Development of Unique Reaction on Boron-doped Diamond Electrode: Coreactant-free Electrogenerated Chemiluminescence and Hydroxide Ion Oxidation

February 2020

Irkham

A Thesis for the Degree of Ph. D. in Science

Development of Unique Reaction on Boron-doped Diamond Electrode: Coreactant-free Electrogenerated Chemiluminescence and Hydroxide Ion Oxidation

February 2020

Graduate School of Science and Technology

Keio University

Irkham

Table of Content

Electrogenerated Chemiluminescence of Luminol & in Situ H_2O_2 on Boron-Doped Diamond Electrode

Study of Hydroxide Ion Oxidation in Basic Solutions Using Boron-doped Diamond Electrodes

Summary & Future Perspective

Chapter 1

General Introduction

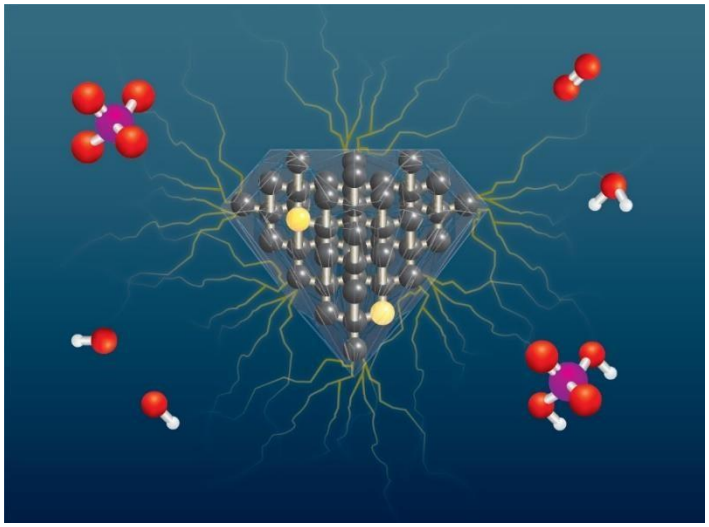

1. Boron-doped diamond

Conductive diamond is now gaining much attention as an electrode material in the field of electrochemistry. In early 1990's, conducting diamond was started to be applied for different electrochemical application as a new carbon electrode material.[1-7] For over decade, many types of conductive diamond including hydrogen terminated undoped diamond, nitrogen-doped diamond (NDD), phosphorus-doped diamond (PDD) has been utilized in many applications.[8-14] Boron-doped diamond (BDD), by far has been the most extensively studied and employed among the conductive diamond types. This is due to the fact boron takes up the same position as displaced carbon atoms effectively with relatively small activation energy (0.37 eV), making high doping levels are possible thus could increase the conductivity in those diamond itself.[15]

In 1996, Angus et al.[16] revealed the high overpotential for both oxygen and hydrogen evolution of a high quality BDD, which lead to a wide electrochemical potential window in aqueous solution (~3 V in 1 M H_2SO_4),[17-20] especially compared to some conventional electrode such as gold, platinum, or other traditional carbon materials. This remarkable feature easily become the strongest characteristic of BDD that lead to its wide range of application including electrochemical electrosynthesis,[21,22] electroanalysis,[23,24] biosensors,[25] CO_2 reduction,[26.27] and metal recovery.[28]

It also has been shown that BDD electrodes could electrogenerates hydroxyl radical from water under polarization at high anodic potential.[29] The hydroxyl radical that generate on the surface of BDD has a weak hydroxyl radical interaction to the electrode, resulting in a low electrochemical activity towards the oxygen evolution. The hydroxyl radical adsorbed on the surface of BDD are very reactive and could easily react with other compound including the electrolyte i.e. sulfate (SO_4^{2-}), phosphate (PO_4^{3-}), and carbonate (CO_3^{2-}), to produce a strong oxidant of peroxydisulfate ($S_2O_8^{2-}$),[20] peroxydiphosphate ($P_2O_8^{2-}$),[30] and peroxydicarbonate ($C_2O_6^{2-}$)[31] respectively. Since the oxygen evolution activity on BDD was low, the efficiency of the production of those strong oxidants are quite high compared to conventional electrode such as platinum. This coupled with it stability as a diamond, low background current, and the fact that generally it assumed that no passivating layers are

formed on BDD surface (unlike metal electrodes), made BDD has been proposed as an anode to perform efficient production of strong oxidants.

On the other hand, these oxidants could be directly used in the phenomenon such as electrogenerated chemiluminesence (ECL), which a complex phenomenon where the generation of light emitting excited state is triggered by electrochemical reaction at the surface of an electrode.[32,33] In particular, ECL system usually applied in the biosensors field, having several advantage such as no background emission, broad dynamic range, low volume, and rapid measurement analysis, therefore push the detection limit to pM range.[34-36] There are two pathways of ECL system in general called annihilation and coreactant pathway, where the later involving a reaction between luminophore and sacrificial reagent so-called coreactant to generate the light emission. Notes that the coreactant are usually needs to be a strong oxidant (or reductant) to be able to generate the excited state of the luminophores. Despite being well established in many analytical applications, coreactant ECL still shows some disadvantages such as toxicity, high vapor pressure, and low solubility in aqueous solutions.[37] Moreover, relatively high coreactant concentrations are usually needed in order to obtain high emission; therein lies a severe drawback in some bioanalytical applications since the existence of high concentrations of coreactant species can interfere with the target biochemical analyte.[38] With the ability of BDD to directly produce strong oxidants at will and in situ from the choice of the electrolyte, we could established a novel *coreactant-free* ECL system which could maintain general application of ECL by overcoming aforementioned drawbacks of toxicity and being able to minimize the interference with the biomolecule, since the active compound is only generated in electrode surface in a short time.

With its low background current and chemical inertness in almost all aggressive aqueous electrolytes, BDD was also has been proposed as a pH sensor.[39] The detection was based on the reduction of hydronium ion, which could be well separated from the hydrogen evolution background. In the same manner, it is expected that the oxidation wave due to oxidation of hydroxide ions can to be separated from the oxygen evolution background in a basic solution, especially on BDD electrode.[40-43] This, makes BDD also a great candidate for

analyzing alkalinity by measuring the hydroxide ion concentration in a solution, since BDD could work well even in the harsh alkaline environment. This could be important because typical electrode that were established as pH sensor, e.g. glass electrode, usually cannot work well on the high alkalinity solution. Moreover, even though the pH in high alkalinity could also be monitored via proton reduction, direct observation of hydroxide ion could give stronger response, due to the fact that hydroxide ion is much more abundant in the alkaline solution, hence lead into a better sensitivity overall.

2. Electrogenerated chemiluminescence

Electrogenerated Chemiluminesence (ECL) is the process in accordance with which, species generated at electrodes undergo high-energy electron-transfer reactions to form excited states that emit light.[32,33] ECL is a form of luminescence where the production of light occurs because of the species that can undergo highly energetic electron-transfer reaction. Figure 1.1 shows the general principles of the ECL generation process.

There are some benefits from ECL compared to other luminescence method. First, in ECL, the electrochemical reaction allows the control of time and position of the emitting light reaction. Control of the time can lead to the delayed light emission until particular reactions take place, such as biochemical reactions. Meanwhile, by controlling the position, the light emission can be precisely located according to the position of detector, increasing the signal-to-noise ratio which lead to the improved sensitivity.[44] Second, ECL is more selective than CL. Thus, varying the electrode potentials can selectively control the generation of light emitting species. Third, ECL, in some cases, is a nondestructive technique, because some of the ECL emitters can be regenerated after the ECL emission. In general, ECL has gained considerable attention as a powerful analytical method owing to its innate features, such as, high sensitivity, selectivity, and wide linear dynamic range for a variety of analyses including oxalate,[45] alkylamines,[46] amino acids,[47,48] NADH,[49-51] and a number of pharmaceutical compounds.[52-55]

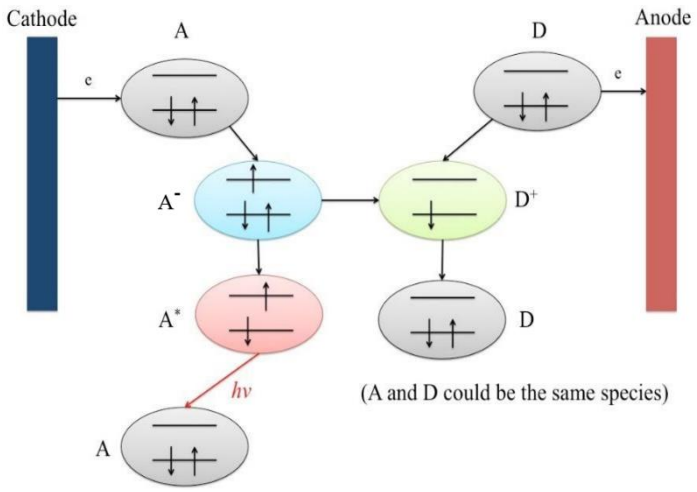

Figure 1.1. Schematic diagrams showing the general principles of electrogenerated chemiluminescence.[33]

In ECL, reactants are, at first, electrochemically generated via two-mechanisms: annihilation and coreactants, resulting in the production of light. Both mechanisms have various advantages and follow different pathways to generate the electronically excited state that eventually emits light. Although one of the most important elements in the generation of efficient ECL is the kinetics of the reaction, however, other fundamental elements are required for efficient ECL generation. These are including radical ion stability of the precursor molecules in the electrolytes, good photoluminescence efficiency, and sufficient energy in the electron-transfer reaction for the production of the excited state.[56]

2.1 Ion annihilation pathway

The early ECL studies were originated via ion annihilation mechnanism.[33] Proceeded by the annihilation pathway, ECL can be generated on reaction between oxidized and reduced species produced on the electrode, either on a single electrode by using an alternating potential or at two separate electrodes. Most of the annihilation ECL processes have been investigated in organic solvents or partially organic solutions because annihilation reactions are very energetic. In addition, aqueous solutions usually exhibit too narrow potential range to allow convenient electrolytic generation of both oxidized and reduced

ECL precursors.[57] Such reactions performed in organic solutions require a supporting electrolyte such as tetrabutylammonium salt. The presence of dissolved oxygen should be avoided as it may sometimes react with radical intermediates and, thus, quench the reaction.[58]

The advantages of the annihilation process lie in its simple approach as it needs only the ECL species (luminophore), solvent, and supporting electrolyte in order to generate light.[58] A common example of the annihilation method is $Ru(bpy)_3^{2+}$ which is first published by Bard's group in 1972.[33] They generated ECL by pulsing the electrode potential to form oxidative $Ru(bpy)_3^{3+}$ and reductive $Ru(bpy)_3^{+}$ which later formed the excited state of ruthenium $Ru(bpy)_3^{2+*}$ with reaction as shown below:

Anode:

$Ru(bpy)_3^{2+} \rightarrow Ru(bpy)_3^{3+} + e^-$

Cathode:

$Ru(bpy)_3^{2+} + e^- \rightarrow Ru(bpy)_3^{+}$

$Ru(bpy)_3^{+} + Ru(bpy)_3^{3+} \rightarrow Ru(bpy)_3^{2+*}$

$Ru(bpy)_3^{2+*} \rightarrow Ru(bpy)_3^{2+} + h\nu$

This annihilation process can be observed only in acetonitrile solution due to the instability of $Ru(bpy)^{3+}$ in aqueous solution. Moreover, the annihilation pathway needs a high-energy potential in general, make it difficult to perform in aqueous solution.

2.2 Coreactant pathway

Currently, the majority of commercially available ECL analytical instrument is based on coreactant technology.[33] The reason lies in the advantage of the coreactant approach that gives assistance in ECL generation even in aqueous solution. This leads to a significantly wider application in the analytical field. Moreover, unlike the annihilation pathway that requires two-directional potential scanning, coreactant ECL requires only one-directional

potential scanning either to the positive potential or negative potential.[58] In annihilation pathway, all starting species can be generated after the light emission, whereas in a coreactant ECL system, only luminophore can be regenerated. Coreactant is consumed during the chemical (or electrochemical) reaction, while the luminophore species can be regenerated on the electrode. Suitable coreactant can be easily oxidized and reduced, which undergo a rapid chemical reaction to form an intermediate species with sufficient power to oxidize or reduce the luminophore leading to the formation of the excited state.[34,37] This is the most important factor to select a good coreactant, although other factors, such as, solubility, stability, kinetics, quenching effect, and ECL background should also be considered.[33,37]

There are four process usually involved in generating ECL light from coreactant system such as (a) redox reactions at electrode, (b) homogeneous chemical reactions, (c) excited-state species formation, and (d) light emission.[33,37] Luminophore and coreactant in coreactant pathway can be first oxidized or reduced at the electrode to form radicals by considering the polarity of the applied potential. The intermediates are thus formed from the coreactant then decompose to produce a strong reducing or oxidizing species that react with oxidized or reduced luminophore to produce the excited states that emit light. Depend on the process, there are two terms being used to specify the reaction. The term "oxidativereductive" ECL used when the intermediate species generate a highly reducing species after an electrochemical oxidation of a coreactant, and "reductive-oxidation" ECL used when highly oxidizing intermediate produced after an electrochemical reduction.[37]

One of the most famous coreactant ECL system is $Ru(bpy)_3^{2+}$/ Tripropylamine (TPrA) system. This system is currently basis for the commercial immunoassays and DNA analyses.[59-61] One of the reasons is the optimum pH of the system. The system is strongly depending on the solution pH, and having the maximum value of the ECL intensity occurs at around pH 7.5, which is very suitable for the application in biological system. The mechanism is "oxidative-reductive" and has been explained in detail in recent years.[59,62] The oxidation of both $Ru(bpy)_3^{2+}$ and TPrA takes place on the electrode surface, and $Ru(bpy)_3^{3+}$ is reduced by TPrA to produce the excited state. The reactions occur as follows:

$Ru(bpy)_3^{2+} \rightarrow Ru(bpy)_3^{3+} + e^-$

$TPrA \rightarrow TPrA^{\bullet+} + e^-$

$TPrA^{\bullet+} \rightarrow TPrA^{\bullet}$

$Ru(bpy)_3^{3+} + TPrA^{\bullet} \rightarrow Ru(bpy)_3^{2+*} + products$

$Ru(bpy)_3^{2+*} \rightarrow Ru(bpy)_3^{2+} + h\nu$

Although having several superior features and attractiveness, it still has some issues to works with. TPrA exhibits several disadvantages such as toxicity, volatility, and relatively low solubility in aqueous solution. Moreover, high concentration (usually up to 100mM) is necessary to obtain good sensitivity.[33]

Another coreactant system that also gain attention is $Ru(bpy)_3^{2+}$/ $S_2O_8^{2-}$. Unlike TPrA system, the coreactant $S_2O_8^{2-}$ is "reductive-oxidation" coreactants. This system produces ECL light by applying a negative potential to the electrode.[63] Consequently, it seems quite difficult to study this kind of ECL systems in aqueous solution due to hydrogen evolution upon applying very negative potential. The ECL emission for $Ru(bpy)_3^{2+}/S_2O_8^{2-}$ system cannot be observed in purely aqueous solutions due to either instability of $Ru(bpy)_3^{+}$ or the rapid quenching by persulfate in aqueous solution.[64] The hydrogen evolution in aqueous solution might also interfere the reaction which makes it difficult to observe the light. The reactions are as follows:

$Ru(bpy)_3^{2+} + e^- \rightarrow Ru(bpy)_3^{+}$

$Ru(bpy)_3^{+} + S_2O_8^{2-} \rightarrow Ru(bpy)_3^{2+} + SO_4^{\bullet-} + SO_4^{2-}$

$Ru(bpy)_3^{+} + SO_4^{\bullet-} \rightarrow Ru(bpy)_3^{2+*} + SO_4^{2-}$

$Ru(bpy)_3^{2+} + SO_4^{\bullet-} \rightarrow Ru(bpy)_3^{3+} + SO_4^{2-}$

$Ru(bpy)_3^{+} + Ru(bpy)_3^{3+} \rightarrow Ru(bpy)_3^{2+*} + Ru(bpy)_3^{2+}$

$Ru(bpy)_3^{2+*} \rightarrow Ru(bpy)_3^{2+} + h\nu$

Bard first reported this ECL system in 1984, with a linear range of 10^{-13} to 10^{-7} M in Acetonitrile-H_2O mixed solution containing persulfate.[65]

Many efforts to ECL system are also performed by other researchers until now. One of the main goal are to move this system to pure aqueous solution for more general application. This become hard not only due to the relatively fast quenching rate of the coreactant peroxodysulfate, but also due to the limitation of the electrode material. As we know in water-based solution, hydrogen evolution could easily occur on conventional electrode and completely hampered the ECL reaction. Even though the ECL reaction are still occur, the tremendous amount of hydrogen bubble will easily cover the weak signal of the ECL making it's hard to be detected.

On the other hand, as previously mentioned, BDD electrode is known having a high overpotential to the hydrogen evolution, makes the ECL reaction easier to be occur even in the water solution. Moreover, also as mentioned before, BDD could in situ produce the coreactant via electrolyte. This makes the system could be more less reactive to the analyte since the reactive coreactant was only produced in the surface of the solution in the short time.

3. Hydroxide oxidation

Sodium hydroxide is one of the most common raw materials used in various industrial and laboratory applications, including electrochemical field. The main uses of concentrated sodium hydroxide globally are in paper pulp, electroplating, alumina and chemical industries as well as in waste water treatment plants.[66] Although it is the largest chemical manufactured in the world, it is highly corrosive that necessitates a need to develop on-line monitoring sensors for its determination in the high concentration range.[66-68]

In aqueous solutions, the cathodic and anodic potential limits are define by the hydrogen and oxygen evolution process that occurs through a complex reaction.[69] It is well established that in acidic solution, for a given electrode material, the peak of hydronium ion reduction can be separated with the hydrogen evolution background.[70-72] In the same manner, hydroxide ion oxidation wave could be expected to be separated with the oxygen evolution background in the basic solution.[69] Generally, the overall electrode process for the hydroxide ions can be written as follows:

$OH^- \rightarrow \frac{1}{4}O_2 + \frac{1}{2}H_2O + e^-$ (1)

The oxidation of hydroxide ion usually occurred on relatively high potential, which makes the phenomena quite difficult to be observed due to overlapping of the oxidation wave with the water oxidation. Moreover, on metal electrode, the hydroxide ion oxidation become more complex due to the background oxide formation, which happen near the hydroxide ion oxidation potential. Despite these, some studies on noble metal electrode such as gold or platinum have shown that a well-defined hydroxide ion oxidation wave can be observed in the basic solution. Although the wave height was found to be proportional to the concentration of hydroxide ion, a steady-state system including a special geometry or a special system of an electrode was necessary.[69,73-75]

On the other hand, BDD electrode, with its high overpotential of water oxidation, it should be possible to distinct the oxidation of hydroxide ion with the water. In addition, unlike metal electrodes, almost no oxide layer forms on the BDD electrode. Combined with high stability in harsh environment, BDD could become a great electrode candidate for observing hydroxide ion oxidation without the needs of special geometry or an electrode system.

4. Outline of the thesis

This thesis will describe (1) the development of several novel *coreactant-free* ECL system using BDD electrode and (2) behaviour of hydroxide ion oxidation in BDD electrode.

In Chapter 2, a unique ability of BDD electrode to electrogenerate strong oxidant efficiently combined with the high overpotential over the hydrogen evolution is described. Generally, a common system of using $Ru(bpy)_3^{2+}$ as luminophore and $S_2O_8^{2-}$ for the coreactant is used. Instead of using coreactant $S_2O_8^{2-}$, Na_2SO_4 solution, which allow the electrogeneration of $S_2O_8^{2-}$ from the oxidation of SO_4^{2-} at the surface of the electrode, was applied. The result showed an efficient ECL generation could be observed at bare BDD electrode in the novel $Ru(bpy)_3^{2+}/SO_4^{2-}$ *coreactant-free* ECL system.

In Chapter 3, another example of *coreactant-free* system of $Ru(bpy)_3^{2+}/CO_3^{2-}$, where CO_3^{2-} will be oxidized at BDD electrode to generate H_2O_2 efficiently that will act as the coreactant, is discussed. The ECL emission was found to be dependent on the concentration of the electrogenerated hydrogen peroxide, therefore it can be controlled through several means such as controlling the pH, oxidation potential, time, and the initial concentration of carbonate electrolyte.

In Chapter 4, using the similar strategy, ECL system of Luminol/CO_3^{2-} is shown. The emission was found to be decreased by the decrease of pH, which is expected on the luminol system due to the needs of luminol to be deprotonated before oxidize.

In Chapter 5, a study of hydroxide ion oxidation on BDD electrode in alkaline solution was described. Hydroxide oxidation peak was found in both oxidized and reduced BDD and showing good linearity versus the hydroxide ion. The current on weak alkaline solution was found to be higher compared to the same hydroxide ion concentration of strong alkaline solution due to the buffering capability of weak basic solution.

5. Reference

1. Tenne, R.; Patel, K.; Hashimoto, K.; Fujishima, A. *J. Electroanal. Chem.* **1993**, *347*, 409.
2. Swain, G. M.; Ramesham, R. *Anal. Chem.* **1993**, *65*, 345.
3. Ramesham, R.; Askew, R. F.; Rose, M. F.; Loo, B. H. *J. Electrochem. Soc.* **1993**, *140*, 3018.
4. Miller, B.; Kalish, R.; Feldman, L. C.; Katz, A.; Moriya, N.; Short K.; White, A. E. *J. Electrochem. Soc.* **1994**, *141*, 41.
5. Yang, N.; Yu, S.; Macpherson, J. V.; Einaga, Y.; Zhao, H.; Zhao, G.; Swain, G. M.; Jiang, X. *Chem. Soc. Rev.* **2019**, *48*, 157
6. Fujishima, A.; Einaga, Y.; Rao, T. N.; Tryk, D. A. *Elsevier and BKC*, **2005**.
7. Yang, N.; Swain, G. M.; Jiang, X. *Electroanalysis* **2016**, *28*, 27.
8. Ke, H.; Liu, M.; Zhuang, L.; Li, Z.; Fan, L.; Zhao, G. *Electrochim. Acta* **2014**, *137*, 146.
9. Ivandini, T. A.; Einaga, Y.; *Chem. Commun.* **2017**, *53*, 1338.
10. Yang, N.; Foord, J. S.; Jiang, X.; *Carbon* **2016**, *99*, 90.
11. Zhou, Y.; Zhi, J. *Talanta* **2009**, *79*, 1189.
12. Vermeeren, V.; Wenmackers, S.; Wagner, P.; Michiels, L. *Sensor* **2009**, *9*, 5600.

13. Zhao, G.; Tang, Y.; Liu, M.; Lei, Y.; Xiao, X. *Chin. J. Chem.* **2007**, *25*, 1445.
14. Li, M.; Zhao, G.; Geng, R.; Hu, H. *Bioelectrochemistry* **2008**, *74*, 217.
15. Macpherson, J. V. *Phys. Chem. Chem. Phys.* **2015**, *17*, 2935.
16. Martin, H. B.; Argoitia, A.; Landau, U.; Anderson, A. B.; Angus, J. C. *J. Electrochem. Soc.* **1996**, *143*, 133.
17. Michaud, P-A.; Panizza, M.; Ouattara, L.; Diaco, T.; Foti, G.; Comninellis, C. *J Appl Electrochem* **2003,** *33*, 151.
18. Serrano, K.; Michaud, P-A.; Comninellis, C.; Savall, A. *Electrochim Acta*, **2002**, *48*, 431.
19. Salazar-Banda, G.; Andrade, L.; Nascente, P.; Pizani, P.; Rocha-Filho, R.; Avaca, L. *Electrochim Acta* **2006**, *51*, 4612.
20. Khamis, D.; Mahe, E.; Dardoize, F.; Devilliers, D. *J. Appl. Electrochem.* **2010**, *40*, 1829.
21. Ivandini, T. A.; Einaga, Y. *Chem. Commun.* **2017**, *53*, 1338.
22. Waldvogel, S. R.; Elsler, B. *Electrochim. Acta* **2012**, *82*, 434.
23. Einaga, Y. *J. Appl. Electrochem.* **2010**, *40*, 1807.
24. Asai, K.; Ivandini, T. A.; Falah, M. M.; Einaga, Y. *Electroanalysis* **2016**, *28*, 177.
25. Asai, K.; Ivandini, T. A.; Einaga, Y. *Sci. Rep.* **2016**, *6*, 32429.
26. Natsui, K.; Iwakawa, H.; Ikemiya, N.; Nakata, K.; Einaga, Y. *Angew. Chem. Int. Ed*. **2018**, *57*, 2639.
27. Tomisaki, M.; Kasahara, S.; Natsui, K.; Ikeminya, N.; Einaga, Y. *J. Am. Chem. Soc.* **2019**, *141*, 7414.
28. Natsui, K.; Yamaguchi, C.; Einaga, Y. *Phys. Status Solidi Appl. Mater. Sci.* **2016**, *2086*, 2081.
29. Kapałka, A.; Foti, G.; Comninellis, C. *Electrochim. Acta*. **2007**, *53*, 1954.
30. Cañizares, P.; Larrondo, F.; Lobato, J.; Rodrigo, M. A.; Sáez, C. *J. Electrochem. Soc.* **2005**, *152*, 191.
31. Ruiz, E. J.; Ortega-Borges, R.; Jurado, J. L.; Chapman, T. W.; Meas, Y. *Electrochem. Solid-State Lett.* **2009**, *12*, 1.
32. Valenti, G.; Zangheri, M.; Sansaloni, S.E.; Mirasoli, M.; Penicaud, A.; Roda, A.; Paolucci, F. *Chem. Eur. J.* **2015**, *21*, 12640.
33. Miao, W. *Chem. Rev.* **2008**, *108*, 2506.
34. Valenti, G.; Rampazzo, E.; Biavardi, E.; Villani, E.; Fracasso, G.; Marcaccio, M.; Bertani, F.; Ramarli, D.; Dalcanale, E.; Paolucci, F.; Prodi, L. *Faraday Discuss*. **2015**, *185*, 299.
35. Li, L.; Chen, Y.; Zhu, J. J. *Anal. Chem.* **2017**, *89*, 358.

36. Liu, Z.; Qi, W.; Xu, G. *Chem. Soc. Rev*. **2015**, *44*, 3117.
37. Richter, M. M. *Chem. Rev*. **2004**, *104*, 3003.
38. Xu, J.; Huang, P.; Qin, Y.; Jiang, D.; Chen, H. *Anal. Chem*. **2016**, *88*, 4609.
39. Fierro, S.; Mitani, N.; Comninellis, C.; Einaga, Y. *Phys. Chem. Chem. Phys*. **2011**, *13*, 16795.
40. Daniele, S.; Baldo, M. A.; Simonetto, F. *Anal. Chim. Acta* **1996**, *331*, 117.
41. Abdelsalam, M. E.; Denuault, G.; Antonietta Baldo, M.; Bragato, C.; Daniele, S. *Electroanalysis* **2001**, *13*, 289.
42. Ciszkowska, M.; Jaworski, A.; Osteryoung, J. G. *J. Electroanal. Chem.* **1997**, *423*, 95.
43. Canhoto, C.; Matos, M.; Rodrigues, A.; Geraldo, M. D.; Bento, M. F. *J. Electroanal. Chem.* **2004**, *570*, 63.
44. Chen, X-M.; Su, B-Y; Song, X-H.; Chen, Q-A.; Chen, X.; Wang X-R. *Trac-Trends Anal Chem.* **2011**, *30*, 665.
45. Rubinstein, I.; Martin, C.R.; Bard, A.J. *Anal Chem.* **1983**, *55*, 1580.
46. Noffsinger, J.B.; Danielson, N.D. *Anal. Chem.* **1987**, *59*, 865.
47. Brune, S.N.; Bobbitt, D.R. *Talanta* **1991**, *38*, 419.
48. Brune, S.N.; Bobbitt, D.R. *Anal. Chem.* **1992**, *64*, 166.
49. Downey, T.M.; Nieman, T.A. *Anal. Chem.* **1992**, *64*, 261.
50. Lee, W-Y.; Nieman, T.A. *Anal. Chem.* **1995**, *67*, 1789.
51. Martin, A.F.; Nieman, T.A. *Anal. Chim. Acta.* **1993**, *281*, 475.
52. Zorzi, M.; Pastore, P.; Magno, F. *Anal. Chem.* **2000**, *72*, 4934.
53. Greenway, G.M.; Nelstrop, L.J.; Port, S.N. *Anal. Chim. Acta.* **2000**, *405*, 43.
54. Park, Y-J.; Lee, D.W. and Lee, W-Y. *Anal. Chim. Acta.* **2002**, *471*, 51.
55. Li, F.; Cui, H. and Lin, X-Q. *Anal Chem Acta*. **2002**, *471*,187.
56. Oldham, P.B.; McCarroll, M.E.; McGown, L.B.; Warner, I.M. *Anal. Chem.* **2000**, *72*, 197.
57. Rubinstein, I.; Bard, A.J. *J. Am. Chem. Soc.* **1981**, *103*, 512.
58. Bertoncello, P.; Forster, R.J. *Biosens. Bioelectron.* **2009**, *24*, 3191.
59. Miao, W.; Choi, J. P.; Bard, A. J. *J. Am. Chem. Soc*. **2002**, *124*, 14478.
60. Yang, Y.; Oh, J. W.; Kim, Y. R.; Terashima, C.; Fujishima, a.; Kim, J. S.; Kim, H. *Chem. Commun*. **2010**, *46*, 5793.
61. Honda, K.; Yoshimura, M.; Rao, T. N.; Fujishima, a. *J. Phys. Chem. B*. **2003**, *107*, 1653.
62. Wightman, R.M.; Forry, S.P.; Maus, R.; Badocco, D. and Pastore, P. *J. Phy. Chem. B.* **2004**, *108*, 19119.

63. Hu, L.; Xu, G. *Chem. Soc. Rev.* **2010**, *39*, 3275.
64. White, H.S.; Bard. A.J. *J. Am. Chem. Soc.* **1982**, *104*, 25.
65. Ege, D.; Becker, W.G.; Bard, A.J. *Anal. Chem.* **1984**, *56*, 2413.
66. Thakur, N.; Kumar, S. A.; Pandey, A. K.; Kumar, S. D.; Reddy, A. V. R. *RSC Adv.*, **2015**, *5*, 72893.
67. Hallam, P. M.; Kampouris, D. K.; Kadara, R. O.; Jenkinson, N.; Banks, C. E. *Anal. Meth.* **2010**, *2*, 1152.
68. De Wael, K.; Adriaens, A. *Talanta* **2008**, *74*, 1562.
69. Daniele, S.; Baldo, M. A.; Bragato, C.; Denuault, G.; Abdelsalam, M. E. *Anal. Chem.* **1999**, *71*, 811.
70. Daniele, S.; Baldo, M. A.; Simonetto, F. *Anal. Chim. Acta* **1996**, *331*, 117.
71. Abdelsalam, M. E.; Denuault, G.; Antonietta Baldo, M.; Bragato, C.; Daniele, S. *Electroanalysis* **2001**, *13*, 289.
72. Ciszkowska, M.; Jaworski, A.; Osteryoung, J. G. *J. Electroanal. Chem.* **1997**, *423*, 95.
73. Abdelsalam, M. E.; Denuault, G.; Baldo, M. A.; Daniele, S. *J. Electroanal. Chem.* **1998**, *449*, 5.
74. Abu-Rabi, A.; Jašin, D.; Mentus, S. *J. Electroanal. Chem.* **2007**, *600*, 364.
75. Pašti, I. A.; Lazarević-Pašti, T.; Mentus, S. V. *J. Electroanal. Chem.* **2012**, *665*, 83.

Chapter 2

Co-reactant-on-Demand ECL: Electrogenerated Chemiluminescence by the in Situ Production of $S_2O_8^{2-}$ at BoronDoped Diamond Electrodes

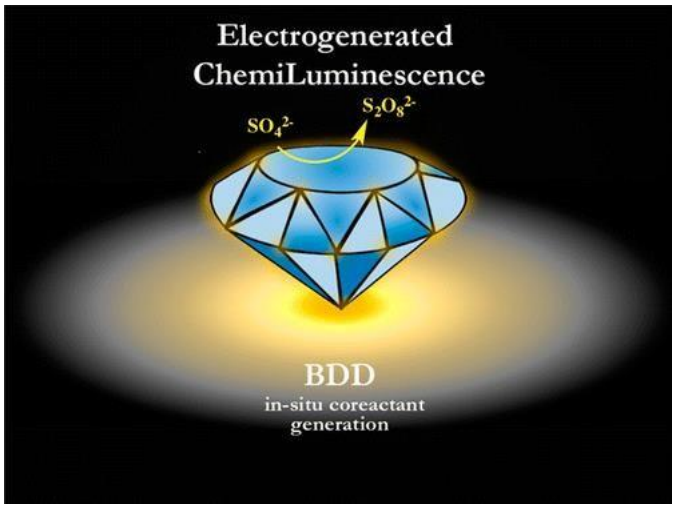

1. Introduction

In Chapter 1, it is already mentioned that the $Ru(bpy)_3^{2+}$/TPA[1-7] system become the basis of commercial ECL immunoassay and DNA analysis devices.[5] Despite its great efficiency in generating ECL in biocompatible environments, TPA shows some disadvantages such as toxicity, high vapor pressure, and low solubility in aqueous solutions.[1] Relatively high coreactant concentrations are usually needed in order to obtain high emission and this may represent a severe drawback in some bioanalytical applications, where the existence of high concentrations of coreactant species can interfere with the target biochemical analyte.[8] Notice that, in some applications, the addition of TPA is not needed, since its role is played by the analyte itself, generally an amine, e.g., sarcosine,[9] dopamine,[10] NADH[11] or other organic compounds.[12,13] Furthermore, opportunely modified fluorophores may also limit the need for added TPA such as, e.g., in recently reported ruthenium(II) complexes carrying Schiff bases cavities. Due to the electrochemical oxidation of phenolic hydroxyl groups and the resonant structure of imino radicals, electrons are transferred intramolecularly to Ru(III) center leading to the efficient generation of the Ru(II)-based excited state.[14]

In order to maintain a more general analytical applicability, the *in-situ generation of coreactant* starting from a relatively unreactive precursor would however represent a promising alternative approach capable to keep the great advantages typical of such a highly sensitive technique. At the same time, it would allow to circumvent most of the aforementioned drawbacks such as toxicity issues and interferences with the biomolecules. In such a context, peroxydisulfate ($S_2O_8^{2-}$) offers some advantages with respect to amines. $S_2O_8^{2-}$ has widely been used as a coreactant in many ECL applications[15-17] where, upon cathodic reduction, it forms the sulfate radical anion ($SO_4^{\bullet-}$), a strongly oxidizing intermediate.[15,18] It has been shown that the ECL efficiency for the $Ru(bpy)_3^{2+}/S_2O_8^{2-}$ is about half that of the annihilation system.[16] Besides being coupled to common luminophores such as Ru complexes, luminol and their derivatives, peroxydisulfate was also shown to exhibit ECL behaviour at magnesium, silver and platinum (Pt) electrodes, where dissolved oxygen can react with $SO_4^{\bullet-}$, thus generating light-emitting species such as $^1O_2$, $^1(^1O_2)_2$ and

$^3(^1O_2)_2$.[19] Several examples based on such an approach have recently been reported, such as a label-free and highly sensitive ECL aptasensor for kanamycin,[20] also coupled to nanocarbons,[21] quantum dots[22] and gold nanoclusters[23,24] for the high sensitive detection of chemicals,[25] antigens[26] and nucleic acids.[27,28] Importantly, peroxydisulfates are commercially prepared by the electrolytic oxidation of aqueous solutions of sulfate precursors, e.g., ammonium sulfate with Pt or platinized titanium anodes at high current densities. Therefore, the in-situ electrogeneration of peroxydisulfate represents a viable strategy to obtain a *coreactant-free* ECL system. In fact, the coreactant would be generated, at will and in-situ, by applying a suitably positive potential in a solution containing the sulfate precursor followed by the step to negative potential that can ignite the ECL emission. Notice that a similar procedure would not be accessible in the case of amines. Given the very high potential required to perform the anodic oxidation of sulfate to peroxydisulfate (E^o = 2.01 V vs. SHE), anode materials displaying very high overpotentials for the oxygen evolution reaction are however needed for the efficient production of peroxydisulfates. Boron−doped diamond (BDD), In particular, BDD has been proposed as anode to perform the efficient oxidization of SO_4^{2-} into peroxydisulfate[29,30] and it has been used for the development of laboratory devices for the determination of sulfates and peroxydisulfates, adapted for the on-line monitoring in process control applications.[31]

Moreover, in recent years, BDD has also been proposed as electrode material for ECL, in particular in applications using $Ru(bpy)_3^{2+}$ with either TPA [6,7,32,33] or with luminol.[34]

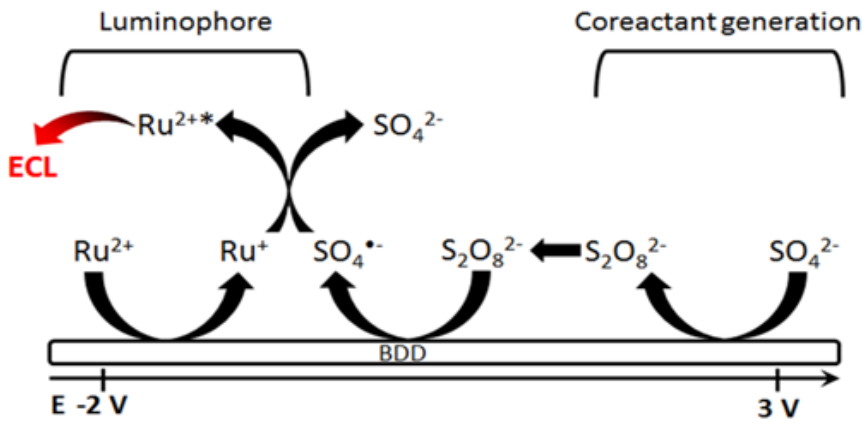

Figure 2.1. Reaction mechanism of electrochemiluminescence generation from $Ru(bpy)_3^{2+}$ on BDD electrode with sulfate ions. Ru = $Ru(bpy)_3$. Adopted from *ref 35* Copyright 2016 American Chemical Society.

Herein we report on a *coreactant-free ECL system* (Figure 2.1) in which the unique ability of BDD (i) to promote peroxydisulfate generation with high efficiency is coupled with (ii) the high overpotential for the hydrogen evolution reaction obtained at the same electrode to allow, in the end, the efficient ECL generation in a $Ru(bpy)_3^{2+}/SO_4^{2-}$ aqueous solution.[35] The procedure is rather straightforward, not requiring any particular electrode geometry, and, since the reactive coreactant $S_2O_8^{2-}$ is only generated on the electrode surface for a short time, the interference with biological samples is minimized.

2. Experimental

Materials. All reagents were obtained commercially and used without further purification. $Ru(bpy)_3Cl_2$ $6H_2O$, Na_2SO_4, $Na_2S_2O_8$, and $KClO_4$ were obtained from Sigma Aldrich. Pure water was doubly distilled with maximum conductivity 18 MΩ obtained from Simply−Lab water system (DIRECT-Q 3 UV, Millipore).

Preparation of BDD. The BDD films were deposited on a silicon (111) wafer by using a microwave plasma-assisted chemical vapor deposition (MPCVD) system (CORNES Technologies / ASTeX−5400). Acetone and trimethoxyborane were used as the source of carbon and boron respectively with atomic ratio of B/C = 1%. The surface morphology of

the BDD was examined with field emission scanning electron microscope (FESEM, JEOL JSM-7600F). Raman Spectra were recorded with an Acton SP2500 (Princeton Instruments) with excitation at 532 nm from a green laser diode in room temperature.

Electrochemiluminescence measurement. All ECL measurements were conducted in a conventional three electrode system in a PTFE cell with a 1% BDD, a Pt spiral, and an Ag/AgCl (Saturated KCl) as working, counter, and reference electrodes, respectively with PGSTAT302 (AUTOLAB Instrument). The ECL signal was measured with a photomultiplier tube (PMT, Hamamatsu R4220p) placed in constant distance inside a dark box. A voltage 750-800 V was supplied to the PMT. The light/current/voltage curves were recorded by collecting the preamplified PMT output signal (by an ultralow-noise Acton research model 181) with the second input channel of the ADC module of the AUTOLAB instrument. For measuring the origin of the light, a voltage of 800V was supplied to the PMT and the light measured directly without amplification. Stabilizing surface of the BDD electrode was carried out before each measurement by electrochemical cleaning by performing ten voltammetric cycles between −3.0 V to 3.0 V followed by ten cycles between 0 V to −3.0 V in 0.1 M $KClO_4$ solution with scan rate 0.3 V/s.

3. Results and discussion

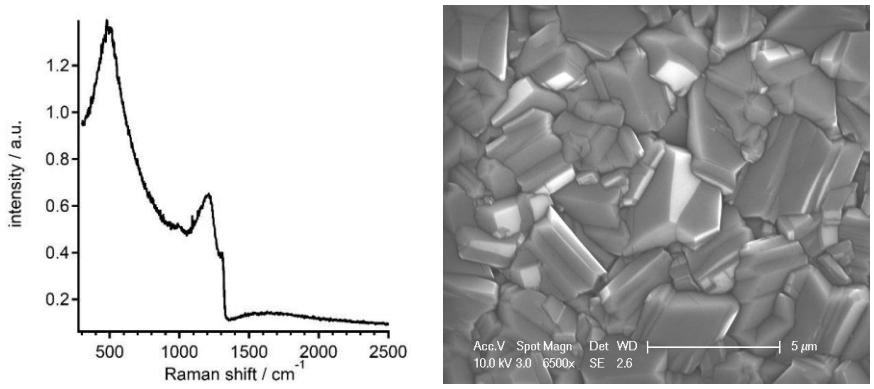

Figure 2.2. Raman spectrum (left) and SEM image (right) of 1% BDD. Adopted from *ref 35* Copyright 2016 American Chemical Society.

To confirm that the film that growth on the silicon surface is BDD, the carbon structure of were investigated using Raman spectroscopy (Figure 2). The BDD used for the electrochemical and ECL measurements showed typical Raman spectrum for highly boron-doped diamond, exhibiting zone-center phonon line observed as a shoulder peak around 1300 cm^{-1}. (Figure 2.2 left).[36] SEM image of the BDD showed predominant facet having three-fold symmetry axis is (111) facet which is known as more electrochemically active domain than (100) (Figure 2.2 right).[32]

The electrochemical and the ECL properties of $Ru(bpy)_3^{2+}$ in 0.1 M Na_2SO_4 aqueous solution on BDD electrodes were firstly investigated by cyclic voltammetry (CV). Figure 2.3 displays the CV curves (a) and the corresponding ECL-potential curves (b) obtained by scanning the potential initially from 0 V to 3.0 V followed by a scan to negative potentials (-2.0 V). The first positive scan is meant to generate, at the BDD electrode surface, a sufficiently high concentration of peroxydisufate ions (eq. 1) to fuel the ECL emission process during the negative potential scan, according to the following general mechanism

positive potential scan:

$$2SO_4^{2-} \rightarrow S_2O_8^{2-} + 2e^- \quad (1)$$

negative potential scan:

$$S_2O_8^{2-} + e^- \rightarrow SO_4^{\bullet -} + SO_4^{2-} \quad (2)$$

$$Ru(bpy)_3^{2+} + e^- \rightarrow Ru(bpy)_3^{+} \quad (3)$$

$$Ru(bpy)_3^{+} + S_2O_8^{2-} \rightarrow Ru(bpy)_3^{2+} + SO_4^{\bullet -} + SO_4^{2-} \quad (4)$$

$$Ru(bpy)_3^{+} + SO_4^{\bullet -} \rightarrow Ru(bpy)_3^{2+*} + SO_4^{2-} \quad (5)$$

$$Ru(bpy)_3^{2+*} \rightarrow Ru(bpy)_3^{2+} + h\nu \quad (6)$$

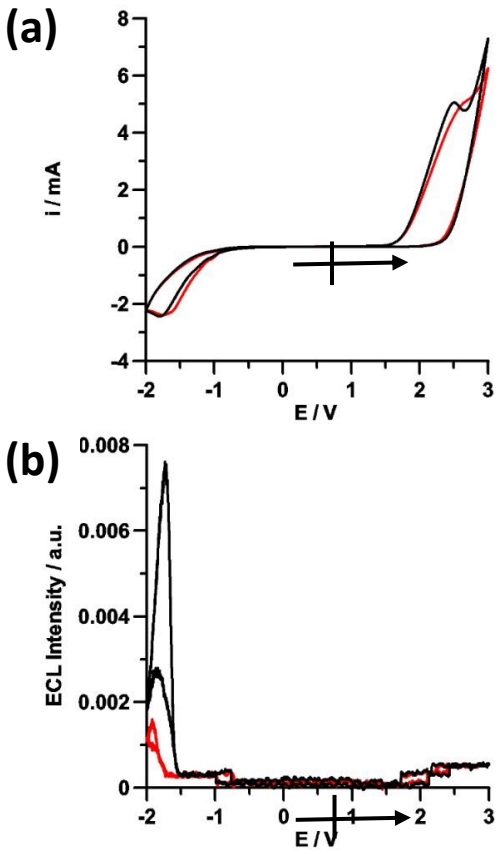

Figure 2.3. (a) CVand (b) ECL comparison between 0.1 M Na_2SO_4 (black) and 0.1 M $KClO_4$ (red) measurement of 5 μM $Ru(bpy)_3Cl_2$ in aqueous media. Scan rate 100 mV/s, potential referred to Ag/AgCl (KCl sat) at room temperature. PMT bias 750 V. Adopted from *ref 35* Copyright 2016 American Chemical Society.

As shown in Figure 2.3a (black line), during the voltammetric cycle in 0.1 M aqueous Na_2SO_4, ECL was efficiently generated at $E° \leq$ -1.5 V, i.e., in the region where reduction of both peroxydisulfate (eq. 2) and $Ru(bpy)_3^{2+}$ (eq. 3) may take place, thus making the sequence of processes outlined by equations 4-6 possible. Notice that, according to the established mechanism depicted above,[16] peroxydisulfate may be reduced to generate sulfate anion radical, either directly at the electrode (eq. 2) or by mediation of $Ru(bpy)_3^{+}$ (eq. 4). The profile of ECL emission vs. potential is similar to that obtained in the $Ru(bpy)_3^{2+}/S_2O_8^{2-}$

system (Figure 2.4), thus substantiating the above hypothesis that $S_2O_8^{2-}$coreactant is effectively produced at the BDD electrode during the first scan at positive potentials. In line with the above hypothesis, an intense ECL signal was only observed when potential was swept in the first scan to sufficiently high values, i.e., where the electrogeneration of peroxydisulfate occurs (Figure 2.5).

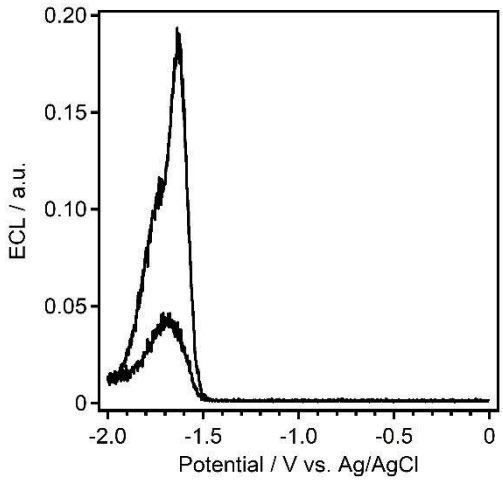

Figure 2.4. ECL of 10 μM $Ru(bpy)_3Cl_2$ and 100 μM $Na_2S_2O_8$ in phosphate buffer solution. Adopted from *ref 35* Copyright 2016 American Chemical Society.

CV in 0.1 M aqueous Na_2SO_4 (Figure 2.3b, black line) shows the broad and intense peak in the first scan at 2.5 V, indicating electrogeneration of peroxydisulfate. On the other hand, CV curve obtained in the absence of sulfate ions, i.e., in 0.1 M aqueous $KClO_4$ (Figure 2.3b, red line) also shows comparable oxidation peak in similar potentials with somewhat duller shape. Such peak prior to intense oxygen evolution reaction (OER) is often observed at BDD electrodes. It is reported that this pre-OER peak is related to water oxidation reaction to generate hydroxyl radical (eq. 7) via surface redox couple of BDD.[37]

$$H_2O \rightarrow OH^{\bullet} + H^+ + e^- \qquad E^\circ = 2.52 \text{ V vs Ag/AgCl} \qquad (7)$$

Hydroxyl radicals are considered to weakly interact with surface of BDD so that eq. 7 is formally written as:

$$BDD + H_2O \rightarrow BDD(OH^{\bullet}) + H^+ + e^- \quad (8)$$

where BDD represents the active site on the electrode surface. This eq. 8 may occur at slightly negative potential to $E°$ for eq. 7 due to weak interaction to the surface of BDD. A. Kapalka et al. reported pre-OER peak attributed to eq. 8 was observed from 1.8 to 2.4 V vs. Ag/AgCl in 1 M $HClO_4$ aqueous solution.[37] Furthermore, D. Khamis et al. reported that in the pre-OER potential domain, indirect oxidation process for generation of peroxydisulfate can occur via surface mediated reaction with $BDD(OH^{\bullet})$ as shown in following equations[29]

$$BDD(OH^{\bullet}) + SO_4^{2-} \rightarrow BDD(SO_4^{\bullet -}) + OH^- \quad (9)$$

$$BDD(SO_4^{\bullet -}) + SO_4^{2-} \rightarrow BDD + S_2O_8^{2-} + e^- \quad (10)$$

where the surface site $BDD(SO_4^{\bullet -})$ is not as oxidative as $SO_4^{\bullet -}$ but sufficient to lead to the generation of peroxydisulfate according to the overall mechanism depicted in eq. 1.[29] In the case of perchlorate solution, the oxidation current observed at pre-OER potential domain is considered as generation of oxygen (eq. 11) following eq. 8.[37]

$$BDD(OH^{\bullet}) \rightarrow BDD + 1/2O_2 + H^+ + e^- \quad (11)$$

In Na_2SO_4 aqueous solutions, this eq. 11 also occurs at pre-OER potential domain as competing reaction with eq. 9. Actually, the CVs conducted in N_2-bubbled 0.1 M Na_2SO_4 showed ORR peak in cathodic scan after sweeping until 2.5 V. Thus, considering $E°$ value and similar oxidation current in pre-OER potential domain in both of Na_2SO_4 and $KClO_4$ solutions, water discharge reaction (eq. 8) is not fast and rate determining step around pre-OER potential domain i.e. around peak potential. Accordingly, in our experiment, it is

considered that peroxydisulfate is mainly generated by indirect oxidation process thorough the eq. 8, 9 and 10.

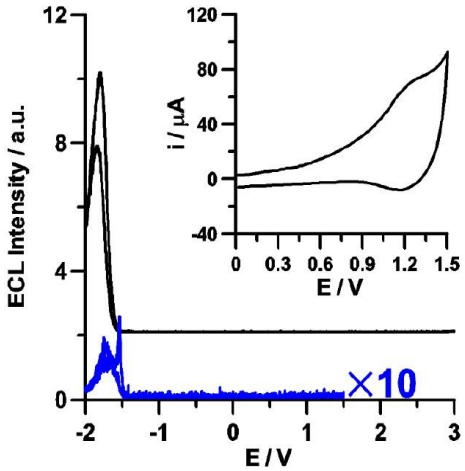

Figure 2.5. ECL of 0.1 M Na_2SO_4 and 5 μM $Ru(bpy)_3Cl_2$ in water solvent at different potential range: 3 V to -2 V (black), 1.5 V to -2 V (blue). Scan rate 100 mV/s, potential referred to Ag/AgCl (KCl saturated) at room temperature. PMT bias 750 V, amplification 000.0 nA. The curves are shifted for clarity. Adopted from *ref 35* Copyright 2016 American Chemical Society.

In cathodic scan, large reduction peak observed starting around −1.0 V in both solutions of Na_2SO_4 and $KClO_4$ is mainly due to oxygen reduction reaction (ORR) since oxygen can be produced in first positive scan (Figure 2.6). The reductions of both peroxydisulfate (eq. 2) and $Ru(bpy)_3^{2+}$ (eq. 3) were considered to be masked with this ORR peak. Despite occurrence of ORR, massive hydrogen evolution reaction (HER) that would more greatly inhibit the process leading to ECL at very negative potentials, could be avoided because of choosing Na_2SO_4 instead of H_2SO_4 or $NaHSO_4$, as precursor of electrogenerated peroxydisulfate.

Furthermore, BDD was uniquely suited to promote ECL emission under such conditions, since parallel experiments carried out with either Pt or GC electrodes were unsuccessful (Figure 2.7); at such electrodes, water oxidation proceeds via different route

and even if hydroxyl radicals can be produced, the radicals would react with electrodes themselves rather than the sulfate ions.

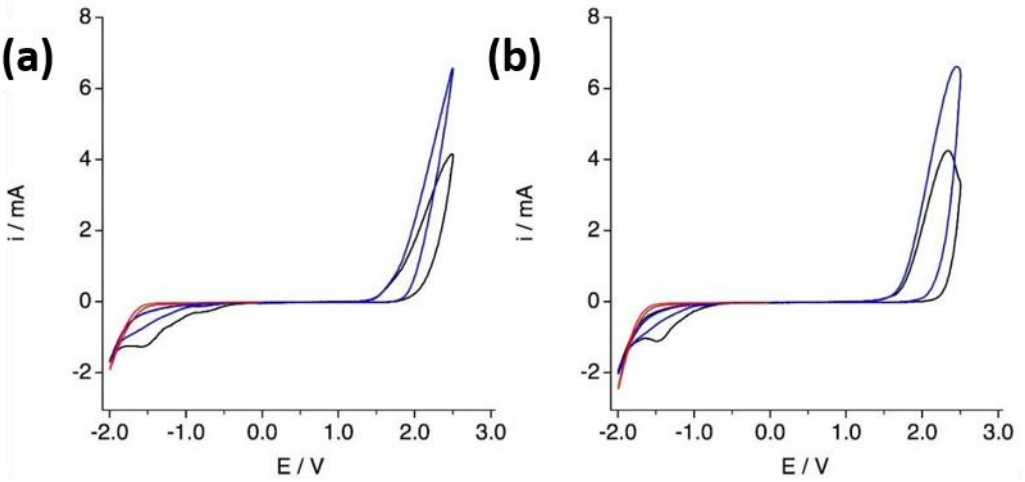

Figure 2.6. Cyclic voltammograms in (a) 0.1 M $KClO_4$ and (b) 0.1 M Na_2SO_4 aqueous solutions. Potential scanned from 0 V to −2.0 V (red), 0 V to 3.0 V to −2.0 V (black), and 0 V to 3.0 V to −2.0 V with pause at 0 V for 3 min before going to −2.0 V (blue). Scan rate 100 mV/s, potential referred to Ag/AgCl (KCl saturated) at room temperature. The solution was bubbled with N_2 gas before measurement. Adopted from *ref 35* Copyright 2016 American Chemical Society.

Importantly, the ECL spectrum (Figure 2.8), recorded during chronoamperometric experiments (v. infra), shows a maximum wavelength at 609 nm, which is expectedly in full agreement with the attribution of the emitted light to the $Ru(bpy)_3^{2+}$ based excited state and excluding that other potential emitters, such as oxygen, may be playing an important role in the observed phenomenon.[16]

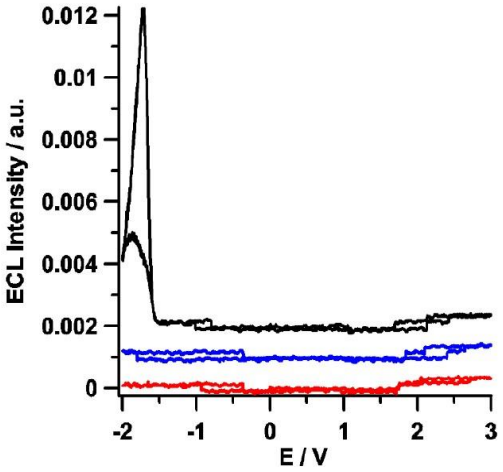

Figure 2.7. Comparison between BDD (black), GC (blue), and Pt (red) electrodes with 5 µM $Ru(bpy)_3Cl_2$ and 0.1 M Na_2SO_4 in water solution from 3.0 V to −2.0 V. Scan rate 100 mV/s, potential referred to Ag/AgCl (KCl saturated) at room temperature. PMT bias 750 V, amplification 000.0 µA. The curves are shifted for clarity. Adopted from *ref 35* Copyright 2016 American Chemical Society.

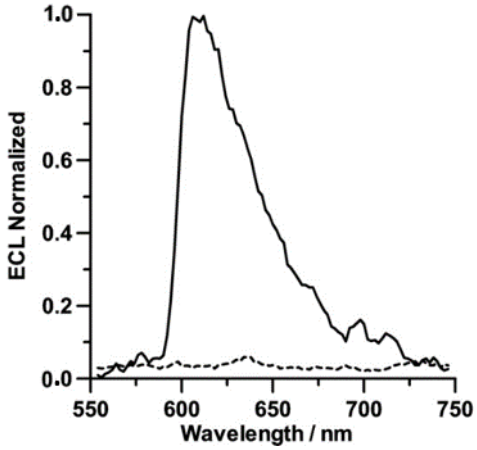

Figure 2.8. Normalized ECL spectrum of 5 µM $Ru(bpy)_3Cl_2$ / 0.1 M Na_2SO_4 system (solid line) and 5 µM $Ru(bpy)_3Cl_2$ / 0.1 M $KClO_4$ system (dashed line) in aqueous solution. PMT bias 800 V. Adopted from *ref 35* Copyright 2016 American Chemical Society.

Interestingly, a weak emission was also obtained when potential was swept in the first scan up to 1.5 V, i.e., at potentials too low to produce peroxydisulfate, but sufficiently high to oxidise the $Ru(bpy)_3^{2+}$ fluorophore ($E°$ = 1.02 V vs Ag/AgCl, Figure 2.6 inset). A possible explanation for such a weak emission is therefore that, in the present system, ECL generation may also take place according to the annihilation route (eq. 12), where $Ru(bpy)_3^{3+}$ generated in the first (positive) scan may react with $Ru(bpy)_3^{+}$ generated in the second (negative) one:[38]

$$Ru(bpy)_3^{+} + Ru(bpy)_3^{3+} \rightarrow Ru(bpy)_3^{2+*} + Ru(bpy)_3^{2+} \qquad (12)$$

Such a mechanism, that involves the couple of fluorophores in either their oxidized or reduced form, is generally unobserved in aqueous media where the prevailing HER prevents formation of the reduced species $Ru(bpy)_3^{+}$ [16] while it would be made possible in the present case by the high overpotential for HER on BDD. In line with such a hypothesis, Figure 2.3 (red line) shows the ECL-potential plot obtained in 0.1 M $KClO_4$ solutions, i.e., in the absence of sulfate ions, displaying a noticeable, although very weak signal, associated to process (12). Notice that annihilation ECL for aqueous $Ru(bpy)_3^{2+}$ solutions was only previously reported in the case of interdigitated carbon microelectrode arrays, with 2 μm width spacing, working in a generation/collection biasing mode.[39] In the present case, instead, annihilation ECL would be obtained from $Ru(bpy)_3^{2+}$ aqueous solutions only by virtue of the unique properties of BDD electrodes, without requiring any particular geometry of the cell and electrodes system.

Further insight in the underlying mechanism and quantification of the ECL emission in the present system, was obtained by performing chronoamperometric experiments where potential was firstly stepped from 0 V to 3.0 V, where it was kept for various time durations (t_{ox}) to generate variable amounts of coreactant, and then to -2.0 V to ignite the ECL process (see Figure 2.9b, inset); the current and ECL light (Figure 2.9b) signals were continuously monitored. While the current curves decrease monotonically, the ECL signal exhibits a steep increase, after each complete oxidation–reduction cycle, followed by a rapid decay,

reflecting the complex sequence of processes described by eqs. 1-6 involving the production and encounter of the reacting species in the diffusion layer. Oxidation currents measured in the first step, in either the presence or absence of sulfate ions, were integrated and were found to increase linearly with the oxidation time t_{ox} (Figure 2.9a), thus suggesting that formation of the surface reactive species (eq. 8), rather than diffusion of the sulfate precursor, controls in the present conditions the oxidation current. By contrast, the integrated ECL signals (measured during the step at -2.0 V) decreases linearly with the square root of t_{ox} (Figure 2.9b, inset) indicating that the efficiency of the overall ECL generation process is limited by diffusion of sulfate precursor to the electrode and of electrogenerated peroxydisulfate towards the bulk of solution.

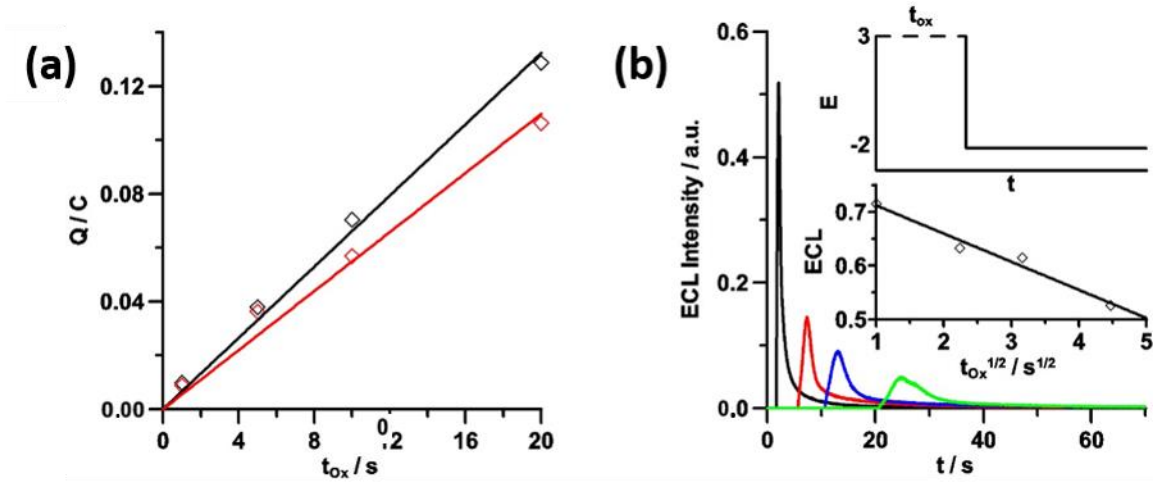

Figure 2.9. (a) Integrated charge at 3V for different oxidation times for 0.1 M Na_2SO_4 (black) and 0.1 M $KClO_4$ (red) and (b) ECL intensity transients measured during chronoamperometric experiments carried out in a 5 μM $Ru(bpy)_3Cl_2$ and 0.1 M Na_2SO_4 aqueous solution; first step from 0 to +3.0 V for t_{ox} = 1, 5, 10 or 20 s, followed by a step to 2.0 V for 50 s. Figure b inset: (above) potential program used in the chronoamperometric experiments; (below) integrated ECL intensity vs square root of time step duration t_{ox}. PMT bias 750 V. Adopted from *ref 35* Copyright 2016 American Chemical Society.

The efficiency of ECL generation was finally investigated at various sulfate concentrations. Current efficiency for sulfuric acid oxidation to peroxydisulfuric acid has been reported to increase with H_2SO_4 concentration.[40] In the present case, the efficiency of peroxydisulfate electrogeneration was in fact found to increase linearly with $[SO_4^{2-}]$ up to ≈ 0.6 M, then deviating negatively at higher concentrations (Figure 2.10) i.e., at significantly lower concentration than the reported maximum current efficiency for peroxydisulfate electrogeneration, obtained with sulfuric acid concentration ≥ 2 M.[51] Importantly, deviations from linearity of the ECL signal as a function of sulfate concentration (in the range 10^{-3}-1 M, Figure 2.11), occurred at significantly lower values than those observed for current, since the signal, following an initial linear increase (up to 0.1 M), reaches a plateau at $[SO_4^{2-}]$ ≈ 0.5 M.

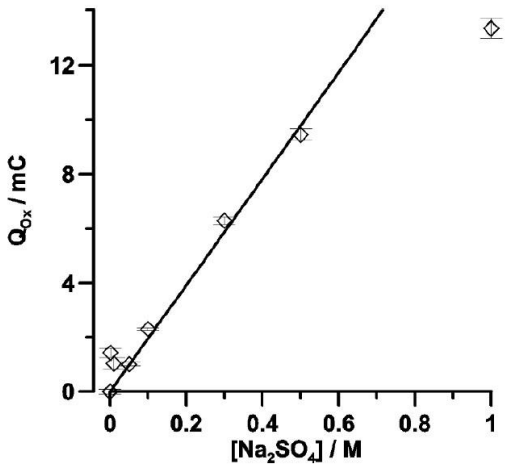

Figure 2.10. Integrated anodic charge as a function of Na_2SO_4 concentration, step at 3.0 V for 1 s. The charge for 0.1 M $KClO_4$ is subtracted. Adopted from *ref 35* Copyright 2016 American Chemical Society.

The observed trend of ECL intensity vs. sulfate precursor concentration can tentatively be ascribed to the known ability of peroxydisulfate ion to effectively quench the excited state $Ru(bpy)_3^{2+*}$.[16] It has been reported that the ECL intensity of the $Ru(bpy)_3^{2+}/S_2O_8^{2-}$ system is in fact a function of $S_2O_8^{2-}$ concentration with a maximum

emission at [$S_2O_8^{2-}$] ≈ 15-20 mM.[16] The dependence of the ECL intensity vs. [SO_4^{2-}] observed in the present case would therefore reflect the increasing competition, as the sulfate ions concentration increases, between the two processes associated to the electrogenerated peroxydisulfate, one leading to a more efficient ECL production (through an increased rate of peroxydisulfate generation) and the other to a faster quenching of the excited state.[41,42]

Finally, analytical applications of the present system can be envisaged within the observed linearity range (1-100 mM). BDD electrodes were proposed for the detection and measurement of sulfate ions, with detection limits in the grams per liter range (≈10 mM), through their anodic oxidation to peroxydisulfate followed by the amperometric detection of peroxydisulfate (eq. 2), and some commercial development has been proposed.[31,43] In such a context, the present ECL-based approach would therefore allow to reach detection limits for sulfate ions in the millimolar range, i.e., at least one order of magnitude lower than the reported amperometric method.

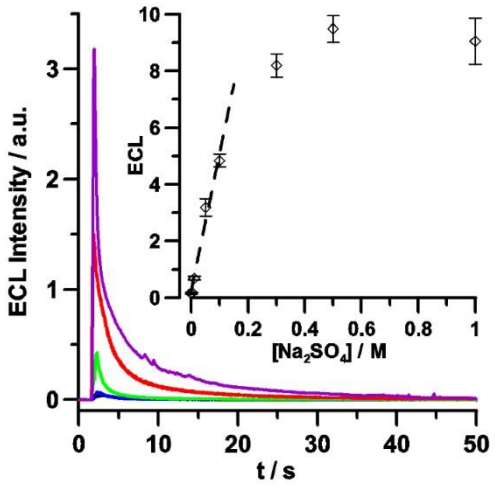

Figure 2.11. ECL intensity transient at various Na_2SO_4 concentrations in 5 μM $Ru(bpy)_3Cl_2$ aqueous solutions; first step 3.0 V for 1 s, followed by a step to −2.0 V for 50 s. Na_2SO_4: 1 mM (blue), 10 mM (green), 0.1 M (red), 1 M (purple) and 0.1 M $KClO_4$ (black), Inset: integrated ECL intensity as function of concentration. PMT bias 750 V. Adopted from *ref 35* Copyright 2016 American Chemical Society.

4. Conclusion

The generation of ECL from aqueous solutions containing the $Ru(bpy)_3^{2+}$ fluorophore and SO_4^{2-} was for the first time reported. The underlying mechanism is similar to that of the $Ru(bpy)_3^{2+}/S_2O_8^{2-}$ system, except that $S_2O_8^{2-}$ is in this case electrogenerated in situ from the sulfate precursor, exploiting the unique ability of BDD electrodes to promote electrochemical reactions with compounds that have highly positive standard potentials. The intensity of the emitted signal was found to increase linearly with $[SO_4^{2-}]$ up to ≈ 0.6 M, thus opening possible analytical uses of the present approach with detection limits for sulfate ions as low as 1 mM. Finally, evidence was also found of ECL emission generated by $Ru(bpy)_3^{2+}$ through the annihilation mechanism, an unprecedented result in aqueous solutions that would also be associated to the wide potential windows achievable with BDD.

5. Reference

1. Richter, M. M. *Chem. Rev.* **2004**, *104*, 3003.
2. Deaver, D. R. *Nature*. **1995**, *377*, 758.
3. Leland, J. K. *J. Electrochem. Soc.* **1990**, *137*, 3127.
4. Noffsinger, J. B.; Danielson, N. D. *Anal. Chem.* **1987**, *59*, 865.
5. Miao, W.; Choi, J. P.; Bard, A. J. *J. Am. Chem. Soc.* **2002**, *124*, 14478.
6. Yang, Y.; Oh, J. W.; Kim, Y. R.; Terashima, C.; Fujishima, A.; Kim, J. S.; Kim, H. *Chem. Commun.* **2010**, *46*, 5793.
7. Honda, K.; Yoshimura, M.; Rao, T. N.; Fujishima, A. *J. Phys. Chem. B* **2003**, *107*, 1653.
8. Xu, J.; Huang, P.; Qin, Y.; Jiang, D.; Chen, H. *Anal. Chem.* **2016**, *88*, 4609.
9. Valenti, G.; Rampazzo, E.; Biavardi, E.; Villani, E.; Fracasso, G.; Marcaccio, M.; Bertani, F.; Ramarli, D.; Dalcanale, E.; Paolucci, F.; Prodi, L. *Faraday Discuss.* **2015**, *185*, 1.
10. Stewart, A. J.; Hendry, J.; Dennany, L. *Anal. Chem.* **2015**, *87*, 11847.
11. De Poulpiquet, A.; Diez-Buitrago, B.; Dumont Milutinovic, M.; Sentic, M.; Arbault, S.; Bouffier, L.; Kuhn, A.; Sojic, N. *Anal. Chem.* **2016**, *88*, 6585.
12. Yuan, Y.; Han, S.; Hu, L.; Parveen, S.; Xu, G. *Electrochim. Acta* **2012**, *82*, 484.
13. Kebede, N.; Francis, P. S.; Barbante, G. J.; Hogan, C. F. *Analyst* **2015**, *140*, 7142.

14. Li, P.; Jin, Z.; Zhao, M.; Xu, Y.; Guo, Y.; Xiao, D. *Dalton Trans.* **2015**, *44*, 2208.
15. Bolleta, F.; Ciano, M.; Balzani, V.; Serpone, N. *Inorganica Chim. Acta* **1982**, *62*, 207.
16. White, H. S.; Bard, A. J. *J. Am. Chem. Soc.* **1982**, *104*, 6891.
17. Ege, D.; Becker, W. G.; Bard, a J. *Anal. Chem.* **1984**, *56*, 2413.
18. Memming, R. *J. Electrochem. Soc.* **1969**, *116*, 785.
19. Reshetnyak, O. V; Koval, E. P. *Electrochem. commun.* **1998**, *43*, 465.
20. Zhao, M.; Zhuo, Y.; Chai, Y. Q.; Yuan, R. *Biomaterials* **2015**, *52*, 476.
21. Wu, L.; Wang, J.; Ren, J.; Li, W.; Qu, X. *Chem. Commun. (Camb).* **2013**, *49*, 5675.
22. Liang, J.; Yang, S.; Luo, S.; Liu, C.; Tang, Y. *Microchim. Acta* **2014**, *181*, 759.
23. Hesari, M.; Workentin, M. S.; Ding, Z. *ACS Nano* **2014**, *8*, 8543.
24. Wang, T.; Wang, D.; Padelford, J. W.; Jiang, J.; Wang, G. *J. Am. Chem. Soc.* **2016**, *138*, 6380.
25. Yuan, D.; Chen, S.; Yuan, R.; Zhang, J.; Zhang, W. *Analyst* **2013**, *138*, 6001.
26. Zhang, F.; Mao, L.; Zhu, M. *Microchim. Acta* **2014**, *181*, 1285.
27. Cheng, Y.; Lei, J.; Chen, Y.; Ju, H. *Biosens. Bioelectron.* **2014**, *51*, 431.
28. Sun, H.; Ma, S.; Li, Y.; Qi, H.; Ning, X.; Zheng, J. *Biosens. Bioelectron.* **2016**, *79*, 92.
29. Khamis, D.; Mahé, E.; Dardoize, F.; Devilliers, D. *J. Appl. Electrochem.* **2010**, *40*, 1829.
30. Hippauf, F.; Dorfler, S.; Zedlitz, R.; Vater, A.; Kaskel, S. *Electrochim. Acta* **2014**, *147*, 589.
31. Provent, C.; Haenni, W.; Santoli, E.; Rychen, P. *Electrochim. Acta* **2004**, *49*, 3737.
32. Honda, K.; Noda, T.; Yoshimura, M.; Nakagawa, K.; Fujishima, A. *J. Phys. Chem. B* **2004**, *108*, 16117.
33. Sentic, M.; Virgilio, F.; Zanut, A.; Manojlovic, D.; Arbault, S.; Tormen, M.; Sojic, N.; Ugo, P. *Anal. Bioanal. Chem.* **2016**, *408*, 7085.
34. Garcia-Segura, S.; Centellas, F.; Brillas, E. *J. Phys. Chem. C* **2012**, *116*, 15500.
35. Irkham; Watanabe, T.; Fiorani, A.; Valenti, G.; Paolucci, F.; Einaga, Y. *J. Am. Chem. Soc.* **2016**, *138*, 15636.
36. Watanabe, T.; Honda, Y.; Kanda, K.; Einaga, Y. *Phys. Status Solidi Appl. Mater. Sci.* **2014**, *211*, 2709.
37. Kapałka, A.; Fóti, G.; Comninellis, C. *Electrochim. Acta* **2007**, *53*, 1954.
38. Tokel, N. E.; Bard, A. J. *J. Am. Chem. Soc.* **1972**, *94*, 2862.
39. Fiaccabrino, G. C.; Koudelka-Hep, M.; Hsueh, Y. T.; Collins, S. D.; Smith, R. L. *Anal. Chem.* **1998**, *70*, 4157.
40. Serrano, K.; Michaud, P. a.; Comninellis, C.; Savall, a. *Electrochim. Acta* **2002**, *48*, 431.

41. White, H. S.; Becker, W. G.; Bard, A. J. *J. Phys. Chem.* **1984**, *88*, 1840.
42. Lewandowska-Andralojc, A.; Polyansky, D. E. *J. Phys. Chem. A* **2013**, *117*, 10311.
43. http://www.neocoat.ch (accessed June 28, 2016).

Chapter 3

Electrogenerated Chemiluminescence by the in Situ Generation of H_2O_2 in Na_2CO_3 Aqueous Solution at Boron-Doped Diamond Electrodes.

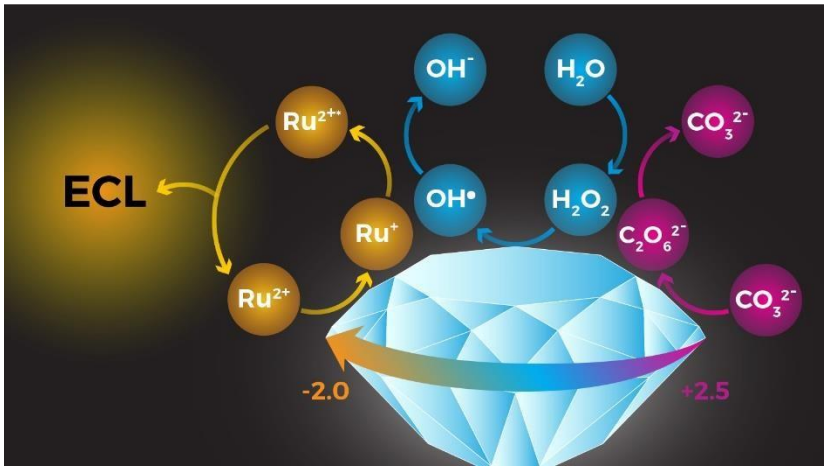

Reprinted (adapted) with permission from Irkham; Fiorani, A.; Kamoshida, N.; Valenti, G.; Paolucci, F.; Einaga,Y. *J. Am. Chem. Soc.* in press (2020). (DOI: 10.1021/jacs.9b11842) Copyright © 2019 American Chemical Society.

1. Introduction

Sensors and biosensors take enormous advantage of electrochemical methods,[1,2] of which electrogenerated chemiluminescence (ECL) is a leading transduction technique, which is used in clinical diagnostics,[3] and is prominent in point-of-care testing.[4] Thanks to the combination of electrochemical stimulus and luminescent response, ECL showed *(i)* the best signal to noise ratio, theoretically without any background emission, with a detection limit typically in the range of pM; *(ii)* broad dynamic range of more than six order of magnitude, *(iii)* rapid measurement (i.e., few seconds), and *(iv)* small working volume for analysis (tenth of a μl).

In chapter 2, we reported a new ECL system, the $Ru(bpy)_3^{2+}/SO_4^{2-}$ system, achieved only at BDD electrode, where peroxydisulfate for the ECL reaction is electrogenerated by oxidation of the unreactive sulfate precursor.[5,6] Since the oxidation of sulfate occurs at high overpotential (E^0 = 2.01 V vs SHE,[7] 2.52-3.08 V vs NHE[8]), the generation of ECL is possible only thanks to the wide potential window of BDD, combined with the electro-oxidation of SO_4^{2-}.[9] Other reactive compounds are also known to be generated using BDD electrodes, such as hydrogen peroxide from hydroxyl oxidation[10–12] (E^0 = 1.77-1.91 V vs SHE),[13–15] which is also a coreactant for ECL.[16,17] Although BDD is able to electrogenerate hydrogen peroxide by oxygen reduction, efficient production requires an acidic pH[9,11,12,18] that might enhance the hydrogen evolution process at cathodic currents, and consequently affect the ECL reductive-oxidation mechanism.

On the other hand, hydrogen peroxide can be conveniently prepared by electro-oxidation of carbonate in aqueous solution ($E^0\ CO_3^{2-/\bullet-}$ = 1.59 V at pH 12 vs NHE)[19–21] at a BDD electrode.[22–25] The electrogeneration mechanism includes the formation of peroxydicarbonate ($C_2O_6^{2-}$), mediated by $OH^\bullet$, which reacts with water to form hydrogen peroxide and carbonate (CO_3^{2-}).

Here, we report on a coreactant free $Ru(bpy)_3^{2+}/CO_3^{2-}$ ECL system that proceeds by the in-situ production of hydrogen peroxide at BDD electrode via carbonate oxidation and subsequent peroxydicarbonate hydrolysis, giving the overall ECL reaction depicted in Figure 3.1.[26]

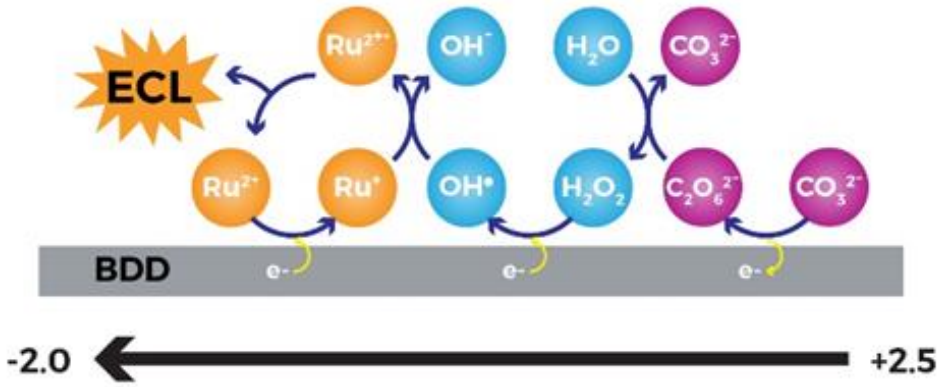

Figure 3.1. ECL scheme of the proposed reaction mechanism for the $Ru(bpy)_3^{2+}/CO_3^{2-}$ system at a BDD electrode. The colors describe the electrochemical reactions on carbonate (pink), the H_2O_2 coreactant (blue), and the ruthenium luminophore (orange). Ru = $Ru(bpy)_3$. Adopted from *ref 26* Copyright 2019 American Chemical Society.

2. Experimental

Materials. All the reagents were obtained commercially and used without further purification. $Ru(bpy)_6Cl_2•6H_2O$ was purchased from TCI (Japan), $HClO_4$, $NaClO_4$, Na_2CO_3, H_2O_2 from Fuji Film (Japan), and $Na_2CO_3•1.5H_2O_2$ from Sigma-Aldrich. D_2O (99.9%) was obtained from Cambridge Isotope Laboratories, Inc. Acetone (TCI) and trimethoxyborane (TCI) were used in the preparation of the BDD. Double distilled water (18.2 MΩ at 25°C) was obtained from a Simply-Lab water system (DIRECT-Q3 UV, Millipore).

Preparation of the BDD Electrodes. BDD films were deposited on silicon (111) wafers (Shinwa Tsusho) using a microwave plasma-assisted chemical vapour deposition (MPCVD) system (CORNES Technologies/ASTeX-5400). Acetone and trimethoxyborane were used as the carbon and boron sources, respectively, with an atomic ratio of B/C ≈ 1% ([B] in BDD ≈ $2 \times 10^{21}/cm^3$). The surface morphology of the BDD was examined with a field emission scanning electron microscope (SEM, JEOL JCM-6000). Raman spectra were recorded with

an Acton SP2500 (Princeton Instruments) with excitation wavelength of 532 nm from a green laser diode at room temperature (Figure 2.2).

Electrochemical Measurements and ECL. All electrochemical measurements were conducted with a potentiostat (PGSTAT302N, Metrohm) using a single-compartment three-electrode Teflon cell with 1% BDD, Pt or GC as the working electrode, a Pt spiral as the counter electrode and an Ag/AgCl (saturated KCl) electrode as the reference electrode. The working electrode area was 0.635 cm^2. The ECL signal was measured with a photomultiplier tube (PMT, Hamamatsu R928) placed at a fixed height from the electrochemical cell, inside a dark box. A high voltage power supply socket assembly with a transimpedance amplifier (Hamamatsu C6271) was used to supply 500 V to the PMT, using an external trigger connection to the potentiostat DAC module. Light/current/voltage curves were recorded by collecting the amplified PMT output signal with the ADC module of the potentiostat. ECL spectra were collected by a SEC2000 Spectra system UV-visible spectrophotometer (ALS Co., JP). Prior to each measurement, the BDD surface was pretreated to guarantee reproducibility, with cathodic reduction at -3.5 V followed by anodic oxidation at +3.5 V (total fixed charge of 0.1 C in each step) in 0.1 M $NaClO_4$ solution. The GC (Tokai Carbon, Japan) and Pt (Nilaco Co., Japan) electrodes were cleaned with a 0.5 μm alumina suspension on cloth tape, then sonicated in double distilled water for 5 min (2 times) and dried with a nitrogen stream. All experiments were carried out at room temperature.

3. Results and discussion

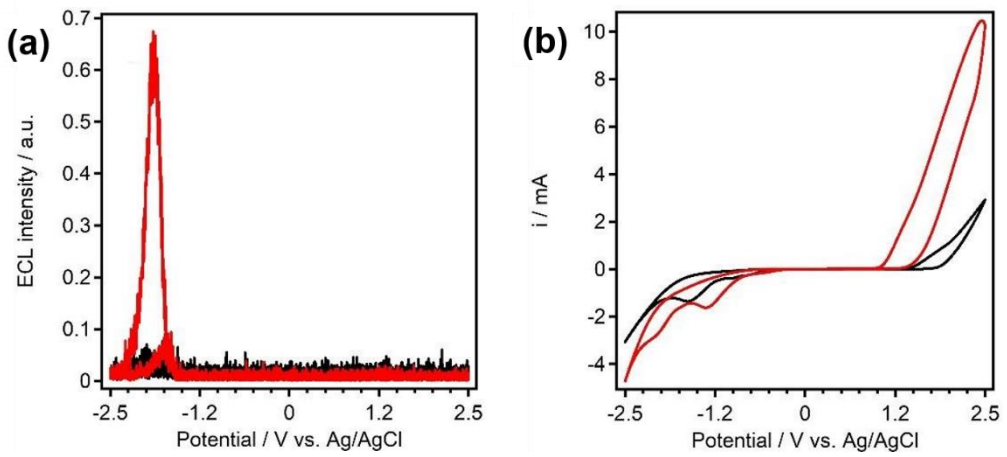

Figure 3.2. (a) ECL and (b) CV comparison between 100 mM Na_2CO_3 (red) and 100 mM $NaClO_4$ (black) measurement of 10 µM $Ru(bpy)_3Cl_2$ in aqueous solution. Potential was first swept to 2.5 V then -2.5 V with scan rate 100 mV/s. Adopted from *ref 26* Copyright 2019 American Chemical Society.

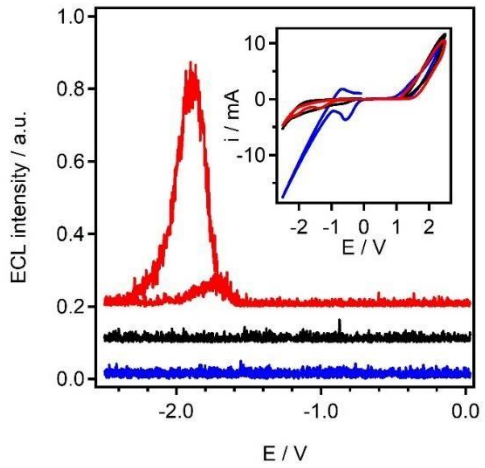

Figure 3.3. Cyclic voltammetry - ECL (curves shifted for clarity) and current (inset) of 10 µM $Ru(bpy)_3Cl_2$ in 100 mM Na_2CO_3 aqueous solution with BDD (red), GC (black), and Pt (blue) electrodes. Potential was first swept to 2.5 V then -2.5 V. Scan rate was 100 mV/s. Adopted from *ref 26* Copyright 2019 American Chemical Society.

The electrochemical and the ECL properties of $Ru(bpy)_3^{2+}$ in Na_2CO_3 aqueous solution at a BDD electrode were first investigated by cyclic voltammetry (CV). The CV was conducted by first scanning the potential from 0 V to 2.5 V followed by scanning to a negative potential up to -2.5 V. Figure 3.2a (red line) shows that a high ECL signal was observed during the CV starting from -1.5 V reaching a peak at around -1.9 V. This ECL emission is due to a combination of the unique properties of BDD, which combine an efficient generation of peroxydicarbonate, and a high overpotential for the hydrogen evolution reaction, allowing ECL to be obtained through reductive-oxidation mechanism. ECL emission was observed only with the carbonate solution, while no significant signal was observed with the $NaClO_4$ solution (Figure 3.2a, black) (see discussion for further details about the background signal). The same experiment conducted with conventional electrode materials such as GC and platinum (Pt) could not generate any ECL signal (Figure 3.3), although carbonate can be oxidized at Pt electrodes,[27] and GC electrodes (Figure 3.3, inset), the higher current for the hydrogen evolution reaction prevents the generation of ECL The first positive scan generated the peroxydicarbonate from the oxidation of carbonate, which further reacts with water to produce hydrogen peroxide according to the following mechanism:[27,28]

$$CO_3^{2-} \rightarrow CO_3^{\bullet -} + e^- \quad (1)$$

$$2CO_3^{\bullet -} \rightarrow C_2O_6^{2-} \quad (2)$$

$$C_2O_6^{2-} + 2H_2O \rightarrow H_2O_2 + 2HCO_3^- \quad (3)$$

Peroxydicarbonate hydrolysis was confirmed with a rotating ring-disk electrode where the current for H_2O_2 oxidation was simultaneously measured during oxidation of the carbonate.[26] At a BDD electrode, the oxidation of the carbonate is mediated by $OH^{\bullet}$ generated from hydroxide oxidation:[10,29]

$$BDD + OH^- \rightarrow BDD(OH^{\bullet}) + e^- \quad (4)$$

Therefore, we can write the overall equation for the oxidation of the carbonate as:[23-25,30]

$$2BDD(OH^{\bullet}) + 2CO_3^{2-} \rightarrow 2BDD + C_2O_6^{2-} + 2OH^- \quad (5)$$

where BDD represents the active site on the electrode surface.

The CV in Na_2CO_3 (Figure 3.2b, red line) shows a significantly higher anodic current compared to that in $NaClO_4$ (Figure 3.2b, black line), confirming the oxidation process of the carbonate. For both electrolytes, an onset oxidation potential of 1.1 V was observed, with a peak at 1.3 V in $NaClO_4$ solution. This was previously reported to be the oxidation of hydroxide ions at a BDD electrode (eq. 4),[31,32] which mediates the oxidation of CO_3^{2-} (eq. 5). The second scan, toward negative potentials, generated the ECL with the H_2O_2 produced from the EC oxidation mechanism of the carbonate, with the following likely mechanism, as proposed by Choi and Bard for the $Ru(bpy)_3^{2+}/H_2O_2$ system:[33]

$$H_2O_2 + e^- \rightarrow OH^{\bullet} + OH^- \quad (6)$$

$$Ru(bpy)_3^{2+} + e^- \rightarrow Ru(bpy)_3^{+} \quad (7)$$

$$Ru(bpy)_3^{+} + OH^{\bullet} \rightarrow Ru(bpy)_3^{2+*} + OH^- \quad (8)$$

$$Ru(bpy)_3^{2+*} \rightarrow Ru(bpy)_3^{2+} + h\nu \quad (9)$$

The ECL emission is obtained after both H_2O_2 (eq. 6) and $Ru(bpy)_3^{2+}$ (eq. 7, E^0 = -1.48 V vs Ag/AgCl) are reduced, followed by homogeneous electron transfer (eq. 8), which leads to the emission of light (eq. 9). In the cathodic scan, the reduction peaks at ≈ -0.8 V are from sp^2-carbon impurities on the BDD surface. The second peak at ≈ -1.5 V for the $NaClO_4$ solution is oxygen reduction,[30,34,35] since it can be easily removed after nitrogen bubbling. The cathodic scan for Na_2CO_3 shows a peak starting at ≈ -1.5 V, at the same potential as ECL, likely to be oxygen and peroxydicarbonate reduction. The ECL spectrum confirms the emission from $Ru(bpy)_3^{2+}$* (Figure 3.4), with a peak emission wavelength at ≈ 620 nm. Without $Ru(bpy)_3^{2+}$, no ECL signal was obtained (Figure 3.5). Furthermore, the ECL emission was triggered by hydrogen peroxide produced in the first positive scan, via

the EC mechanism of electrogenerated peroxydicarbonate, and not from hydroxyl radicals produced by hydroxide oxidation[36] (eq. 4) or H_2O_2 from the recombination of hydroxyl radicals,[11] because only slightly detectable ECL signal was observed in the $NaClO_4$ solution (Figure 3.2a, black line).

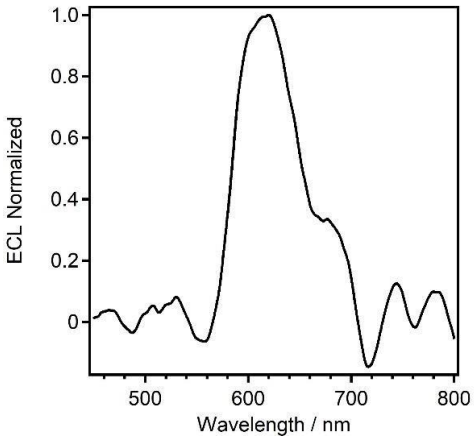

Figure 3.4. Normalized ECL spectra of 10 μM $Ru(bpy)_3Cl_2$ and 100 mM Na_2CO_3 system in aqueous solution collected by using two steps chronoamperometry: E_1 = 2.5 V, t_1 = 1 s; E_2 = -2.0 V; t_2 = 30 s. Adopted from *ref 26* Copyright 2019 American Chemical Society.

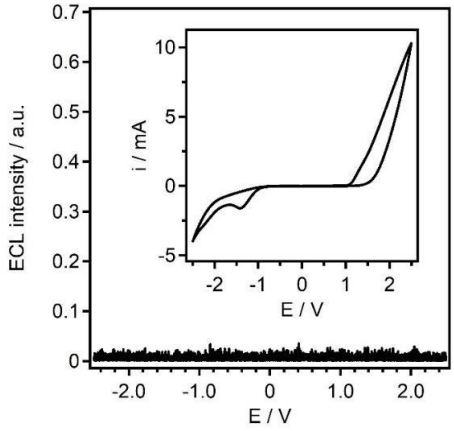

Figure 3.5. ECL of 100 mM Na_2CO_3 aqueous solution, without $Ru(bpy)_3Cl_2$, at BDD electrode by using cyclic voltammetry with potential range from 2.5 V to -2.5 V, starting at 0 V. Scan rate was 100 mV/s. Adopted from *ref 26* Copyright 2019 American Chemical Society.

In line with this hypothesis, no ECL was observed when the first positive scan was swept to a value insufficient to generate peroxydicarbonate (Figure 3.6), although in this case, a weak ECL signal could be observed. This signal is likely to have originated from the annihilation reaction mechanism between oxidized $Ru(bpy)^{2+}$, electrogenerated at $E^0 = 1.07$ V (vs Ag/AgCl), and the reduced $Ru(bpy)^{2+}$, as follows[37]:

$$Ru(bpy)_3^{3+} + Ru(bpy)_3^{+} \rightarrow Ru(bpy)_3^{2+*} + Ru(bpy)_3^{2+} \qquad (10)$$

Moreover, the background emission in the $NaClO_4$ solution (Figure 3.2a, black line) can be ascribed to this mechanism.

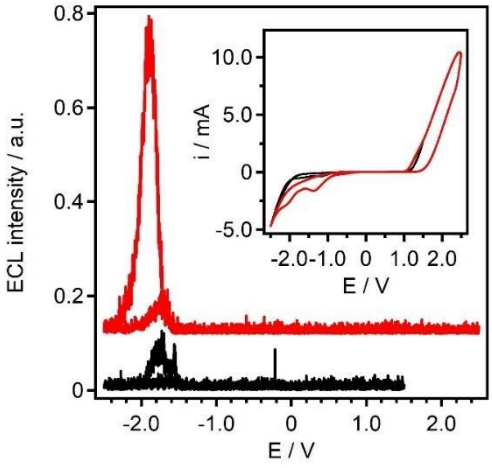

Figure 3.6. ECL intensity of 10 µM $Ru(bpy)_3Cl_2$ in 100 mM Na_2CO_3 aqueous solution at BDD electrode by using cyclic voltammetry with different potential range: 2.5 V to -2.5 V (red) and 1.5 V to -2.5 V (black), starting from 0 V. Scan rate was 100 mV/s. ECL signal was shifted for clarity. Inset: corresponding cyclic voltammograms. Adopted from *ref 26* Copyright 2019 American Chemical Society.

In order to support the hypothesis of the ECL mechanism with H_2O_2, we carried out experiments comparing carbonate solution with percarbonate ($Na_2CO_3 \cdot 1.5H_2O_2$), and hydrogen peroxide solutions (Figure 3.7). The two solutions contained the same amount of

hydrogen peroxide at a concentration of 10 mM and the CVs were directly swept from 0 V to -2.5 V. The ECL signals appear to be similar in all three systems, therefore supporting the hypothesis that hydrogen peroxide is the coreactant in the $Ru(bpy)_3^{2+}/CO_3^{2-}$ system, as outlined in the reaction sequence given in eqs. 6-9.

To gain an insight into the ECL emission mechanism of the present system, the effect of the oxidation potential was investigated using two-potential step chronoamperometry (CA). In the first step, an oxidation potential is applied for a fixed time (1s), while in the second step a potential of -2.0 V triggers the ECL reaction (Figure 3.9). The ECL signal in the second step was integrated to quantify the emission as a function of the oxidation potential of the first step (Figure 3.9, inset). The ECL emission was found to increase linearly from 1.8 V to 2.5 V, which indicates an increase in hydrogen peroxide from the electrogenerated peroxydicarbonate. The weak ECL emission at 1.5 V was assumed to be due to the annihilation reaction of $Ru(bpy)^{2+}$ (eq. 10). The present ECL system can work at a potential of 1.8 V, which is 500 mV lower than that with our previously reported $Ru(bpy)_3^{2+}/SO_4^{2-}$ system in Chapter 2 (Figure 3.10, 3.11).

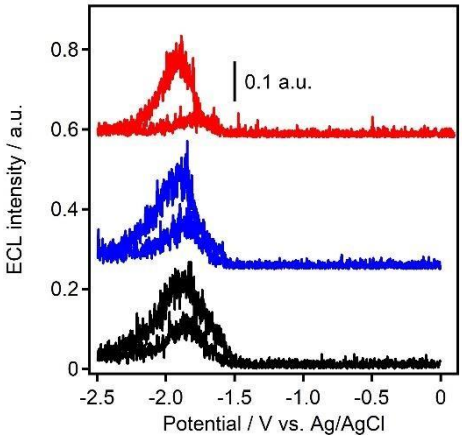

Figure 3.7. 10 µM $Ru(bpy)_3Cl_2$ ECL emission comparison between 10 mM H_2O_2 (blue) and 6.7 mM $Na_2CO_3.1.5H_2O_2$ (black) in pH 7 PBS with potential scanned to -2.0 V (blue) with potential scanned to -2.0 V, and 25 mM Na_2CO_3 with potential first scanned to 2.5 V then -2.0 V (red). Scan rate was 100 mV/s. Signal was shifted for clarity. Adopted from *ref 29* Copyright 2019 American Chemical Society.

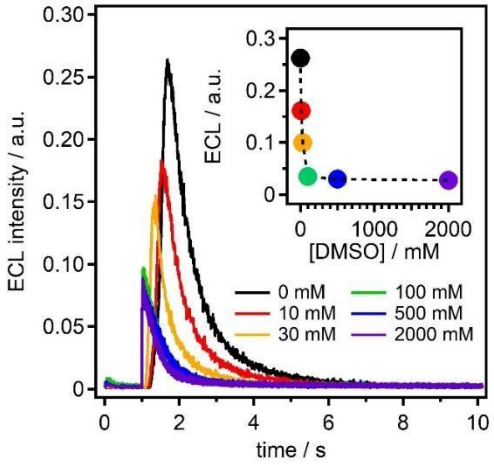

Figure 3.8. ECL intensity of 10 µM $Ru(bpy)_3Cl_2$ in 100 mM Na_2CO_3 aqueous solution at BDD electrode by using two steps chronoamperometry with increasing concentration of DMSO. E_1 = 2.5 V, t_1 = 1 s; E_2 = -2.0 V, t_2 = 30 s. Inset: integrated ECL intensity for 6 s as function of DMSO concentration. Adopted from *ref 26* Copyright 2019 American Chemical Society.

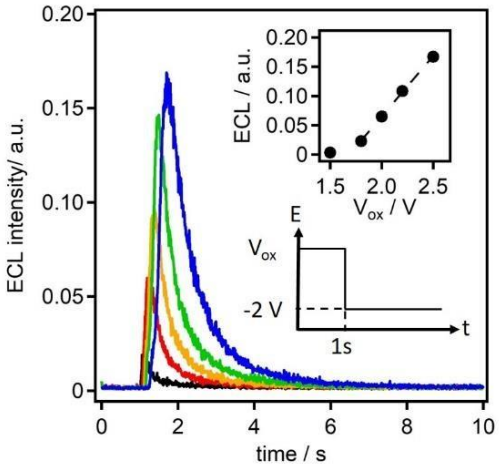

Figure 3.9. ECL intensity by CA for 100 mM Na_2CO_3 and 10 µM $Ru(bpy)_3Cl_2$ with first oxidation step from 0 V to 1.5 V (black), 1.8 V (red), 2.0 V (orange), 2.2 V (green), and 2.5 V (blue) for 1s, followed by step to -2.0 V. Inset: (top) plot of integrated ECL value as a function of oxidation potential; (bottom) potential program used in the chronoamperometry. Adopted from *ref 26* Copyright 2019 American Chemical Society.

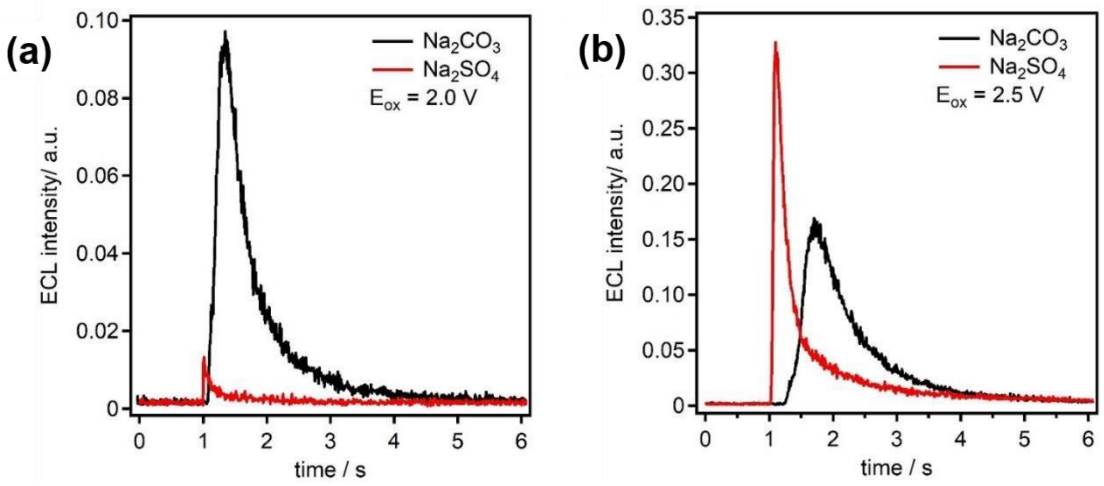

Figure 3.10. ECL intensity of 10 µM $Ru(bpy)_3Cl_2$ in 100 mM Na_2CO_3 (black) and 100 mM Na_2SO_4 (red) aqueous solutions at BDD electrode by using two steps chronoamperometry: (a) E_1 = 2.0 V and (b) E_1 = 2.5 V, t_1 = 1 s; E_2 = -2.0 V, t_2 = 30 s. Adopted from *ref 26* Copyright 2019 American Chemical Society.

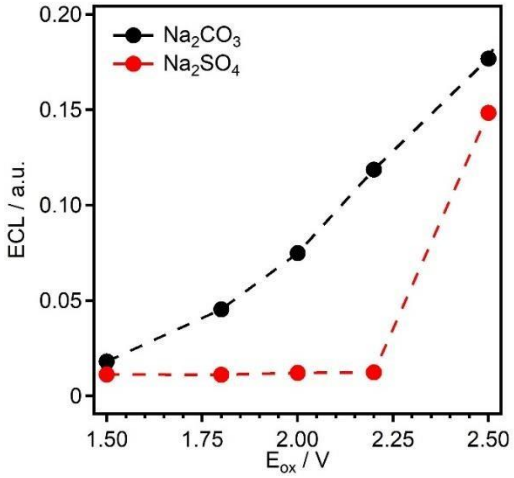

Figure 3.11. 6s of Integrated ECL of 10 µM $Ru(bpy)_3Cl_2$ and 100 mM Na_2CO_3 (black) and 100 mM Na_2SO_4 (red) at different oxidation potential by using two steps chronoamperometry: E_1 = E_{ox} V, t_{ox} = 1 s; E_2 = -2.0 V, t_2 = 30 s. Adopted from *ref 26* Copyright 2019 American Chemical Society.

Furthermore, the influence of the oxidation time (t_{ox}) on the system was also investigated by CA to find the highest ECL emission. The current measured at a potential of 2.5 V during the first step in the presence of carbonate was integrated and found to increase linearly with the square root of oxidation time (Figure 3.12a), suggesting that the oxidation process was controlled by carbonate diffusion,[40] with increasing amounts of peroxydicarbonate, therefore hydrogen peroxide. On the other hand, the integrated ECL emission showed an increase up to 5 s, then nearly stable emission up to 20 s (Figure 3.12b). The ECL is highly affected by the gradient of the coreactant in the diffusion layer, which gives a lower peak intensity and broader emission. In fact, the diffusion layer thickness for carbonate with 1 to 20 s oxidation times ranges roughly from 100 to 600 µm.[41,42]

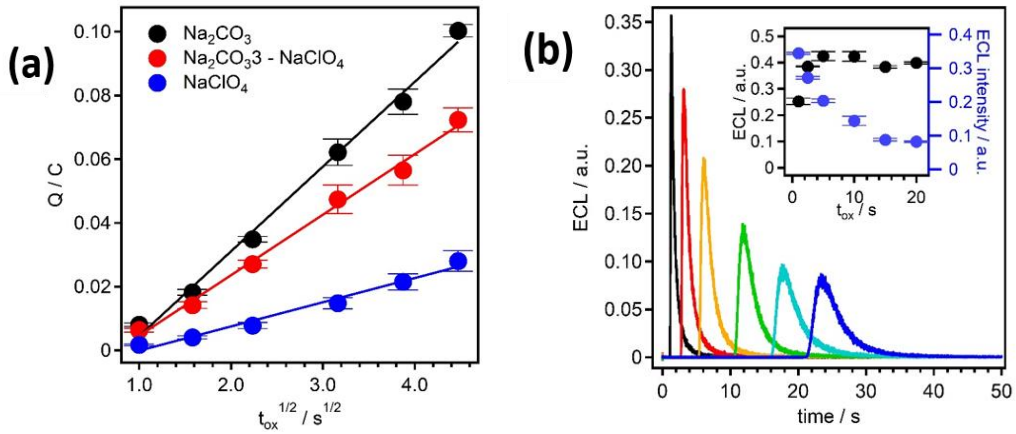

Figure 3.12. (a) Integrated charge at 2.5 V for different oxidation times for 10 µM $Ru(bpy)_3Cl_2$ in 100 mM Na_2CO_3 (black), 100 mM $NaClO_4$ (blue), and the difference (red). (b) ECL intensity by chronoamperometry: E_1 = 2.5 V, t_{ox} = 1s (black), 2.5s (red), 5s (orange), 10s (green), 15s (sky blue), and 20s (blue); E_2 = -2.0 V, t_2 = 30 s. Inset: plot of integrated ECL (black), and ECL intensity peak (blue) as a function of oxidation time. Adopted from *ref 26* Copyright 2019 American Chemical Society.

The effect of pH on the ECL signal was investigated using CV measurements from pH 11.5, the pH of the starting Na_2CO_3 solution, to pH 4 (Figure 3.13). The oxidation current, ascribed to CO_3^{2-}, was found to decrease with decreasing pH, suggesting less

peroxydicarbonate, and thus less H_2O_2, was generated. This might be the effect of pH on the equilibrium of the carbonate species, with the following reactions:

$CO_3^{2-} + H_2O \rightleftharpoons HCO_3^- + OH^-$ pKa = 10.33 (11)

$HCO_3^- + H_2O \rightleftharpoons H_2CO_3 + OH^-$ pKa = 6.35 (12)

$H_2CO_3 \rightleftharpoons CO_{2(aq)} + H_2O$ (13)

$CO_{2(aq)} \rightleftharpoons CO_{2(g)}$ (14)

In the neutral region, the concentration of carbonate is less dominant compared to the bicarbonate, and as the current decreases in the oxidation scan, we can infer that it is the carbonate ions that is oxidized rather than hydrogenated species such as bicarbonate or carbonic acid. However, the ECL signal increases as the pH decreases from 11.5, reaching a maximum at pH 7, while a further decrease down to pH 4 almost suppresses the ECL completely. In this case, the stability of the hydrogen peroxide generated in the solution seems to be the main factor for the ECL emission, since hydrogen peroxide is more stable when the pH is neutral or acidic.[43–45] Moreover, carbonate can promote the decomposition of hydrogen peroxide.[46] In conclusion, the ECL emission peak at pH 7 is due to two trends, (i.e., the decreasing CO_3^{2-} oxidation current and the increasing $OH^{\bullet}$ stability). Hydrogen evolution at pH 4 can hardly be the reason for the decrease in ECL, since we have already demonstrated that this pH does not affect the ECL emission at BDD electrode.[5]

The ECL emission as a function of Na_2CO_3 concentration was investigated from 25 mM to 1000 mM using CA (Figure 3.14). In the present system, the ECL signal is stable and it was found to be linear within the range of 25 mM to 200 mM and reaches a plateau at 500 mM Na_2CO_3. The decrease at 1 M Na_2CO_3 can be explained by the possibility of hydrogen peroxide quenching the $Ru(bpy)_3^{2+}$*, since it can be seen that the carbonate oxidation charge (Figure 3.14b) increased with carbonate concentration, suggesting that hydrogen peroxide is also increasing. This phenomena has previously been reported by Choi and Bard[33] with the maximum ECL emission achieved at 1 mM of H_2O_2 in 100 µM $Ru(bpy)_3Cl_2$ in a pH 7.5 phosphate buffer, with a quenching rate constant of 5.7×10^6 M^{-1} s^{-1}.

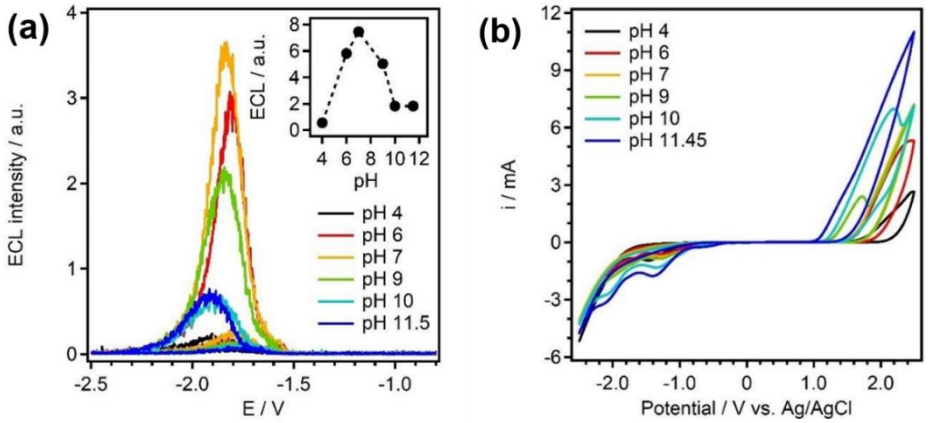

Figure 3.13. (a) ECL intensity and (b) current by CV for 100 mM Na_2CO_3 and 10 µM $Ru(bpy)_3Cl_2$ with pH of 4 (black), 6 (red), 7 (orange), 9 (green), 10 (light blue) and 11.5 (blue). Potential was first swept to 2.5 V then -2.5 V with scan rate 100 mV/s. Inset: Plot of integrated ECL value as a function of ph. Adopted from *ref 26* Copyright 2019 American Chemical Society.

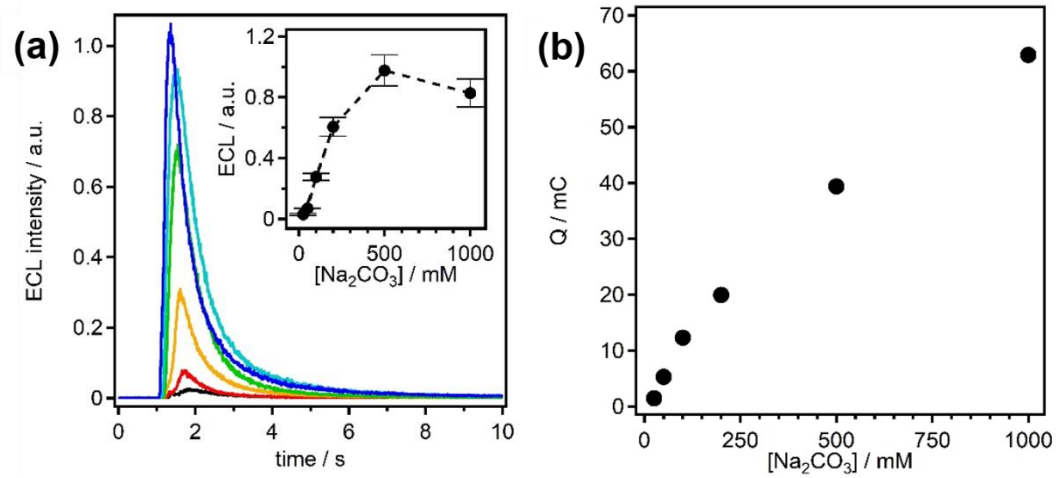

Figure 3.14. (a) ECL intensity of 10 µM $Ru(bpy)_3Cl_2$ in 5 mM (black), 50 mM (red), 100 mM (orange), 200 mM (green), 500 mM (light blue), 1000 mM (blue) Na_2CO_3 solution with first step of 2.5 V for 1s followed by a step to -2.0 V for 30s. Inset: integrated ECL as function of initial Na_2CO_3 concentration. (b) Integrated anodic charge as a function of Na_2CO_3 concentration. Adopted from *ref 26* Copyright 2019 American Chemical Society.

Finally, we considered the energy needed to form $Ru(bpy)_3^{2+}$*. The Gibbs free energy for formation of the excited state, ΔG_{es}, can be written as:[47]

$$\Delta G_{es}\,(eV) \approx E^{0\prime}(Ru(bpy)^{2+/+}) - E^{0\prime}(OH^{\bullet}/OH^{-}) + E_{es}(Ru(bpy)_3^{2+}*)$$

where E_{es} is the energy of the excited state of $Ru(bpy)_3^{2+}$* (2.12 eV).[32] $E^{0\prime}(Ru(bpy)^{2+/+}$ is −1.28 V (vs SHE), while $E^{0\prime}(OH^{\bullet}/OH^{-})$ is 1.77 - 1.91 V (vs SHE)[13-15], therefore the ΔG_{es} is −0.93/1.07 eV, enough to populate the excited states of $Ru(bpy)_3^{2+}$.

4. Conclusion

A *coreactant-free* ECL system using $Ru(bpy)_3^{2+}$ as the luminophore in aqueous solutions containing carbonate is reported. The underlying mechanism involves the oxidation of carbonate to peroxydicarbonate, which hydrolysis leads to the in-situ production of the coreactant, hydrogen peroxide. This ECL system was made possible only by using a BDD electrode, which has a wide potential window and promotes direct oxidation of hydroxide, allowing the mediated oxidation of carbonate, while at the same time suppressing hydrogen evolution at the cathodic currents where the ECL reaction takes place. The ECL emission was found to be dependent on the carbonate concentration, so can be applied to carbonate detection, while it can be controlled by several parameters such as the pH, the oxidation potential and time to tune the ECL intensity.

5. Reference

1. Ronkainen, N. J.; Halsall, H. B.; Heineman, W.R. *Chem. Soc. Rev.* **2010**, *39*, 1747.
2. Wang, Z.; Yu, R.; Zeng, H.; Wang, X.; Luo, S.; Li, W.; Luo, X.; Yang, T. *Microchim. Acta.* **2019**, *186*, 1.
3. Zanut, A.; Fiorani, A.; Rebeccani, S.; Kesarkar, S.; Valenti, G. *Anal. Bional. Chem.* **2019**, *411*, 4375.
4. Gao, W.; Saqib, M.; Qi, L.; Zhang, W.; Xu, G. *Curr. Opin. Electrochem.* **2017**, *3*, 4.
5. Fiorani, A.; Irkham; Valenti, G.; Paolucci, F.; Einaga, Y. *Anal. Chem.* **2018**, *90*, 15636.

6. Irkham; Watanabe, T.; Fiorani, A.; Valenti, G.; Paolucci, F.; Einaga, Y. *J. Am. Chem. Soc.* **2016**, *138*, 15636.
7. Memming, R. *J. Electrochem. Soc.* **1969**, *116*, 785.
8. Eberson, L. *Adv. Phys. Org. Chem.* **1982**, *18*, 79.
9. Michaud, P. A.; Mahé, E.; Haenni, W.; Perret, A.; Comninellis, C. *Electrochem. Solid-State Lett.* **2000**, *3*, 77.
10. Marselli, B.; Garcia-Gomez, J.; Michaud, P.-A.; Rodrigo, M. A.; Comninellis, C. *J. Electrochem. Soc.* **2003**, *150*, 79.
11. Thostenson, J. O.; Ngaboyamahina, E.; Sellgren, K. L.; Hawkins, B. T.; Piascik, J. R.; Klem, E. J. D.; Parker, C. B.; Deshusses, M. A.; Stoner, B. R.; Glass, J. T. *ACS Appl. Mater. Interfaces* **2017**, *9*, 16610.
12. Katsuki, N. *J. Electrochem. Soc.* **1998**, *145*, 2358.
13. Koppenol, W. H.; Liebman, J. F. *J. Phys. Chem.* **1984**, *88*, 99.
14. Schwarz, H. A.; Dodson, R. W. *J. Phys. Chem.* **1984**, *88*, 3643.
15. Kläning, U. K.; Sehested, K.; Holcman, J. *J. Phys. Chem.* **1985**, *89*, 760.
16. Leca, B.; Blum, L. J. *Analyst* **2000**, *125*, 789.
17. Sakura, S. *Anal. Chim. Acta* **1992**, *262*, 49.
18. Martin, H. B. *J. Electrochem. Soc.* **1996**, *143*, 133.
19. Zuo, Z.; Cai, Z.; Katsumura, Y.; Chitose, N.; Muroya, Y. *Radiat. Phys. Chem.* **1999**, *55*, 15.
20. Bisby, R. H.; Johnson, S. A.; Parker, A. W.; Tavender, S. M. *J. Chem. Soc. Faraday Trans.* **1998**, *94*, 2069.
21. Huie, R. E.; Clifton, C. L.; Neta, P. *Radiat. Phys. Chem.* **1991**, *38*, 477.
22. Ruiz, E. J.; Ortega-Borges, R.; Jurado, J. L.; Chapman, T. W.; Meas, Y. *Electrochem. Solid-State Lett.* **2009**, *12*, 1.
23. Saha, M. S.; Furuta, T.; Nishiki, Y. *Electrochem. Commun.* **2004**, *6*, 201.
24. Velazquez-Peña, S., Sáez, C.; Cañizares, P.; Linares-Hernández, I.; Martínez-Miranda, V.; Barrera-Díaz, C.; Rodrigo, M. A. *Chem. Eng. J.* **2013**, *230*, 272.
25. Saha, M. S.; Furuta, T.; Nishiki, Y. *Electrochem. Solid-State Lett.* **2003**, *6*, 5.
26. Irkham; Fiorani, A.; Kamoshida, N.; Valenti, G.; Paolucci, F.; Einaga,Y. *J. Am. Chem. Soc.* **2019**, in press (2020). (DOI: 10.1021/jacs.9b11842)
27. Zhang, J.; Oloman, C. W. *J. Appl. Electrochem.* **2005**, *35*, 945.

28. Flanagan, J.; Jones, D. P.; Griffith, W. P.; Skapski, A. C.; West, A. P. *J. Chem. Soc. Commun.* **1986**, *1*, 20.
29. Michaud, P-A.; Panizza, M.; Outtara, L.; Diaco, T.; Foti, G.; Comninellis, C. *J. Appl. Electrochem.* **2003**, *33*, 151.
30. Macpherson, J. V. A *Phys. Chem. Chem. Phys.* **2015**, *17*, 2935.
31. Irkham; Watanabe, T.; Einaga, Y. *Anal. chem.* **2017**, *89*, 7139.
32. Irkham; Einaga, Y. *Analyst* **2019**, *144*, 4499.
33. Choi, J. P.; Bard, A. J. *Anal. Chim. Acta* **2005**, *541*, 143.
34. Mahé, É.; Bornoz, P.; Briot, E.; Chevalet, J.; Comninellis, C.; Deviliers, D. *Electrochim. Acta* **2013**, *102*, 259.
35. Watanabe, T.; Honda, Y.; Kanda, K.; Einaga, Y. *Phys. Status Solidi A* **2014**, *211*, 2709.
36. Kapałka, A.; Fóti, G.; Comninellis, C. *Electrochim. Acta* **2009**, ***254***, 2018.
37. Tokel, N. E.; Bard, A. J. *J. Am. Chem. Soc.* **1972**, *94*, 2862.
38. Garcia-Segura, S.; Centellas, F.; Brillas, E. *J. Phys. Chem. C* **2012**, *116*, 15500.
39. Bardouki, H.; Barcellos da Rosa, M.; Mihalopoulos, N.; Palm, W.-U.; Zetzsch, C. *Atmospheric Environ.* **2002**, *36*, 4627.
40. Bard, A. J.; Faulkner, L. R. *John Wiley & Sons, Inc.: New York*, **2001**; pp 210-216.
41. Bard, A. J.; Faulkner, L. R. *John Wiley & Sons, Inc.: New York*, **2001**; pp 34-35.
42. Zeebe, R. E. *Geochim. Cosmochim. Acta* **2011**, *75*, 2483.
43. Duke, F. R.; Haas, T. W. *J. Phys. Chem.* **1961**, *65*, 304.
44. Staehelin, J.; Holgné, J. **1982**, *16*, 676.
45. Hickel, B.; Corfitzen, H.; Sehested, K. *J. Phys. Chem.* **1996**, *100*, 17186.
46. Lee, H. H. B.; Park, A. H.; Oloman, C. W. *TAPPI J.* **2000**, *83*, 94.
47. Valenti, G.; Rampazzo, E.; Kesarkar, S.; Genovese, D.; Fiorani, A.; Zanut, A.; Palomba, F.; Marcaccio, M.; Paolucci, F.; Prodi, L. *Coord. Chem. Rev.* **2018**, *367*, 65.

Chapter 4

Electrogenerated Chemiluminescence of Luminol & in Situ H_2O_2 on Boron-Doped Diamond Electrode

1. Introduction

Luminol (5-amino-2,3-dihydro-1,4-phthalazinedione) is one of popular luminophore that has been widely used in ECL system at various electrode material such as platinum,[1] gold,[2] indium tin oxide,[3] and carbon-based material.[4,5] It has emission characteristic of light at λ_{max} = 425 nm derivate from excited state of 3-aminopthalte dianion in alkaline medium.[5-8] Although it could generate light emission by direct oxidation of its deprotonated state in alkaline solution,[7] usually the application of ECL luminol are coupled by reactive oxygen species (ROS), typically oxygen and hydrogen peroxide, which enhance the ECL emission via charge transfer reaction. This behavior makes luminol ECL system could be used as ROS detector,[9] or even bioanalytical application via indirect quantification of substrate whose enzymatically produces ROS.[10-12]

Boron-doped diamond (BDD) electrode also known for its ability to generate a ROS such as H_2O_2 from water, which could be used to fuel the luminol ECL system. Despite of that, efficient productions are usually carried in acidic environment, which is not the most suitable condition for generating ECL from luminol system. On the other hand, In Chapter 3 it was mentioned that a convenient source of hydrogen peroxide is peroxydicarbonate ($C_2O_6^{2-}$), a compound that are prepared by electro-oxidation of carbonate in aqueous solution ($E^0\ CO_3^{2-/\bullet-}$ = 1.59 V at pH 12 vs NHE)[13–15] and also easily obtained at a BDD electrode.[16-19] This peroxide is unstable and reacts with water to form hydrogen peroxide and carbonate. The generation of peroxydicarbonate occurred optimally at high pH, which make a perfect match for the luminol ECL system that also work best at alkaline solution.

Here, we report on a coreactant free luminol/CO_3^{2-} ECL system that proceeds by the in-situ production of H_2O_2 at BDD electrode via carbonate oxidation and subsequent peroxydicarbonate hydrolysis (Figure 4.1).

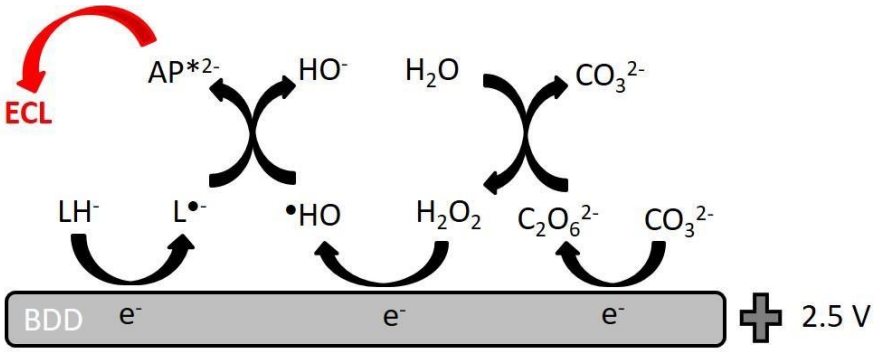

Figure 4.1. ECL scheme of the proposed reaction mechanism for the Luminol/CO_3^{2-} system at a BDD electrode. LH^- = deprotonated luminol, $L^{\bullet-}$ = luminol anion radical, AP^{2-}* = 3-aminopthalte excited state.

2. Experiment

Materials. All the reagents were obtained commercially and used without further purification. Luminol were purchased from TCI (Japan), while $HClO_4$, $NaClO_4$, Na_2CO_3, H_2O_2 from Fuji Film (Japan). For BDD preparation, acetone (TCI) and trimethoxyborane (TCI). Double distilled water (18.2 MΩ•cm at 25°C) was obtained from a Simply-Lab water system (DIRECT-Q3 UV, Millipore).

Preparation of BDD Electrodes. BDD films were deposited on silicon (111) wafers (Shinwa Tsusho) using a microwave plasma-assisted chemical vapor deposition (MPCVD) system (CORNES Technologies/ASTeX-5400). Acetone and trimethoxyborane were used as the carbon and boron sources, respectively, with an atomic ratio of B/C = 1% ([B] in BDD $\approx 2 \times 10^{21}/cm^3$).

Electrochemical Measurements and ECL. All electrochemical measurements were conducted with a potentiostat (PGSTAT302N, Metrohm) using a single-compartment threeelectrode teflon cell with an 1% BDD, a Pt spiral as counter electrodes and an Ag/AgCl (saturated KCl) as the reference electrode. The electrode area of was 0.635 cm^2. The ECL signal was measured with a photomultiplier tube (PMT, Hamamatsu R928) placed at a fixed height from the electrochemical cell, inside a dark box. A high voltage power supply socket assembly with a transimpedance amplifier (Hamamatsu C6271) was used to supply 500 V

to the PMT, using an external trigger connection to the potentiostat DAC module. Light/current/voltage curves were recorded by collecting the amplified PMT output signal with the ADC module of the potentiostat. ECL spectra was collected by a SEC2000 Spectra system UV-visible spectrophotometer (ALS Co., JP). Prior to each measurement, BDD surface was pretreated to guarantee reproducibility, with cathodic reduction at −3.5 V followed by anodic oxidation at +3.5 V (total fixed charge of 0.1 C each steps) in 0.1 M $NaClO_4$ solution. All experiments were carried at room temperature.

3. Results and discussion

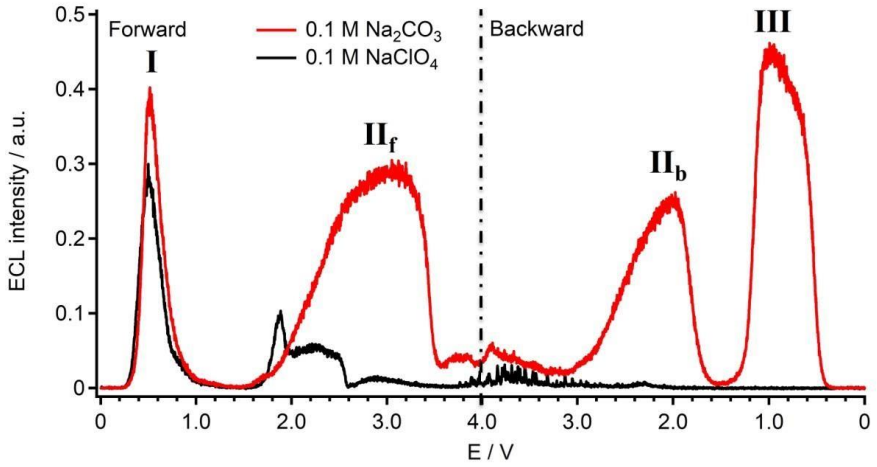

Figure 4.2. CV−ECL measurement of 100 µM luminol in 0.1 M Na_2CO_3 (red) and 0.1 M $NaClO_4$ (black) pH 12. The potential was scanned from 0 V to 4.0 V then back to 0 V with scan rate was 100 mV/s.

The ECL properties of 100 µM luminol in 0.1 M Na_2CO_3 were investigated using cyclic voltammetry (CV) measurement. Figure 4.2 Shows the forward and backward CV−ECL. The potential was scanned from 0 V 4.0 V to be able to observe all possible peak clearly. It can be seen that the system gives several peaks of ECL both in the forward and the backward scan (Figure 4.2, red line). First peak could be observed starting around 0.25 V and reach maximum at 0.52 V (Peak I). This peak is previously reported to be the direct

oxidation of luminol at the surface of the electrode in the alkaline solution (Scheme 4.1).[1,11] This was also supported by the fact that measurement in 0.1 M $NaClO_4$ solution (Figure 4.2, black line) also gives similar peak, meaning that the ECL is observed even without the presence of any oxidant.

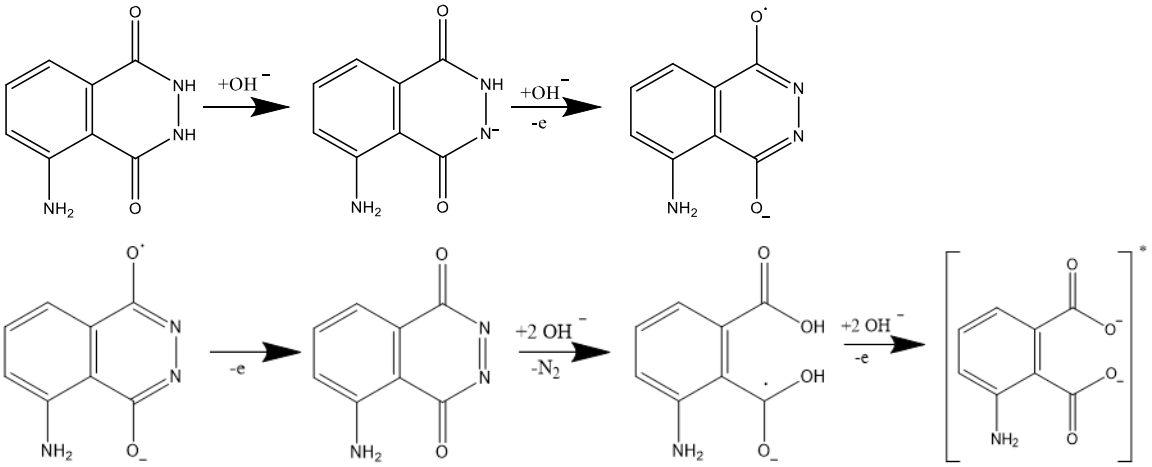

Scheme 4.1. Reaction mechanism proposed for Peak I.

Second peak was observed starting at around 1.5 V reaching a broad peak at 3.0 V (Peak II_f) and decrease with further increase of potential due to the water oxidation that was not only dominate the reaction at the electrode but also producing oxygen that blocking the ECL signal to the PMT. The high ECL emission in this region was able to be observed due to the unique ability of BDD to efficiently oxidize carbonate to generate hydrogen peroxide, which act as coreactant to the luminol with following reaction:[16-19]

$$BDD + OH^- \rightarrow BDD(OH^\bullet) + e^- \quad (1)$$

$$2BDD(OH^\bullet) + 2CO_3^{2-} \rightarrow 2BDD + C_2O_6^{2-} + 2OH^- \quad (2)$$

$$C_2O_6^{2-} + 2H_2O \rightarrow H_2O_2 + 2HCO_3^- \quad (3)$$

In pH 12, H_2O_2 would exist in both its conjugate base (HO_2^-) where both is electroactive species that will oxidize in the surface of the electrode producing oxygen via generation of superoxide with reaction as follows:

$$H_2O_2 + OH^- \rightarrow HO_2^- + H_2O \quad (4)$$

$$HO_2^- \rightarrow HO_2^{\bullet} + H^+ \quad (5)$$

$$HO_2^{\bullet} \rightarrow O_2^{\bullet -} + H^+ \quad (6)$$

The superoxide would then react with the oxidized luminol to form an excited state of 3-aminophtalate leading to the emission of light (Scheme 4.2). This mechanism was also assumed to be responsible for the ECL emission the peak observed at around 2.1 V at the backward scan (peak II_b).

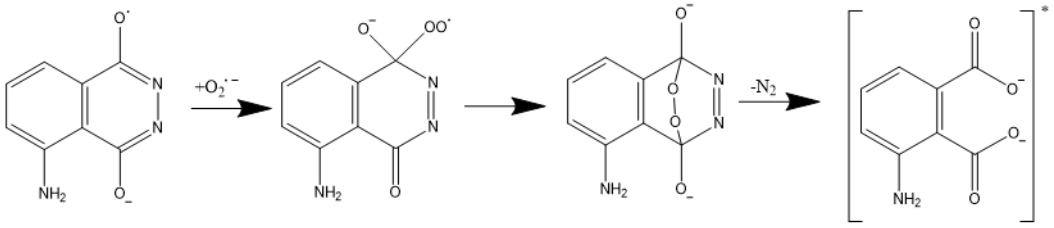

Scheme 4.2. Reaction mechanism proposed for Peak II starting from luminol radical.

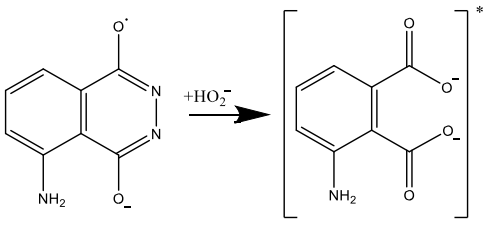

Scheme 4.3. Reaction mechanism proposed for Peak III starting from luminol radical.

The last peak at the backward scan was observed starting at around 1.5 V reaching peak at 0.9 V and completely chased at 0.3 V (Peak III). The ECL emission was increase again after the reaction at peak II_b finished, suggesting that the reaction responsible for this ECL emission was between the unoxidized H_2O_2 with luminol radical (Scheme 4.3). Notes that even in luminol/H_2O_2 (scanned up to 4.0V), this peak could only be observed in the presence of buffer in the solution (Figure 4.3). This could be explained due to the high positive potential scan lead to enormous oxygen evolution reaction (OER) to be occurred, where it releases proton as by product of the reaction in the surface of electrode. The proton would then protonate the luminol back to its neutral state, thus decreasing the ECL signal overall. Furthermore, the measurement with lower scan potential will give an increase to the peak III in luminol/H_2O_2 system, which further support the hypothesis that OER is affecting this peak (Figure 4.4). So, the ECL signal in present measurement could be observed due to the efficient generation of H_2O_2 coupled with the natural buffering capability from Na_2CO_3 solution.

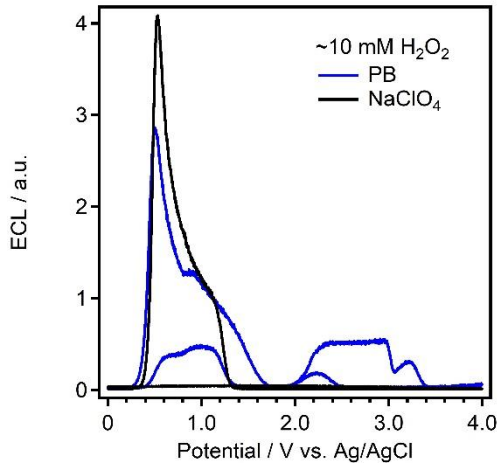

Figure 4.3. ECL comparison of 100 µM Luminol and 10 mM H_2O_2 in phosphate buffer and $NaClO_4$ solution pH 12 with scan rate of 100 mV/s.

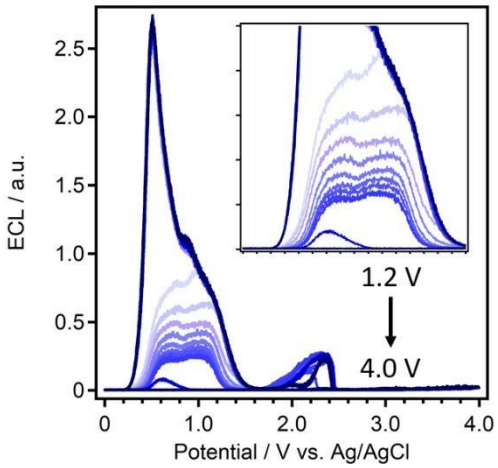

Figure 4.4. Effect of scanned potential of 100 µM Luminol and 10 mM H_2O_2 in phosphate buffer solution pH 12 with scan rate of 100 mV/s.

On the other hand, without the presence of carbonate, that is 0.1 M $NaClO_4$ solution, a weak signal of ECL could be observed in the region of peak II. This ECL emission is possibly happen due to the ability of BDD to generate $OH^{\bullet}$ from water oxidation which also lead to the generation of hydrogen peroxide with following reaction:

$$BDD(OH^{\bullet}) + H_2O \rightarrow H_2O_2 + BDD + H^+ \qquad (7)$$

Notes that the amount of H_2O_2 produced from the water was significantly lower compared to the generation from the carbonate which make a big difference to the ECL emission at peak II. This combine with the fact that $NaClO_4$ didn't have pH buffering capability makes the ECL at peak III could not be observed in this solution.

Importantly, all the ECL spectrum taken with CV shows maximum wavelength at around 438 nm which still in agreement with the attribution of the emitted light to the 3-aminopthalate excited state (Figure 4.5, Scheme 4.4).[20-22]

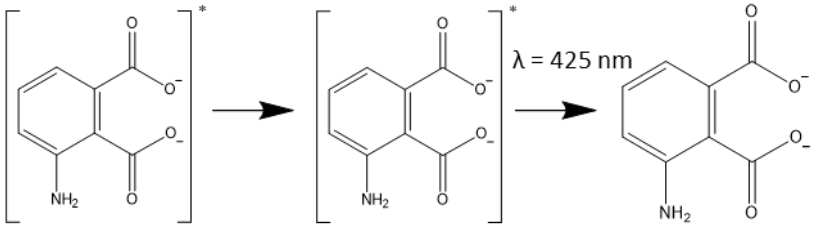

Scheme 4.4. Light excitation mechanism of 3-aminopthalte dianion excited state.

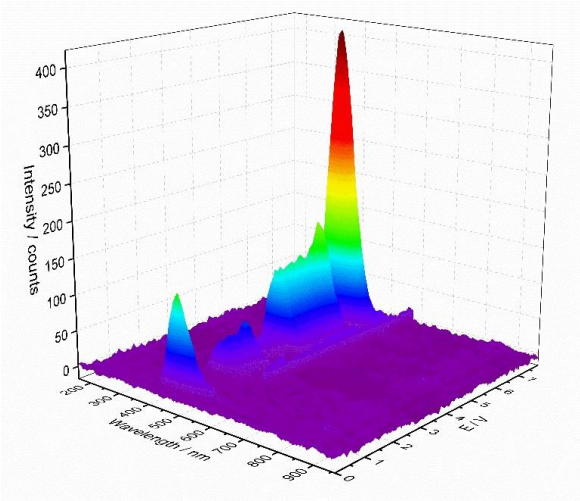

Figure 4.5. 3D surface plot of ECL spectrum with a BDD electrode as a function of applied potential. The solution is 1 mM luminol in 0.5 M Na_2CO_3 pH 12 with scan rate of 100 mV/s. Integration time for the spectrum: 100 ms.

In order to confirm the hypothesis, a CV measurement with a range of scan rate was conducted (Figure 4.6). The result shows that ECL at peak I, II_f, and III are proportionally increase to the scan rate. These indicates that the ECL generated at the surface of electrode are controlled by the diffusion of both luminol and carbonate precursor with the diffusion of electrogenerated hydrogen peroxide towards the bulk solution. On the other hand, ECL emission result at peak II_b was rather decrease with the increase of the scan rate. These might be due to the fact that oxygen that generated at high potential was affecting this peak, making the trend for this peak at rather hard to discuss.

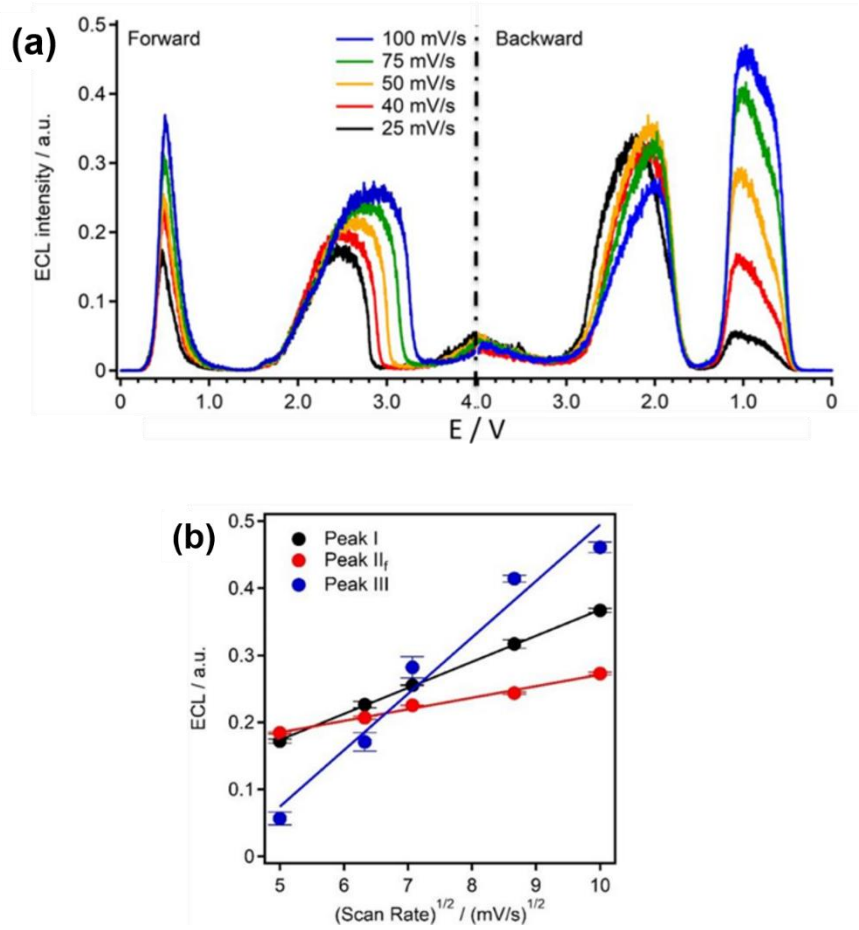

Figure 4.6. (a) ECL measurement at various scan rates of 100 µM luminol in 0.1 M Na_2CO_3 pH 12. (b) ECL peak as a function of the square root of the scan rate (N = 3). The potential was scanned from 0 to 4.0 V.

The effect of the pH on the ECL emission was investigated using CV at pH 12 to 8 (Figure 4.7). ECL signal at peak II_f was found to be rather stable up to pH 10 while further decrease of the pH gives a steep decrease until the signal completely unobservable at pH 8. Meanwhile, other ECL peaks (I, II_b, III) are decrease with the with the decrease of pH. These might be mainly due to the needs of deprotonation of luminol before initiating the oxidation which lead to the generation of ECL emission.

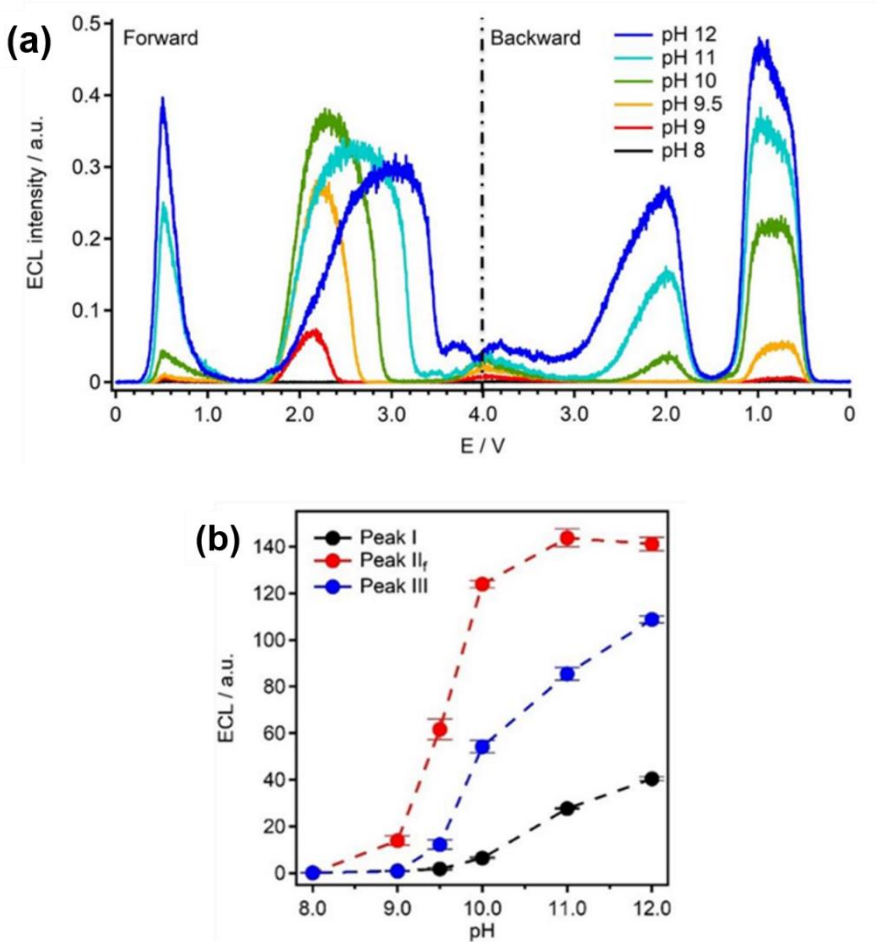

Figure 4.7. (a) ECL intensity by CV for 100 mM Na_2CO_3 and 100 µM luminol with different pH adjusted by adding appropriate amounts of $HClO_4$ to the solution. The potential was swept to 0 V then 4.0 V then back to 0 V with scan rate was of 100 mV/s. (b) Plot of integrated ECL intensity for each peak as a function of pH (N = 3).

With the decrease of pH, the deprotonation rate of luminol would be decrease hence the ECL signal for each peak, which all originated from luminol. This might be due to decrease amount of starting CO_3^{2-} in the equilibrium of carbonate species, with following equation:

$$CO_3^{2-} + H_2O \rightleftharpoons HCO_3^- + OH^- \qquad pKa = 10.33 \qquad (8)$$

$HCO_3^- + H_2O \rightleftharpoons H_2CO_3 + OH^-$ pKa = 6.35 (9)

This was in line with our previous result on $Ru(bpy)_3^{2+}/CO_3^{2-}$ system, where the main species that oxidized to generate peroxydicarbonate is CO_3^{2-}, not HCO_3^- nor H_2CO_3. In conclusion, current luminol/CO_3^{2-} would work best in the alkaline solution.

The ECL emission as function of Na_2CO_3 concentration was investigated in the range of 10−200 mM (Figure 4.8). First, the ECL emission at peak I was found not affected by the changed of initial carbonate concentration. This result was expected due to the origin of peak I was direct oxidation of luminol, and not related to carbonate. On the other hand, ECL emission at peak II_f and III are found to be increase with the carbonate concentration. These results indicate that both peaks are affected by the carbonate concentration, which support our proposed mechanism that both peaks are originated from the reaction between luminol and electrogenerated hydrogen peroxide (Scheme 4.2−4.4). Peak II shows a more broadening peak instead increase in the intensity with the increase of carbonate ion, which suggest that the generation of ECL in this peak is rather slow compared to other peaks. This might also explain the relatively high ECL intensity in the back scan on the same region (peak II_b), which is some excess of II_f. Nevertheless, the ECL area at peak II shows a good linearity to the carbonate concentration with regression analysis of the experimental data yielded (ECL/a.u.) = 22.07 + 0.58 mM and $r^2 = 0.999$.

However, unlike the good linearity of peak II_f, peak III doesn't gives a linear increase to the carbonate concentration. This possibly due to the enormous generation of oxygen at the first scan to the 4.0 V which affecting the quantification of peak III by (i) hindering the light that generate in the surface to travel to the PMT hence lowering the ECL response and (ii) generating proton as the side product of water oxidation that will reduce the surface local pH which lead to the decrease of ECL signal.

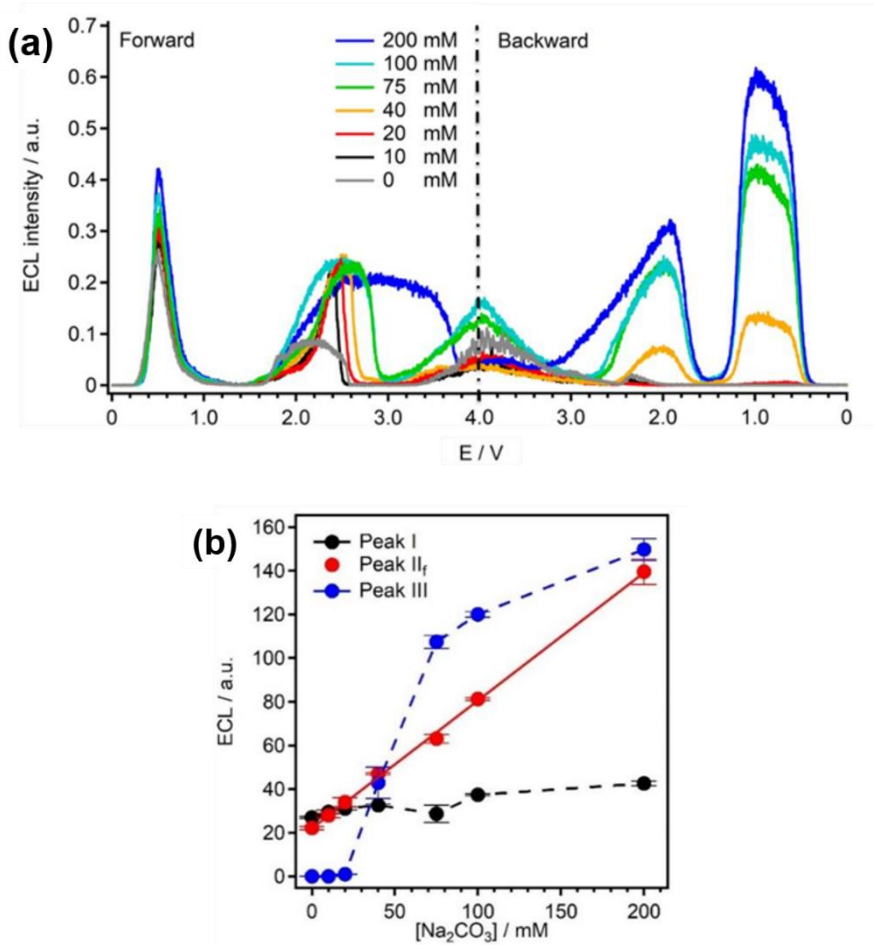

Figure 4.8. (a) ECL intensity for 10 µM $Ru(bpy)_3Cl_2$ in different concentration Na_2CO_3 solutions pH 12. The potential was swept to 0 V then 4.0 V then back to 0 V with scan rate was of 100 mV/s. (b) integrated ECL as a function of Na_2CO_3 concentration (N = 3).

Despite of the nonlinear result, the peak III still give a strong sharper peak compared to the peak II_f which have a rather broadening shape, especially with the increase of carbonate concentration. This suggest that peak III might be a better peak to exploit for analytical application. To overcome the nonlinearity problem on the analytical application, a three-step chronoamperometry measurement was conducted. In the first step, 0 V potential is applied for 5 s to stabilize the system. In the second

step, a potential of 2.5 V was applied for 10 s. This potential was chosen so that the system could generate enough hydrogen peroxide without triggering significant OER. In fact, the CV result of peak III for 2.5 V was almost the same as 4.0 V (Figure 4.9). Lastly in the third step, 1.1 V potential was applied for 10 s to triggering the ECL emission at previously mentioned peak III. Furthermore, for analytical purpose, the concentration luminol was increased to 1 mM to have a higher ECL signal and phosphate buffer was used to have a more stable buffering capacity in the surface of the electrode. The ECL signal in the third step was integrated to quantify the emission as a function of the initial carbonate solution (Figure 4.10). In the presence case, the ECL signal was found to be linear at the range of 0 to 25 mM with regression analysis of the experimental data yielded (ECL/a.u.) = 0.47 + 1.25 mM and $r^2 = 0.997$.

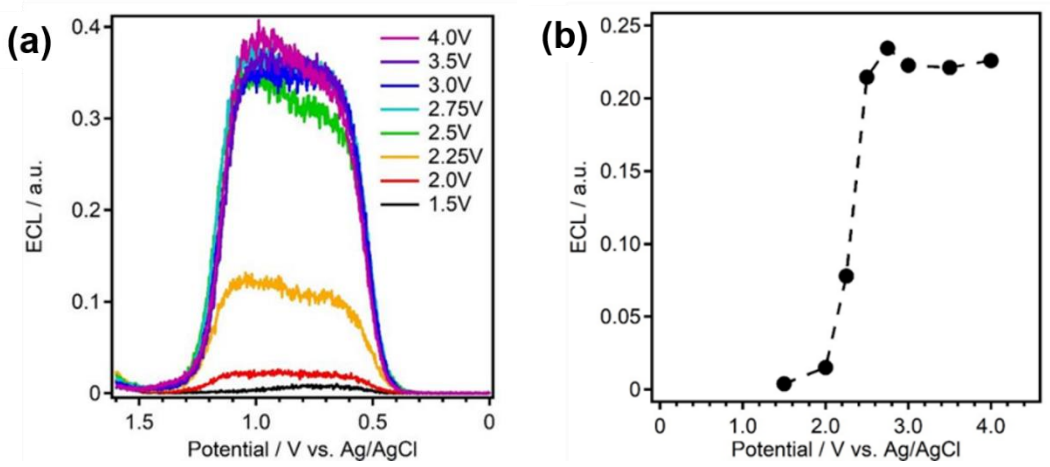

Figure 4.9. (a) Effect of scanned potential to the peak III at 0.1 M Na_2CO_3 100 µM Luminol. (b) integrated ECL as a function of maximum scanned potential.

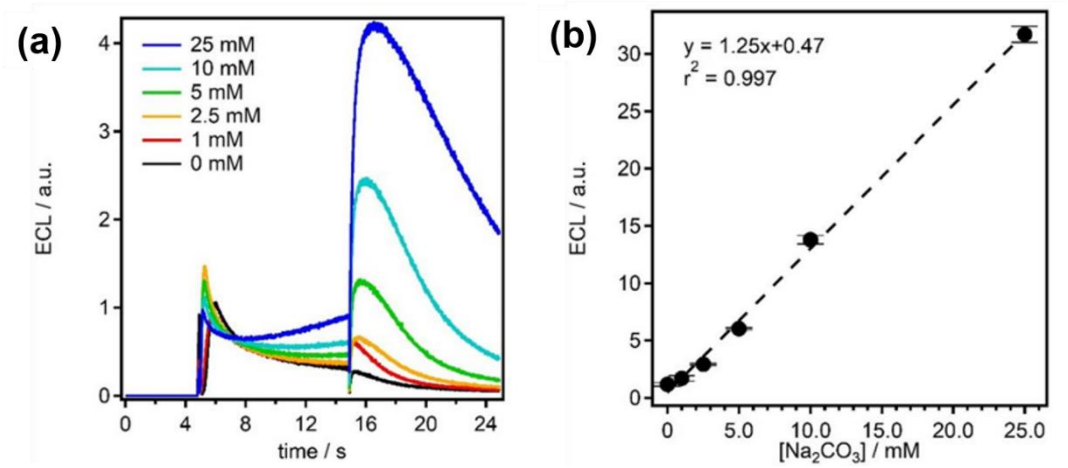

Figure 4.10. (a) ECL intensity for 1 mM $Ru(bpy)_3Cl_2$ in 0 mM (black), 1 mM (red), 2.5 mM (orange), 5 mM (green), 10 mM (sky blue), and 25 mM (blue) Na_2CO_3 solutions. (b) integrated ECL as a function of Na_2CO_3 concentration (N = 3). Three-step chrono-amperometry: E_1 = 0 V, t_1 = 5 s; E_2 = 2.5 V, t_2 = 10 s E_2 = 1.1 V.

4. Conclusion

The *coreantant-free* ECL using luminol in carbonate solution was conducted for the first time. ECL-CV measurement results show 3 kinds of peaks, which all found to be derivate from the excited state of 3-aminopthalte dianion with each respective mechanism. The system could be achieved due to the unique ability of BDD to promote an efficient H_2O_2 generation which could enhance the ECL emission. Moreover, the system also having buffering capability, which further enhance the light intensity compared the non-buffered solution. The emission was found to be decrease by the decrease of pH, which is expected on the luminol system due to the needs of luminol to be deprotonated before oxidized in the surface of electrode.

5. Reference

1. Lin, X. Q.; Sun, Y. G.; Cui, H. Chin. *J. Anal. Chem.* **1999**, 27, 497.
2. Dong, Y-P.; Cui, H.; Wang, C-M. *J. Phys. Chem. B* **2006**, *110*, 18408.
3. Wilson, R.; Akhavan-Tafii, H.; Desilva, R.; Schaap, A. P. Electroanalysis **2001**, *13*, 1083.
4. Sun, Y. G.; Cui, H.; Lin, X. Q. *Acta Chim. Sin.* **2000**, *58*, 567.
5. Cui, H.; Zou, G-M.; Lin, X-Q. *Anal. Chem.* **2003**, *75*, 324.
6. Liu, Z.; Qi, W.; Xu, G. *Chem. Soc. Rev.* **2015**, *44*, 3117.
7. Han, J. H.; Jang, J.; Kim, B. K.; Choi, H. N.; Lee, W. Y. *J. Electroanal. Chem.* **2011**, *660*, 101.
8. Gross, E.M.; Maddipati, S. S.; Snyder, S. M. *Bioanalysis* **2016** *8*, 2071.
9. Liu, X.; Qi, W.; Gao, W.; Liu, Z.; Zhang, W.; Gao, Y.; Xu, G. *Chem. Commun.* **2014**, *50*, 14662.
10. Marquette, C.A.; Blum L. J. *Anal. Chim. Acta* **1999**, *381*, 1.
11. Marquette, C.A.; Leca, B. D. *Luminescence* **2001**, *16*, 159.
12. Pazur, J.H.; Kleppe, K. *Biochemistry* **1964**, *3*, 578.
13. Zuo, Z.; Cai, Z.; Katsumura, Y.; Chitose, N.; Muroya, Y. *Radiat. Phys. Chem.* **1999**, *55*, 15.
14. Bisby, R. H.; Johnson, S. A.; Parker, A. W.; Tavender, S. M. *J. Chem. Soc. Faraday Trans.* **1998**, *94*, 2069.
15. Huie, R. E.; Clifton, C. L.; Neta, P. *Radiat. Phys. Chem. Int. J. Radiat. Appl. lnstrum., Part C* **1991**, *38*, 477.
16. Ruiz, E. J.; Ortega-Borges, R.; Jurado, J. L.; Chapman, T. W.; Meas, Y. *Electrochem. Solid-State Lett.* **2009**, *12*, 1.
17. Saha, M. S.; Furuta, T.; Nishiki, Y. *Electrochem. Commun.* **2004**, *6*, 201.
18. Velazquez-Pena, S.; Saez, C.; Canizares, P.; Linarez-Hernandez, I.; Martines-Miranda, V.; Barrea-Diaz, C.; Rodrigo, M.A. *Chem. Eng. J.* **2013**, *230*, 272.
19. Saha, M. S.; Furuta, T.; Nishiki, Y. *Electrochem. Solid-State Lett.* **2003**, *6*, 5.
20. Shi, M.-J.; Cui, H. *Electrochim. Acta* **2006**, *52*, 1390.
21. Cui, H.; Zhang, Z.-F.; Zou, G.-Z.; Lin, X.-Q. *J. Electroanal. Chem.* **2004**, *566*, 305.
22. Cui, H.; Zou, G.-Z.; Lin, X.-Q. *Anal. Chem.* **2003**, *75*, 324.

Chapter 5

Study of Hydroxide Ion Oxidation in Basic Solutions Using Boron-doped Diamond Electrodes

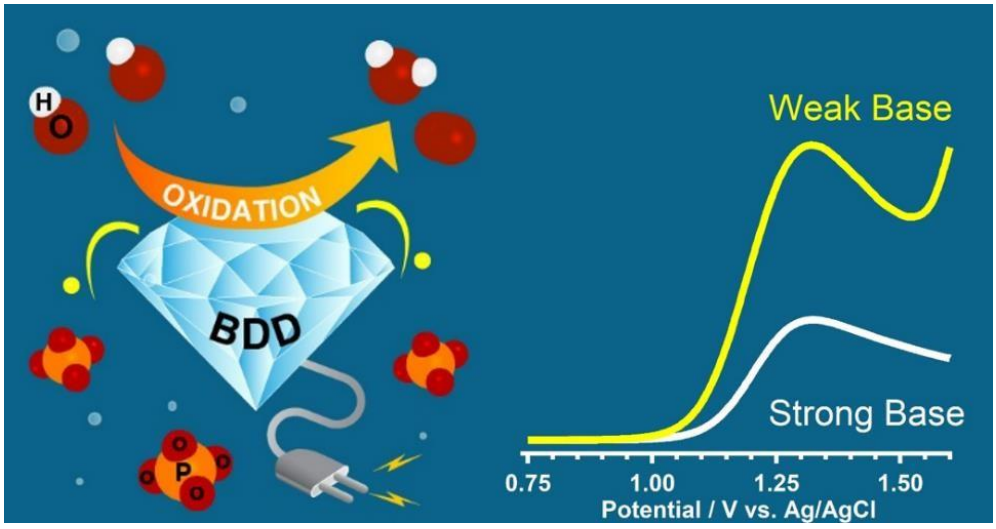

1. Reprinted (adapted) with permission from Irkham; Watanabe, T.; Einaga, Y. *Anal. chem.* **2017**, *89*, 7139-7144. Copyright © 2017 American Chemical Society.
2. Irkham; Einaga, Y. *Analyst* **2019**, *144*, 4499-4504. Reproduced by permission of The Royal Society of Chemistry.

1. Introduction

Hydroxide is used worldwide in many industrial processes and research, including in the electrochemical field application,[1,2] making the study of this compound is important to this field. Particularly, hydroxide ion can be directly oxidize at the surface of the electrode with reaction:

$$OH^- \rightarrow \tfrac{1}{4}O_2 + \tfrac{1}{2}H_2O + e^- \qquad (1)$$

The electrochemical oxidation of hydroxide ion occurs at high overpotential, usually in the region of 1.3 to 1.6 V (vs. SCE).[2,3] In aqueous solution, this high overpotential makes the phenomena quite difficult to be observed due to overlapping of the oxidation wave with the oxygen evolution reaction (OER). Despite of that, reports shown that the hydroxide ion oxidation still can be observed on metal electrodes such as gold, platinum, or nickel. Daniele *et al.* have already explored the electrochemical oxidation of hydroxide ions in aqueous solution using gold microelectrodes in a steady state system.[4–6] The steady-state limiting current was proved to be proportional to the hydroxide ion concentration.[4] Mentus *et al.* also added to the study that cathodic pretreatment on gold electrodes influence the peak of hydroxide ion oxidation.[3] Later Banks and coworkers reported that hydroxide ion could also be observed at low micro-molar to milli-molar range using a nickel oxide screen-printed electrode.[2] However, without a special geometry or a steady state electrode system, the hydroxide ion oxidation is hard to observed due to the background oxide formation of the metal electrodes that overlap with the hydroxide ion oxidation itself.

On the other hand, despite of its popularity, there are still no reports about the study of hydroxide ions oxidation on Boron-doped diamond (BDD) electrode. Since BDD have high overpotential of water oxidation, it should be possible to distinct the oxidation waves of hydroxide ions with the OER. In addition, unlike metals electrodes, oxide layer formation will not occur in BDD electrode. This further makes study of the hydroxide ion oxidation easier, without the needs of particular geometry or electrode system such as micro-sized electrode or a steady state system.

Herein we report the study of hydroxide ion oxidation at BDD electrode in basic aqueous solutions. The study is including comparison of simple NaOH as strong alkaline solution and the phosphate as weak alkaline solution with buffering effect.[7,8] The surface pretreatment effect of the BDD to the behavior of the hydroxide ions oxidation was also studied due to the pretreatment at BDD electrodes have been reported giving a different surface condition, making some differences on the electrochemical behavior.[9,10–12] Moreover, in this chapter, we also showed that BDD electrode might give a new way to estimate buffer capacity value of the solution by simple electrochemical measurement.

2. Experimental

Materials. All reagents were obtained commercially (Fuji Film, Japan) and used without further purification. Pure water was doubly distilled with maximum conductivity 18 MΩ obtained from Simply−Lab water system (DIRECT-Q 3 UV, Millipore).

Preparation of BDD. The BDD films were deposited on a silicon (111) wafer by using a microwave plasma-assisted chemical vapor deposition (MPCVD) system (CORNES Technologies / ASTeX−5400). Acetone and trimethoxyborane were used as the source of carbon and boron respectively with atomic ratio of B/C = 1%. The surface morphology of the BDD was examined with field emission scanning electron microscope (SEM, JEOL JCM6000). Raman Spectra were recorded with an Acton SP2500 (Princeton Instruments) with excitation at 532 nm from a green laser diode in room temperature.

Electrochemical Measurement. The electrochemical measurements were conducted with potensiostat (PGSTAT302N, AUTOLAB Instrument) using a single-compartment threeelectrode cell with 1% BDD as working electrode, Pt spiral as counter electrode, and Ag/AgCl (Saturated KCL) as reference electrode. The electrode area of BDD was 0.096 cm^2. Unless otherwise specifically mentioned, there are two steps of pretreatment conducted before each measurement to stabilize the surface of the BDD electrode. First is electrochemical cleaning by performing 10 voltammetric cycle between −3.0 and 3.0 V. Second step is either anodic oxidation by 10 voltammetric cycle between 0 and 3.0 V or

cathodic reduction by 10 voltammetric cycle between 0 and −3.0 V. Depends on the pretreatment, these BDD later will be referred as anodic oxidized BDD (AO-BDD) and cathodic reduced BDD (CR-BDD), respectively. The entire pretreatment is conducted at a scan rate of 300 mV/s in 0.1 M $NaClO_4$ solution. Phosphate and borate solution was prepared by to adjusting the pH from the pH meter (LAQUA F-74, Horiba, Japan) of the H_3PO_4 or H_3BO_3 solution using NaOH. All the measurements were carried out in 0.1 M or 0.3 M $NaClO_4$ solution as the main electrolyte at room temperature after bubbling N_2 gas through the solutions for 1 hour to remove dissolved oxygen. The measurement was scanned from potential 0 V to +2.0 V with scan rate of 20 mV/s.

Buffer Capacity Calculation. The buffer capacity value from the electrochemical measurement were compared with the theoretical value. Theoretical buffer capacity (β)was calculated using simplified equation:

$$\beta = \frac{dn}{dpH} = 2.303\left(\frac{K_w}{[H^+]} + [H^+] + \sum\left(\frac{C_{buf}K_a[H^+]}{(K_a + [H^+])^2}\right)\right)$$

Where K_w is the water dissociation constant, C_{buf} is the buffer concentration, and K_a is the acid dissociation constant. The concentration of proton was thermodynamically corrected using activity coefficient with equation:

$$\log f_z = \frac{-Az^2\sqrt{I}}{1 + \sqrt{I}}$$

f_z denotes the activity coefficient of an ion with total ion charge z and I is the ionic strength of the aqueous solution.

3. Results and discussion

3.1. Hydroxide ion oxidation at boron-doped diamond in strong alkaline solution

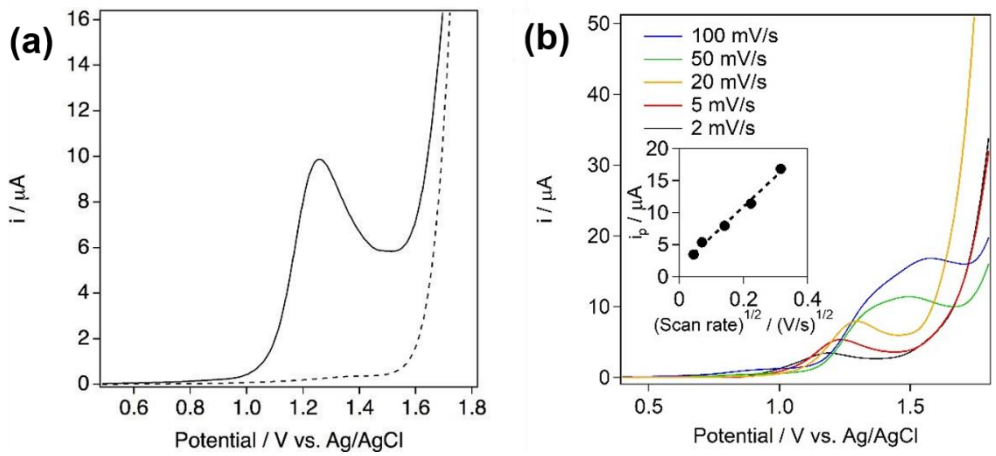

Figure 5.1. (a) LSVs recorded at 20 mV/s on an AO-BDD in 0.1 M $NaClO_4$ solution with (solid line) and without (dotted line) the presence of 1.0 mM NaOH. (b) LSVs at various scan rate in 1.0 mM NaOH with 0.1 M $NaClO_4$ using AO-BDD. Inset: peak current as a function of square root of scan rate. The potential was scanned from 0 V to 2.0 V. Adopted from *ref 7* Copyright 2017 American Chemical Society.

Figure 5.1a (solid line) displays the linear sweep voltammogram (LSV) of 1.0 mM NaOH in 0.1 M $NaClO_4$ solution after bubbling N_2 gas for 1 hour with AO-BDD. Bubbling was needed to remove the dissolved oxygen from the solution that might influence the equilibrium of reaction 1. The peak at around 1.25 V assumed to be the hydroxide ion oxidation at the surface of the electrode. Waves similar to those shown in figure 5.1a (solid line) was reported as hydroxide ion oxidation at metal electrodes in a steady stead system.[2–4,6,13] In the present case, the hydroxide ion oxidation can be observed at BDD electrode without any particular geometry of the cell and electrode system. Such kind of peak near OER was also reported as oxidation peak of sp^2-bonded carbon at the BDD electrodes.[14–18]

However, sp^2-bonded carbon peak was not observed from raman result for the BDD that used in this experiment (Chapter 2, Figure 2.2). Additionally, there are no peaks observed at the background measurement, where there are no presences of NaOH (Figure 5.1a, dotted line).

In order to investigate whether the main peak occurred due to hydroxide ion oxidation, or surface oxidation of sp^2-bonded carbon on the BDD, LSV measurements over a range of scan rates also conducted to (Figure 5.1b). The results show that peak currents were found to be proportional to the square root of the scan rate. The regression analysis of the experimental data yielded $(i_{max}/\mu A) = 1.49 \times 10^{-6} + 4.71 \times 10^{-5}$ (V/s) and $r^2 = 0.992$. This result indicates that the main peak was appeared due to diffusion-controlled reaction of hydroxide ion oxidation, rather than surface oxidation of the electrode. Thus, above results and considerations suggest that the main peak maybe due to the oxidation of hydroxide ion. This phenomenon become possible due to the high overpotential of OER on BDD electrode, making the hydroxide ion oxidation separated with the OER which occurred at more positive potential. Moreover, unlike metal electrodes, the oxidation of hydroxide ion didn't have any competition with oxide formation at the surface of the BDD electrode.

3.2. Effect of surface pretreatment on hydroxide ion oxidation at BDD electrode

BDD has been reported having different electrochemical behavior with different surface pretreatment.[9,10,19–21] Therefore, the effect of surface pretreatment was also important to be investigated. In this experiment, two kinds of pretreatment are used, anodic oxidation (AO-BDD) and cathodic reduction (CR-BDD). Anodic oxidation is reported capable to convert the surface termination of the BDD into oxygen termination.[12,23] It is also reported that anodic oxidation of as-deposited BDD increase the oxygen to carbon (O/C) ratio from 0.02 up to 0.3.[12,22] Characterization of such anodically-oxidized BDD surface by XPS shows that it contains many C-O functional groups.[12,24–26] On the other hand, cathodic pretreatment are reported to be able to reduce the O/C ratio of the BDD's surface.[8] Compared to the AO-

BDD, the hydroxide oxidation peak potential (and the overpotential) on CR-BDD was slightly shifted toward negative potential (Figure 5.2). One possible reason for this result is the electrostatic interaction between the surface and the hydroxide ion. AOBDD surface that rich in C-O functionalities, believed to be in an electrostatically negative state due to the relatively high electronegativity of the oxygen atoms.[27] The relatively negative surface of AO-BDD gives higher repulsion to hydroxide ions, which also have negative charge, makes it harder for hydroxide ion to be oxidized at the surface of the electrode. As a result, the oxidation potential of hydroxide ion was higher at AO-BDD. Another possible explanation for this shifting potential is because of the different polarity on the surface results from electrostatic interactions which can raise or lower the energy levels of the valence and conduction bands.[18]

Additionally, in the transition stages, a shoulder waves were observed at around 0.9 V at CR-BDD (referred as pre-peak). This kind of behavior was formerly reported in gold electrode.[3,4,6] In the case of BDD electrode, the splitting of the hydroxide ion oxidation might happen between different surface-active site of the BDD. Considering that the peak was not observed at AO-BDD, the pre-peak was interpreted as the oxidation of hydroxide ion at "reduced surface" of the BDD, while the peak observed after that was interpreted as the oxidation of hydroxide ion at the "oxidized surface" of the BDD.

In order to investigate the origin of the pre-peak, various cycle number of cathodic pretreatments was conducted (Figure 5.3a). It can be seen that the pre-peak was increase along with the increase of the number of cycle at the cathodic pretreatment. This might be due to the increase of the "reduced surface" of the BDD with the increase number of reduction cycle, leads to the increase of the current signal at the pre-peak. Repetitive measurement without any pretreatment on CR-BDD shows that the pre-peak was not observed at second measurement (Figure 5.3b). It is suggested that the "reduced surface" of the BDD was removed on the first LSV scan. This "reduced surface" might be oxidized along the first scan, where the potential was scanned to 2.0 V. The behavior of the second LSV scan was similar to the AO-BDD. In fact, when more number of scan on the repetitive measurement was conducted (with every solution exchange), the peak current values were

decline in oxidation peak and shifted toward more positive potential, indicates that the surface of BDD was changed through the oxidation process (Figure 5.3c). Empirically, in BDD electrode, good signal stability can be obtained by electrochemical pretreatment as mentioned in the experimental section, which is difficult to apply to other types of electrode.

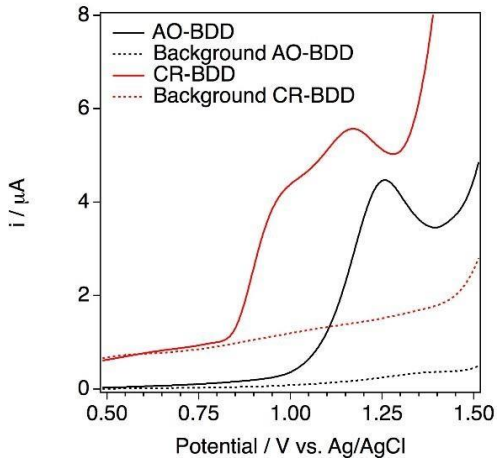

Figure 5.2. LSVs measurements in 0.1 M $NaClO_4$ aqueous solution with absence (dotted line) and with the presence (solid line) of 1.0 mM NaOH at scan rate 20 mV/s on AO-BDD (black) and CR-BDD (red). The potential was scanned from 0 V to 2.0 V. Adopted from *ref 7* Copyright 2017 American Chemical Society.

To see the correlation between hydroxide ion concentration and the current peak, LSV measurement at different concentration of NaOH in 0.1 M $NaClO_4$ solution using AO-BDD was conducted (Figure 5.4a). The peak current at around 1.25 V was plotted as function of hydroxide ion concentration at the range of 0.5 mM to 10 mM. The regression analysis of the experimental data yielded $(i_p/\mu A) = -6.21 \times 10^{-6} + 1.67 \times 10^{-5}$ (mM) and $r^2 = 0.999$. Meanwhile, the peak current at around 1.15 V derived from CR-BDD also gives a good linearity versus the concentration of hydroxide ion in the solution (Figure 5.4b). The regression analysis of the experimental data yielded $(i_p/\mu A) = -1.14 \times 10^{-5} + 2.12 \times 10^{-5}$ (mM) and $r^2 = 0.996$. This good linearity indicates that BDD electrode can be promoted for the evaluation of the concentration of hydroxide ion. Notes that the experiment was carried out in bare BDD without any special geometry and without optimization in the experimental

condition. Nevertheless, from the results, AO-BDD is more suitable for evaluating the concentration of hydroxide ion, since pre-peak phenomena not occurred and gives more stable measurement result.

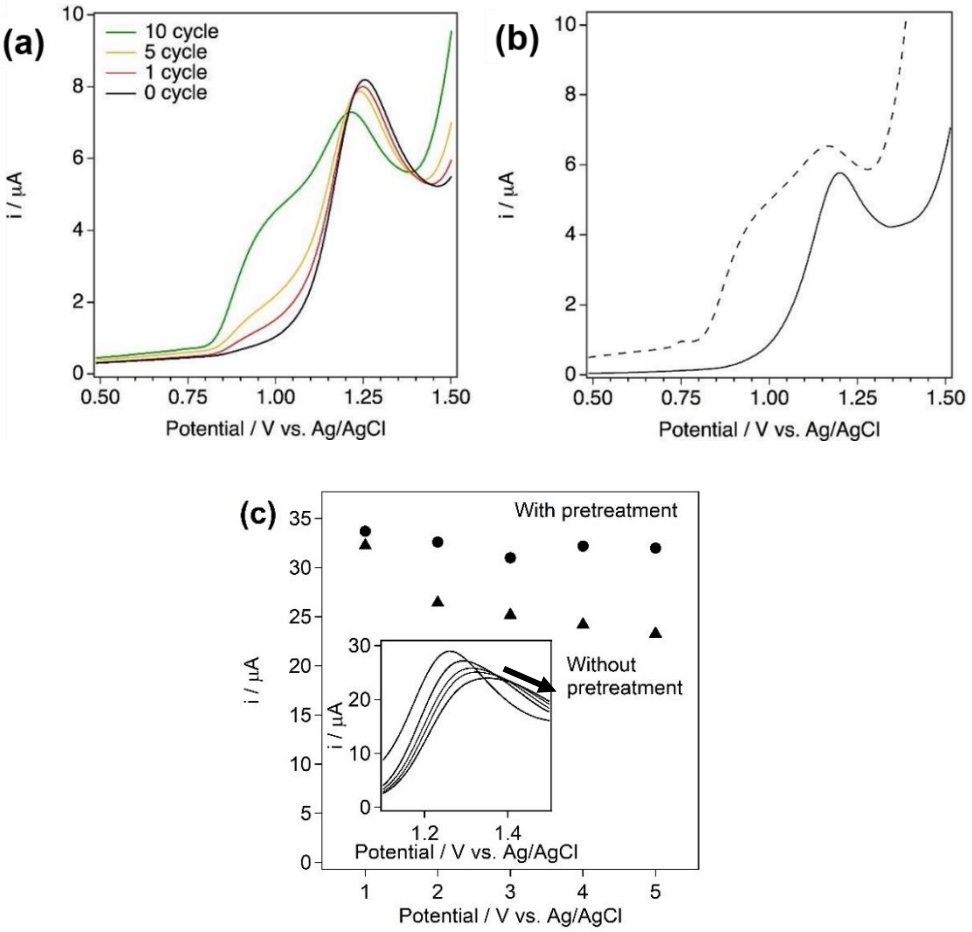

Figure 5.3. (a) LSVs of 1.0 mM NaOH in 0.1 M $NaClO_4$ solution with different number of voltammetric cycle in the cathodic pretreatment. (b) 1st (dotted line) and 2nd (solid line) consecutive LSV of 1.0 mM of NaOH in $NaClO_4$. (c) The variation of peak current in consecutive measurement of LSV for 2.0 mM NaOH in 0.1 M $NaClO_4$. Inset: consecutive LSVs for 2.0 mM NaOH in 0.1 M $NaClO_4$. The working electrode was CR-BDD with potential scanned from 0 V to 2.0 V at scan rate 20 mV/s. Adopted from *ref 7* Copyright 2017 American Chemical Society.

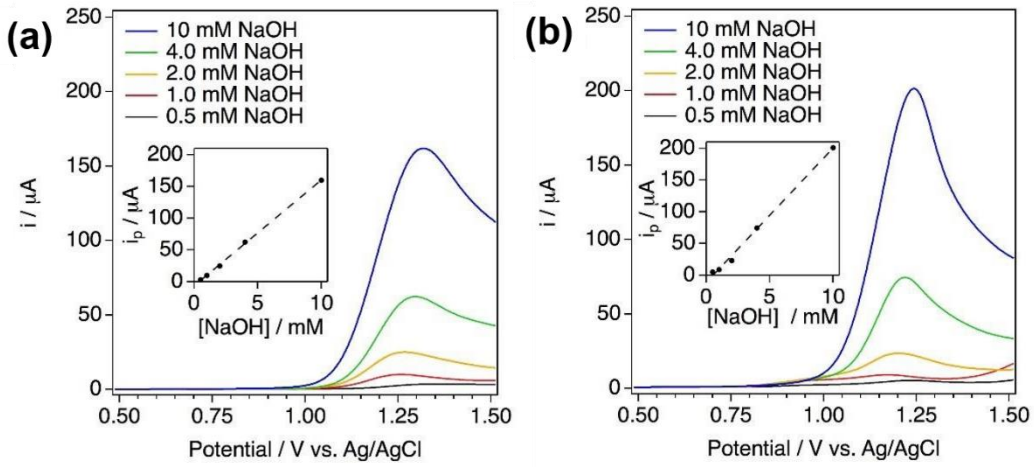

Figure 5.4. LSVs for different concentration of NaOH in 0.1 M $NaClO_4$ solution with scan rate 20 mV/s at (a) AO-BDD (b) CR-BDD. The potential was scanned from 0 V to 2.0 V. Inset: peak current as a function of NaOH concentration. Adopted from *ref 7* Copyright 2017 American Chemical Society.

3.3. Effect of phosphate on the oxidation of hydroxide ions

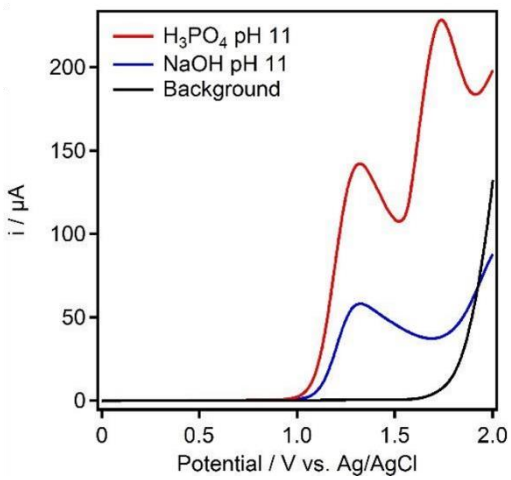

Figure 5.5. LSVs of different types of basic solution at pH 11 using AO-BDD in 0.3 M $NaClO_4$ solution. Background was 0.3 M $NaClO_4$ solution at pH 7. Scan rate was 20 mV/s. Reproduce from *ref 8* by permission of The Royal Society of Chemistry.

Figure 5.5 (red line) shows linear sweep voltammetry measurement (LSV) of 20 mM of H_3PO_4 with pH 11 in 0.3 M $NaClO_4$. There are two clear peaks that can be observed in the voltammograms, first peak at potential around 1.3 V and second peak at potential 1.75 V. The first peak can be assumed to be due to oxidation of the hydroxide ions since the solution has a relatively high concentration of hydroxide ions (around 1 mM), and a peak at a similar potential is observed with the NaOH solution (Figure 5.5, blue line). As for the second peak, this might be due to the oxidation of phosphate ions forming peroxodiphosphate at the surface of the BDD electrode, which can be a direct or indirect reaction via the generation of hydroxide radicals.[23,28] Both of these peaks can be observed due to the unique characteristics of BDD which is that it has a high overpotential for water oxidation making it easier for other compounds to be oxidized at the surface with less competition with water. In order to check the correlation between the hydroxide ion concentration and the peak current, LSV measurements at different hydroxide ion concentrations (by adjusting the pH using a pH meter) were conducted.

Figure 5.6 shows the LSVs for different hydroxide ion concentrations in 20 mM H_3PO_4 solutions. The maximum peak current at around 1.3 V is plotted as a function of hydroxide ion concentration in solutions ranging from 0.1 mM to 10 mM. Regression analysis of the experimental data yielded $(i_p/\mu A) = 39.54 + 93.122$ (mM) with $r^2 = 0.996$, which shows there is good linearity between the peak current and the hydroxide ion concentration. Thus, our conclusion is that the peak is due to the oxidation of hydroxide ions in weak basic solutions. Note that in pH lower than 10, the peak at around 1.3 V was not observed while the peak at around 1.75 V was still observed until pH around 7 due to the high enough amount of phosphate in the solution (Figure 5.7).

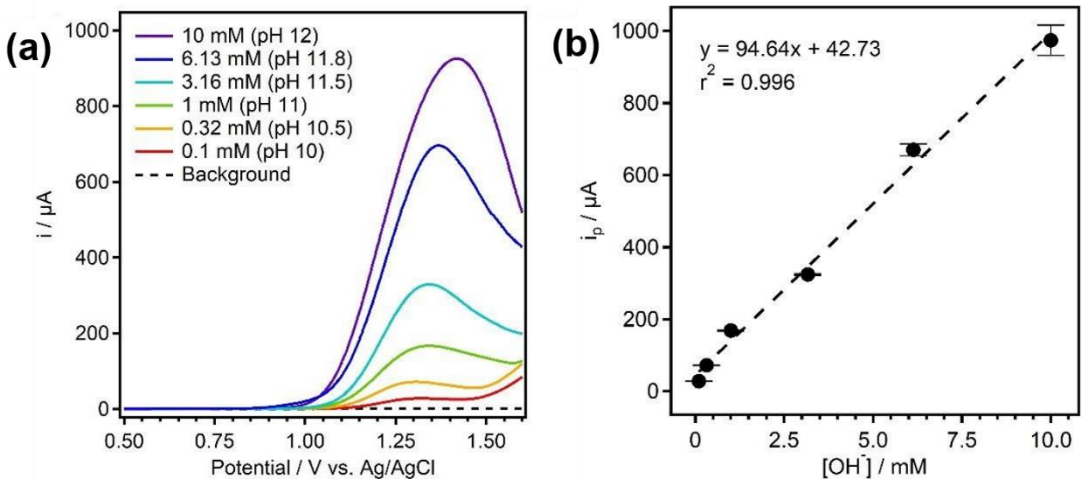

Figure 5.6. (a) LSVs for different hydroxide ion concentrations in 20 mM H_3PO_4 buffer solutions with pH ranging from 10 to 12 at AO-BDD with scan rate of 20 mV/s. (b) peak current as a function of the hydroxide ion concentration (N = 3). Reproduce from *ref 8* by permission of The Royal Society of Chemistry.

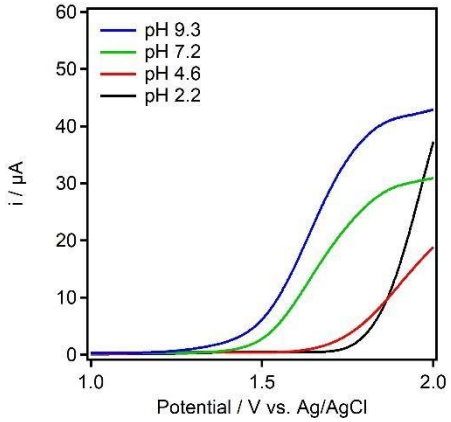

Figure 5.7. LSVs for different hydroxide ion concentrations in 20 mM H_3PO_4 buffer solutions with pH ranging from 2.2 to 9.3 at 0.1 M $NaClO_4$ using AO-BDD. The potential was scanned from 0 V to 2.0 V with a scan rate of 20 mV/s. Reproduce from *ref 8* by permission of The Royal Society of Chemistry.

In Figure 5.5, although the peaks due to oxidation of the hydroxide ions appear at similar potentials, there is a significant difference between the peak currents for the solution with H_3PO_4 (red line) and that without H_3PO_4 (blue line), where the solution with H_3PO_4 has a higher peak current, even though the amounts of hydroxide ions in the solutions are the same. This higher peak current is assumed to be due to the presence of phosphate ions in the solution, which gives a buffering capability to the hydroxide ions with the following equilibrium reactions:

$$PO_4^{3-} + H_2O \rightleftharpoons HPO_4^{2-} + OH^- \quad (2)$$

$$HPO_4^{2-} + H_2O \rightleftharpoons H_2PO_4^- + OH^- \quad (3)$$

$$H_2PO_4^- + H_2O \rightleftharpoons H_3PO_4 + OH^- \quad (4)$$

From reactions (2) − (4), we can see that if there is sufficient phosphate present, and that the hydroxide ions oxidized at the surface can be replaced, it will make oxidation of hydroxide ions at the surface of the electrode easier, leading to an increase in current compared to the basic NaOH solution.

To confirm this hypothesis, LSV measurements of solutions with different H_3PO_4 concentrations with the same hydroxide ion concentration (or same pH) were conducted (Figure 5.8). The pH of the solution was 11.5 in order to see the peak more clearly. The peak current for oxidation of the hydroxide ions increases linearly with increasing phosphate concentration (Figure 5.8b), even though the hydroxide ion concentration was the same for all the solutions (3.16 mM). This is possible because increasing the amount of phosphate ions to balance the solution also increases the buffering capability of the solution. Thus, the equilibrium provides more hydroxide ions and suppresses the proton concentration in the solution. This again means the hydroxide ions are more easily oxidized and a higher current signal obtained, in agreement with our results. It is also noted that the peak current of phosphate oxidation at 1.75 V is also linear to the increase of phosphate concentration (Figure 5.8c). From these data, it can be concluded that the peak current for the oxidation of hydroxide ions in a weak base solution is affected not only by the hydroxide ion

concentration but also the concentration of the acid or base itself. This suggests that these two parameters are related to the buffering capacity of a weak acid or base solution.

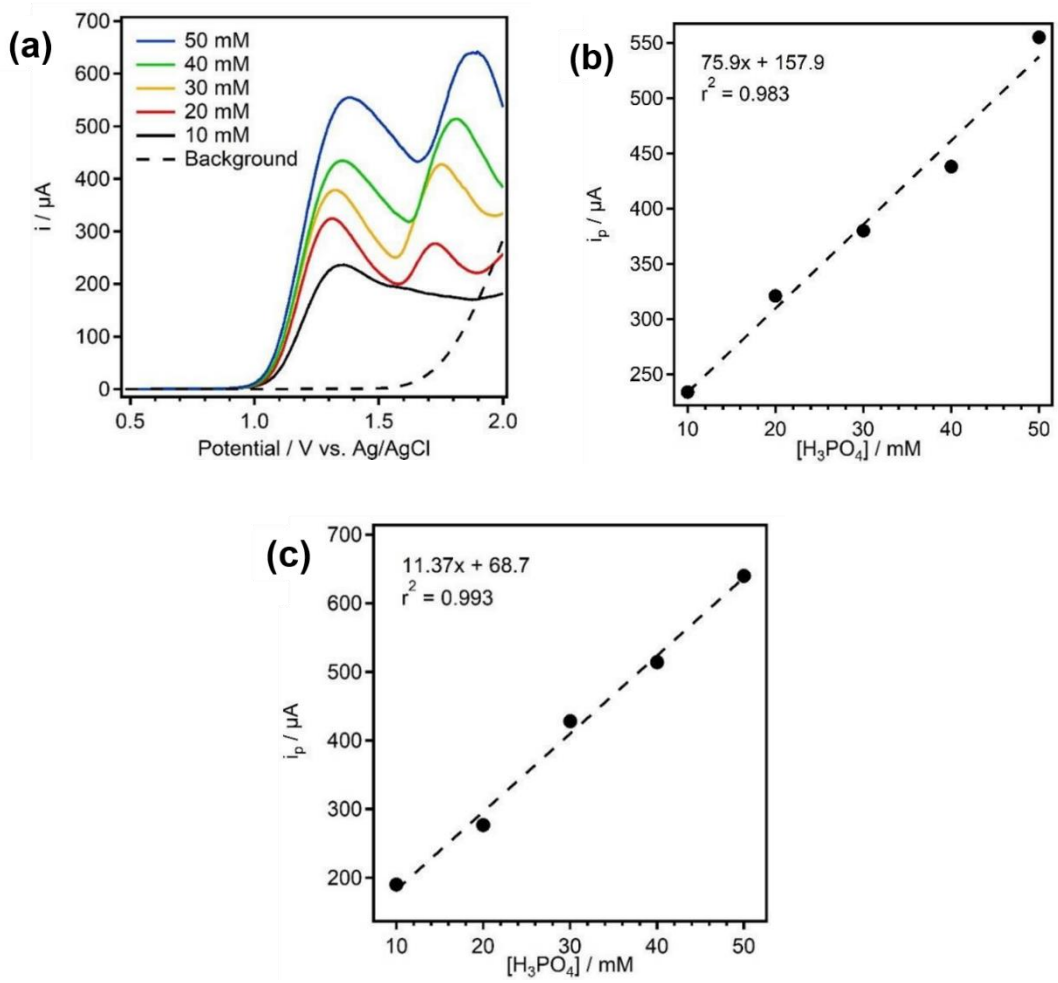

Figure 5.8. (a) LSVs for different concentrations of H_3PO_4 solution at pH 11.5 using AO-BDD with scan rate of 20 mV/s. (b) peak current at 1.3 V as a function of phosphate concentration. (c) peak current at 1.75 V as a function of phosphate concentration. (N = 3). Reproduce from *ref 8* by permission of The Royal Society of Chemistry.

Here, the relationship between the peak for hydroxide ions at 1.3 V and the buffer capacity of the solution estimated by theoretical calculations (see experimental section) was also investigated (Figure 5.9). We assume that the peak current difference between the

H_3PO_4 solution (buffer solution) and the NaOH solution (non-buffer solution) depends solely on the buffering capacity of the H_3PO_4 solution. It can be seen that when the peak current of the NaOH solution is subtracted from the peak current of the H_3PO_4 solution, the value is proportional to the calculated buffer capacity. Importantly, with this approach, it might be possible to evaluate the buffer capacity of a solution. Moreover, compared to the conventional way of determining buffer capacity such as by titration, electrochemical measurements using BDD electrodes are faster, easier, and also do not require extra chemicals. Note that in the low pH region, the current due to oxidation of the hydroxide ions was harder to detect using the present setup due to its low value.

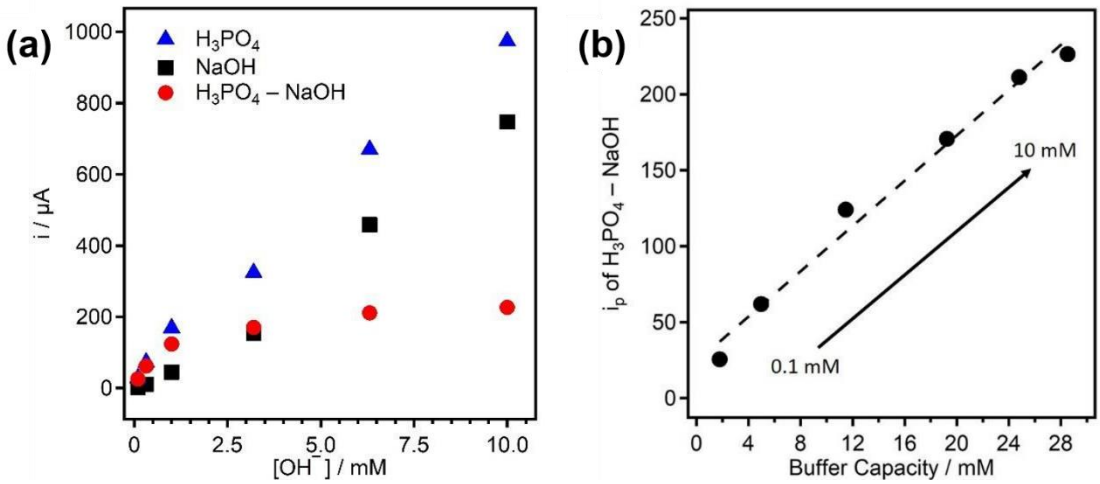

Figure 5.9. Plot of (a) peak current versus hydroxide ion concentration for a 20 mM H_3PO_4 solution (blue), NaOH solution (black), and the difference in peak current between those solutions (red) using AO-BDD. (b) The peak current difference between the 20 mM H_3PO_4 and NaOH solutions versus theoretically calculated buffer capacity. The pH of the solutions ranges from 10 to 12. Reproduce from *ref 8* by permission of The Royal Society of Chemistry.

3.4. Behavior of hydroxide ions in other weak bases

The behavior of hydroxide ions in borate solutions was also investigated. Figure 5.10 shows LSVs of borate solutions (pH 11.5) with different boric acid concentrations. Similar to phosphate solutions, the current signal for oxidation of the hydroxide ions increases with increasing boric acid concentration. The same behavior was observed due to the fact that borate solutions also have buffering capabilities that can supply hydroxide ions to the surface. The reaction for the borate solution is:

$$B(OH)_3 + OH^- \rightleftharpoons B(OH)_4^- \qquad (5)$$

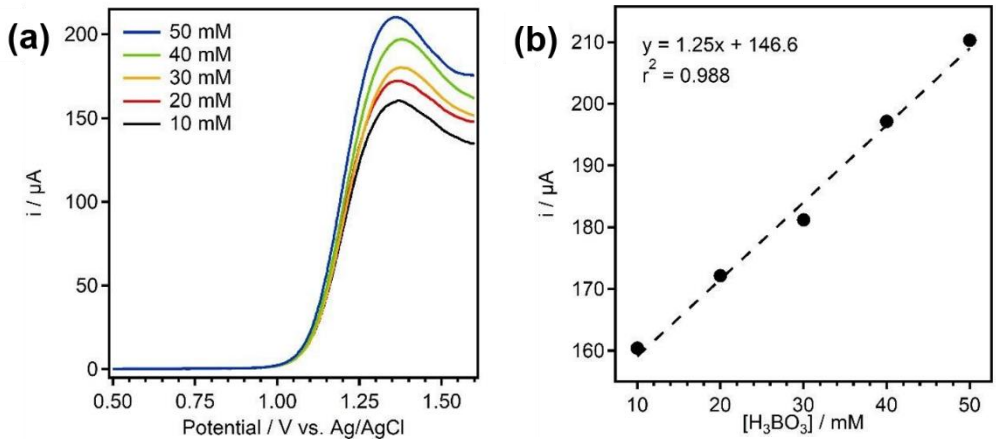

Figure 5.10. (a) LSVs for different concentrations of H_3BO_3 solution at pH 11.5 using AO-BDD with scan rate of 20 mV/s. (b) Peak current as a function of borate concentration. Reproduce from *ref 8* by permission of The Royal Society of Chemistry.

Moreover, a linear relationship between the hydroxide ion concentration and the peak current was observed for borate solutions in the range from 0.316 mM to 3.16 mM (Figure 5.11a), which means that the peak current is affected by the concentrations of both the borate and hydroxide ions. Notes that the peak current signal of borate solution is smaller compared to the phosphate solution. Although we still cannot formulate how is the direct relation between the buffering capacity and the increase of the current signal when compared to the

non-buffer solution, this might be due to weaker buffering capacity that borate buffer has compared to the phosphate buffer in the range of pH used in this experiment.

Lastly, Figure 5.11b shows a plot of the difference between the current for the borate solution and the simple NaOH solution at the same pH versus calculated buffer capacity of the borate solution. It can be seen that this plot is linear, suggesting that the current can also be used to determine the buffer capacity of the borate solution. This behavior is also in agreement with our previous result for the phosphate solution (Section 3.3), which further confirms that the behavior of hydroxide ions in weak basic solutions is related to the buffering capability of the solution.

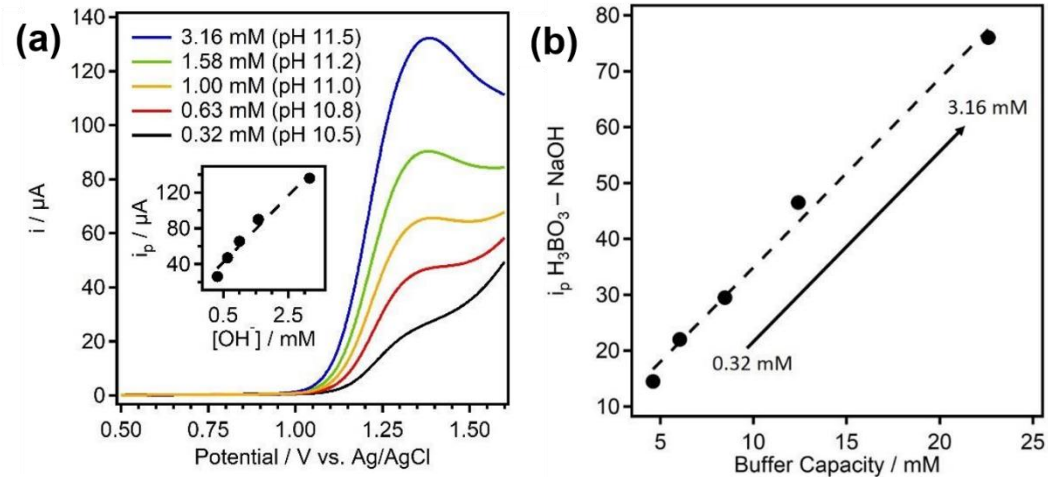

Figure 5.11. (a) LSVs for different concentrations of hydroxide ions in 40 mM H_3BO_3 buffer solution at AO-BDD. inset: peak current as a function of hydroxide ion concentration. (b) Plot of the peak current difference between the 40 mM H_3BO_3 and NaOH solutions versus theoretically calculated buffer capacity. The pH of the solution ranging from 10.5 to 11.5. Reproduce from *ref 8* by permission of The Royal Society of Chemistry.

4. Conclusion

The oxidation behavior of hydroxide ion at BDD electrodes was investigated. The hydroxide ion oxidation was observed at BDD without needs neither a special geometry nor a special electrode system. This was possible due to the high overpotential of the OER and no competition with oxide formation on the surface of the electrodes. The oxidation behavior is found to be depends on the surface condition of the BDD electrodes. In comparison to AO-BDD, the hydroxide ion oxidation at CR-BDD are shifted to more negative potential and shows a pre-peak at around 0.9 V which interpreted as hydroxide ion oxidation at the "reduced surface" of the BDD. The value of the peak current at both AO- and CR-BDD was similar at the same NaOH concentration, and shows good linearity versus the hydroxide ion concentration. Moreover, behavior of hydroxide ion oxidation in a weak basic solution, which in this case is alkaline phosphate solution, was found to be similar with the behavior in simple strong basic solution. Compared to the same concentration of hydroxide ion in the NaOH solution, phosphate solution having higher current signal due to the equilibrium of the phosphate that involving on the increase of hydroxide ion, making it easier to be oxidized on the surface of the solution. The current signal of the hydroxide ion oxidation was found to depend on not only the hydroxide ion, but also the concentration of the phosphate in the solution. It was found that the signal current was also related to the buffer capacity, opening a possibility for BDD electrode to become a new electrochemical method to determine the buffer capacity of a solution electrochemically.

5. References

1. Wael, K. D; Adriaens, A. *Talanta* **2008**, *74*, 1562.
2. Hallam, P. M.; Kampouris, D. K.; Kadara, R. O.; Jenkinson, N.; Banks, C. E. *Electroanalysis* **2010**, *2*, 1152.
3. Abu-Rabi, A.; Jasin, D.; Mentus, S. *J. Electroanal. Chem.* **2007**, *600*, 364.
4. Abdelsalam, M. E.; Denuault, G.; Antonietta Baldo, M.; Bragato, C.; Daniele, S. *Electroanalysis* **2001**, *13*, 289.
5. Abdelsalam, M. E.; Denuault, G.; Baldo, M. A.; Daniele, S. *J. Electroanal. Chem.* **1998**, *449*, 5.
6. Daniele, S.; Baldo, M. A.; Bragato, C.; Denuault, G.; Abdelsalam, M. E. *Anal. Chem.* **1999**, *71*, 811.
7. Irkham; Watanabe, T.; Einaga, Y. *Anal. chem.* **2017**, *89*, 7139.
8. Irkham; Einaga, Y. *Analyst* **2019**, *144*, 4499.
9. Asai, K.; Ivandini, T. A.; Falah, M. M.; Einaga, Y. *Electroanalysis* **2016**, *28*, 177.
10. Brocenschi, R. F.; Hammer, P.; Deslouis, C.; Rocha-Filho, R. C.; Brazil, P.; Brazil, P. *Anal. Chem.* **2016**.
11. Popa, E.; Notsu, H.; Miwa, T.; Tryk, D. A.; Fujishima, A. *Electrochem. Solid-State Lett.* **1999**, *2*, 49.
12. Notsu, H.; Yagi, I.; Tatsuma, T.; Tryk, D. A.; Fujishima, A. *Electrochem. Solid-State Lett.* **1999**, *2*, 522.
13. Daniele, S.; Baldo, M. A.; Bragato, C.; Abdelsalam, M. E.; Denuault, G. *Anal. Chem.* **2002**, *74*, 3290.
14. Kapałka, A.; Fóti, G.; Comninellis, C. *Electrochim. Acta* **2007**, *53*, 1954.
15. Granger, M. C.; Witek, M.; Xu, J.; Wang, J.; Hupert, M.; Hanks, A.; Koppang, M. D.; Butler, J. E.; Lucazeau, G.; Mermoux, M.; Strojek, J. W.; Swain, G. M. *Anal. Chem.* **2000**, *72*, 3793.
16. Duo, I.; Fujishima, A.; Comninellis, C. *J. Appl. Electrochem.* **2004**, *34*, 935.
17. Bennett, J. A.; Wang, J.; Show, Y.; Swain, G. M. *J. Electrochem. Soc.* **2004**, *151*, 306.
18. Macpherson, J. V. *Phys. Chem. Chem. Phys.* **2015**, *17*, 2935.
19. Yagi, I.; Notsu, H.; Kondo, T.; Tryk, D. A.; Fujishima, A. *J. Electroanal. Chem.* **1999**, *473*, 173.
20. Ferro, S.; Battisti, A. De. *J. Phys. Chem. B* **2003**, *107*, 7567.

21. Granger, M. C.; Swain, G. M. *J. Electrochem. Soc.* **1999**, *146*, 4551.
22. Ivandini, T. A.; Rao, T. N.; Fujishima, A.; Einaga, Y. *Anal. Chem.* **2006**, *78*, 3467.
23. Cañizares, P.; Larrondo, F.; Lobato, J.; Rodrigo, M. A.; Sáez, C. *J. Electrochem. Soc.*, **2005**, *152*, 191.
24. Salazar-banda, G. R.; Andrade, L. S.; Nascente, P. A. P.; Pizani, P. S.; Rocha-Filho, R. C.; Avaca, L. A. *Electrochim. Acta* **2006**, *51*, 4612.
25. Wang, M.; Simon, N.; Decorse-pascanut, C.; Bouttemy, M.; Etcheberry, A.; Li, M.; Boukherroub, R.; Szunerits, S. *Electrochim. Acta* **2009**, *54*, 5818.
26. Girard, H.; Simon, N.; Ballutaud, D.; Herlem, M.; Etcheberry, A. *Diam. Relat. Mater.* **2007**, *16*, 316.
27. Honda, Y.; Ivandini, T. A.; Watanabe, T.; Murata, K.; Einaga, Y. *Diam. Relat. Mater.* **2013**, *40*, 7.
28. Weiss, E.; Sáez, C.; Groenen-Serrano, K.; Cañizares, P.; Savall, A.; Rodrigo, M. A. *J. Appl. Electrochem.*, **2008**, *38*, 93–100.

Chapter 6

Summary & Future Perspective

1. Summary

In this thesis, we show the advantage of the boron-doped diamond (BDD) as working electrode to promote unique reaction for developing novel system of electrogenerated chemiluminescence (ECL) and observing the hydroxide ion oxidation in basic solution.

In Chapter 2, the first study on novel *coreactant-free ECL system* in which a unique ability of BDD to promote peroxydisulfate from sulfate with high efficiency is coupled with the high overpotential for the hydrogen evolution reaction to allow the efficient ECL generation in a $Ru(bpy)_3^{2+}/SO_4^{2-}$ aqueous solution was described. The mechanism is similar to the $Ru(bpy)_3^{2+}/S_2O_8^{2-}$, except that in this case the $S_2O_8^{2-}$ is electrogenerated in situ from the SO_4^{2-} electrolyte. The intensity of the light signal was found to be linear to the sulfate concentration up to around 0.6 M, where further increase of the concentration lead to negative deviation due to the ability of $S_2O_8^{2-}$ to quench the excited of $Ru(bpy)_3^{2+*}$. The detection limit to the sulfate was found to be in the range of gram per liter (~1 mM), which is 1 order magnitude lower compared to the previously promoted amperometric method at BDD electrode.

In Chapter 3, with similar strategy, another *coreactant-free* ECL system of $Ru(bpy)_3^{2+}/CO_3^{2-}$ system in aqueous solution was discussed. In this system, CO_3^{2-} was oxidized to $C_2O_6^{2-}$ then further react with the water lead to generation of H_2O_2. This H_2O_2 will then work as coreactant to generate excited state of $Ru(bpy)_3^{2+*}$ in the cathodic scan, lead to generation of ECL light. The carbonate system could work starting in the potential of 1.8 V, which is around 0.7 V lower compared to previous sulfate system. The ECL emission was found to be depend on the concentration of the electrogenerated hydrogen peroxide, therefore it can be controlled through several means such as controlling the pH, oxidation potential, time, and the initial concentration of carbonate electrolyte.

Using similar strategy, Chapter 4 described a *coreactant-free* ECL system where $Ru(bpy)_3^{2+}$ was replaced with luminol, another luminophore that also works with H_2O_2. The results show 3 kinds of peaks could be observed in this luminol/CO_3^{2-} system which all found to be derivate from the excited state of 3-aminopthalte dianion with each respective

mechanism. The emission was found to be decrease by the decrease of pH, which is expected on the luminol system due to the needs of luminol to be deprotonated before even oxidize in the surface of electrode. Although the mechanism seems like more complicated compared to other two ruthenium system in this report (chapter 2 and 3), luminol system have the advantage of having higher ECL intensity and could be achieve possibly by applying one step potential of oxidation. In addition, we also showed the possibility of this system to evaluate the value of carbonate or CO_2 in the water.

Lastly, chapter 5 is discussed about the study of hydroxide ion oxidation on BDD electrode in alkaline solution. The study is including comparison of simple NaOH as strong alkaline solution and the phosphate as weak alkaline solution with buffering effect. In strong alkaline solution, although a pre-peak was found in reduced BDD, both oxidized and reduced BDD are showing good linearity versus the hydroxide ion. This shows that the increase of the current signal was solely depends on the hydroxide ion concentration. Meanwhile, in a weak alkaline solution, the current was found to be higher compared to the same hydroxide ion concentration of strong alkaline solution due to the buffering capability of weak basic solution which make it possible to maintain the hydroxide ion via equilibrium. The plot of peak current signal versus buffer capacity shows a good linearity, suggesting that peak current was not affected by only hydroxide ion concentration but also the buffer capacity of the solution.

2. Future perspective

The remarkable properties of BDD have been exploited by electrochemist for a wide range of applications. Here in this thesis, we successfully develop another way of using BDD as working electrode by taking advantage of its characteristic especially on the wide potential window and its ability to generate an efficient amount of strong oxidant. The results did not only show. the superiority of the BDD electrode, but also opening a new system or application in the field of electrochemistry especially on the electrogenerated chemiluminescence and pH sensing. The study is not complete by any means, and still needs some improvement which will be discuss and suggested in each section bellow.

2.1 *Coreactant-free* electrogenerated chemiluminesence

Nowadays, development of ECL system was led to the aqueous based solution for the more general application. In particular, ECL have several advantages such as no background emission, broad dynamic range, low vo1ume, and rapid measurement analysis, therefore push the detection limit up to pM range. Despite the general reaction mechanism is being dictated by the choice of luminophore and its coreactant, the electrode material and its surface state also playing an important role that affect the ECL signal measured on the system. In this report we show how BDD could become a good candidate to use as working electrode by developing a novel *coreactant-free* system due to its wide potential window and its unique properties to promote strong oxidant from the electrolyte. This could open a new way applying ECL since the use of coreactant, which usually was needed to help generating the ECL in aqueous solution, was technically unnecessary. Although in this thesis we show how ECL using BDD system could simply measure inorganic ion (e.g. SO_4^{2-} or CO_3^{2-}), it still quite far for this kind of system to be applied in clinical purpose where ECL system is already applied for real measurement. The obstacle to this system was the needs of relatively high over-potential to generate the in situ coreactant efficiently, which might lead to the problem of (i) cost and (ii) the oxidation of the target itself. In addition, unlike the usual coreactant system which needs only one step potential (either oxidation or reduction), two step potential was required for application. This led to the challenge on designing the measurement system for such kind of application. It is highly suggested for continue the study in the “magnetic beads” ECL system for detecting some antigen, which is the typical ways on applying ECL for the clinical purpose. As for the design of the system, it might be better to apply the 2 working electrode system such as interdigitated array electrode system where 1 electrode meant for generating the coreactant from the electrolyte, while the other electrode for carrying the ECL. In addition, it also important to search even more electrolyte that could lead to even more efficient generation of in situ coreactant in the lower potential.

2.2. Hydroxide ion oxidation at boron-doped diamond

Many reports already promoting BDD electrode as a pH sensor material due to its inert nature of diamond even in extremely acid or alkaline solution which quite impossible for the normal glass electrode. Unsurprisingly, the research is more focusing on either the direct observation of the hydrogen reduction or some surface sensitive reaction towards the change of pH. Both approaches are possible due to the wide potential window and the unique surface state of BDD electrode. On the other hand, in this study we show another new possible approach for pH sensing using BDD electrode by the observation of hydroxide ion oxidation behavior, again by taking the advantage of BDD to promote unique reaction at its surface. Although both in strong and weak alkaline solution, the current peak signal using cyclic voltammetry was found to be linear with the hydroxide ion concentration, the value of the current peak is still difference for different source of hydroxide ion e.g. non-buffer and buffer. It is recommended to have more deep study to overcome this problem by possibly using different electrochemical technique or by using some special type of cells. Furthermore, in the buffered solution, it was found that the oxidation behavior was also dictated by the buffering capacity of the solution. These interesting results should be more intensely investigate since it leads to the possibility for BDD to evaluate the buffer capacity of the solution directly, which is still quite hard things to observe by other method including electrochemical method itself.

List of Publications and Conferences

Published paper presented in this thesis

(1)Irkham, Fiorani, A., Valenti, G., Kamoshida, N., Paolucci, F. and Einaga, Y.,
"Electrogenerated chemiluminescence by in situ production of coreactant hydrogen peroxide in carbonate aqueous solution at a boron-doped diamond electrode",
Journal of the American Chemical Society, in press (2020). (DOI: 10.1021/jacs.9b11842)

(2)Irkham and Einaga, Y.,
"Oxidation of hydroxide ions in weak basic solutions using boron-doped diamond electrodes: effect of the buffer capacity",
Analyst, Vol. 144, pp. 4499-4504 (2019). [**Highlighted in outside back cover**]

(3)Irkham, Watanabe, T. and Einaga, Y.,
"Hydroxide ion oxidation in aqueous solutions using boron-doped diamond electrodes",
Analytical Chemistry, Vol. 89, No. 13, pp. 7139-7144, (2017).

(4)Irkham, Watanabe, T., Fiorani, A., Valenti, G., Paolucci, F. and Einaga, Y.,
"Co-reactant-on-demand ECL reactant-on-demand ECL: electrogenerated chemiluminescence by the in situ production of $S_2O_8^{2-}$ at boron-doped diamond electrodes",
Journal of the American Chemical Society, Vol. 138, No. 48, pp. 15636-15641, (2016).

Other publication

(1) Muharam, S., Jiwanti, P.K., Irkham, Gunlazuardi, J., Einaga, Y., and Ivandini T.A.,
"Electrochemical oxidation of palmitic acid solution using boron-doped diamond electrodes",
Diamond and Related Materials, Vol. 99, No. 107464 (8 pages), (2019**)**.

(2)Wulandari, R., Ivandini, T.A., Irkham, Saepudin, E. and Einaga, Y.,
"Modification of boron-doped diamond electrodes with platinum to increase the stability and sensitivity of haemoglobin-based acrylamide sensors",
Sensors and Materials, Vol. 31, No. 4, pp. 1105-1117, (2019).

(3) Fiorani, A., Irkham, Valenti, G., Paolucci, F. and Einaga, Y.,
"Electrogenerated chemiluminescence with peroxydisulfate as a coreactant using boron doped diamond electrodes",
Analytical Chemistry, Vol. 90, No. 21, pp. 12959-12963, (2018).

International Conference

(1) Irkham, Fiorani, A., Sakanoue, K. and Einaga, Y.,
"Electrogenerated chemiluminescence at boron-doped diamond electrodes",
The 4th International Symposium on Current Progress in Functional Material, Bali, Indonesia, November 6 (2019).
(2) Irkham, Fiorani, A. and Einaga, Y.
"ECL by the in situ generation of H_2O_2 in Na_2CO_3 aqueous solution at boron-doped diamond electrodes",
International symposium on diamond electrochemistry, Yokohama, Japan, March 6 (2019).
(3) Irkham and Einaga, Y.,
"Study of hydroxide ion oxidation in buffer solutions using boron-doped diamond electrodes",
69th Annual Meeting of the International Society of Electrochemistry, Bologna, Italy, September 4 (2018).
(4) Irkham, Watanabe, T. and Einaga, Y.,
"Hydroxide ion oxidation in aqueous solutions using boron-doped diamond electrodes",
68th Annual Meeting of the International Society of Electrochemistry, Providence, America, August 29 (2017).
(5) Irkham, Watanabe, T., Fiorani, A., Valenti, G., Paolucci, F. and Einaga, Y.,
"Co-reactant-ondemand ECL: electrogenerated chemiluminescence by the in situ production of $S_2O_8^{2-}$ at boron-doped diamond electrodes",
International Conference on Electrogenerated Chemiluminescence, Bordeaux, France, August 30 (2016).
(6) Irkham, Watanabe, T., Fiorani, A., Valenti, G., Paolucci, F. and Einaga, Y.,
"Electrogeneration of $S_2O_8^{2-}$ at BDD electrodes in a electrogenerated chemiluminesence system",
International Symposium on Current Progress in Functional Material, Bali, Indonesia, July 27 (2016).
(7) Irkham, Watanabe, T. and Einaga, Y.
"Electrochemical behavior of weak bases on diamond electrode",
21st China-Japan Bilateral Symposium on Intelligent Electrophonic Materials and Molecular Electronics, Xiamen, China, September 11 (2015).

Domestic Conference

(1) Irkham, Fiorani, A., Sakanoue, K. and Einaga, Y.,
"Electrogenerated chemiluminescence at boron-doped diamond electrodes",
33rd Diamond Symposium, Tokyo, Japan, November 14 (2019).
(2) Irkham, Fiorani, A. and Einaga, Y.,
"ECL by the in situ generation of H_2O_2 in Na_2CO_3 aqueous solution at boron-doped diamond electrodes",
ECSJ Spring Meeting, Kyoto, Japan, March 27 (2019).

(3) Irkham and Einaga, Y.,
"Hydroxide ion oxidation in buffer and non-buffer aqueous solutions using boron-doped diamond electrodes",
ECSJ Spring Meeting, Tokyo, Japan, March 10 (2018).
(4) Irkham, Watanabe, T. and Einaga, Y.,
"Electrogeneration of $S_2O_8^{2-}$ using BDD electrodes for ruthenium electrogenerated chemiluminesence system.
ECSJ Spring Meeting, Osaka, Japan, March 30 (2016).

Others

(1) Fiorani, A., Irkham, Valenti, G., Einaga, Y. and Paolucci, F.,
"Diamond Electrodes for Electrogenerated Chemiluminescence",
Nanocarbon Electrochemistry; John Willey & Sons, Inc.: New York, pp 285-321, (2019).

Acknowledgment

In the name of Allah, the most gracious, the most merciful. I would like to dedicate my works in this dissertation to my beloved family. My best partner of life, my wife, Fathima Assilmia, which is the best supporter that I could ask for going through all of the PhD life. *Terima kasih, untuk kesabaran dan dukungannya selalu, istriku.* My beloved parents, even though there are a lot of trouble just for us to be connected, I know that both of you are always pray the best for me and pray for my success on all of my study progress. All my lovely sister and brothers, which always support me in all ways and make me feel better and less guilty for staying in Japan because I know all of you will take care of our parents. I would devote this works to my parents in law, whose also always support me far away from home. *Terima kasih untuk kalian semua keluarga ku tercinta yang selalu memberikan dukungannya dalam segala hal, walau kita berada di tempat yang jauh, aku selalu merasakan keberadaan kalian semua.*

I would like to address my biggest gratitude to my advisor, Prof. Yasuaki Einaga for having me for more than 5 years in his group, giving me a chance to really study a lot not only science and chemistry, but also a lot about life. Being a foreigner in a foreign land is

absolutely not an easy thing to do. But with the help of your support, your guidance, and your positive attitude, it really making my life and my study in Japan so much easier. I also would like to thanks to Dr. Andrea Fiorani (Ando-san) for all of the advice, guidance, and friendship especially in my ECL research, I really couldn't have complete my PhD without your help. I would like to also say my gratitude to Dr. Takashi Yamamoto, even though that you might not realize, that actually always motivate me to become a better scientist in one way or another.

In addition, I would like to thank you to all the reviewer of my doctoral defense, Prof. Daniel Citterio, Dr. Taku Hasobe, and Dr. Eisuke Nihei for all the useful question and comments towards my work. I also thank you for the revision of this dissertation book, which makes this book so much beautiful and better.

それから、いつも日本語の勉強や研究を共にした栄長研の皆様、スタッフの皆様や後輩の皆様にも感謝いたします。常に優しく接してくださった、吉井さん、赤井さん、細美さん、西谷さん、様々な面で日本での生活を手伝ってくれてありがとうございました。5 年もの間、共に勉強したり、遊んでくれた私の親友、かいちゃんとトミッキー、そして博士号を一緒に取得した外国人チームの皆様にも感謝いたします。私と以心伝心の友セイジ、内山チームのうっちーとヨネダマオ、研究室で楽しませてくれてありがとうございました。私の趣味を分かってくれた、オタクの友達ピーもサンキューです。そしてとなりの席で私の煩さに我慢し、モンハンと ECL の研究を共にやっていたエスくんにも grazie mille です。

Lastly, I also would like to send best gratitude to Keio "Design the Future" Award for International Students that support my academic and financial through all this 3 year of Doctoral Program. Without the help of the scholarship I couldn't even start my PhD let alone finish it.

I hope that all the works done in this dissertation could be helpful, even for just a little, for the advancement of science and technology, especially in the field of electrochemistry and ECL using BDD.

Japan, February 2020

Irkham